SYNTHESIS OF THIOPHENE-CONTAINING HETEROCYCLES AND THEIR APPLICATION AS ANTICANCER AGENTS

by

Joseph Michael Salamoun

B.S., University of Virginia, 2011

Submitted to the Graduate Faculty of

The Kenneth P. Dietrich School of Arts and Sciences in partial fulfillment

of the requirements for the degree of

Doctor of Philosophy

University of Pittsburgh

2017

UNIVERSITY OF PITTSBURGH

THE KENNETH P. DIETRICH SCHOOL OF ARTS AND SCIENCES

This dissertation was presented

by

Joseph Michael Salamoun

It was defended on

August 1, 2017

and approved by

Alexander Deiters, Professor, Department of Chemistry

Kazunori Koide, Associate Professor, Department of Chemistry

John S. Lazo, Harrison Distinguished Teaching Professor, Department of Pharmacology, University of Virginia

Dissertation Advisor: Peter Wipf, Distinguished University Professor, Department of Chemistry

SYNTHESIS OF THIOPHENE-CONTAINING HETEROCYCLES AND THEIR APPLICATION AS ANTICANCER AGENTS

Joseph Michael Salamoun, PhD

University of Pittsburgh, 2017

Five-membered heterocycles represent a privileged scaffold in drug discovery and are the focus of analog design. The first chapter presents the synthesis and biological evaluation of analogs of NSC 652287, which targets the renal carcinoma cell line A498. The Pd-catalyzed Suzuki-Miyaura cross-coupling with halogenated furan, thiophene, and selenophene led to generally high overall yields for the construction of heterocyclic triads. C-H bond activation provided an efficient strategy for the Pd-catalyzed cross-coupling at C(2) of oxazoles. Further analog variation was achieved with a copper-catalyzed azide-alkyne cycloaddition to form a 1,4-substituted 1,2,3-triazole. Potency and selectivity of the final hydroxymethyl products were determined in the NCI-60 cell assay. Two lead compounds were tested *in vivo* and compared to NSC 652287. The evaluation of these compounds continues with a thermal shift assay coupled with differential mass spectrometry for biological target identification. The chemical stability of select triads are also discussed.

The second chapter details the synthesis of thienopyridone and thienopyrimidine dione analogs as inhibitors of protein tyrosine phosphatase 4A3 (PTP4A3), an attractive anticancer target. Derivatization by photooxygenation led to a compound with a unique structural motif, high potency, and excellent selectivity towards PTP4A3. An automated synthesis strategy using Lilly's Automated Synthesis Lab was employed for analog synthesis.

TABLE OF CONTENTS

LIST OF TABLES

LIST OF FIGURES

LIST OF SCHEMES

LIST OF ABBREVIATIONS

μW .....microwave

APL.....Automated Purification Lab

aq.....aqueous

ASL.....Automated Synthesis Lab

ATR.....attenuated total reflectance

Bn.....benzyl

Brettphos.....2-(dicyclohexylphosphino)3,6-dimethoxy-2′,4′,6′-triisopropyl-1,1′-biphenyl

BRSM .....based on recovered starting material

calcd .....calculated

CFL .....compact fluorescent lamp

conc.....concentrated

Davephos.....2-dicyclohexylphosphino-2′-(*N*,*N*-dimethylamino)biphenyl

dba.....dibenzylideneacetone

DDQ.....2,3-dichloro-5,6-dicyano-1,4-benzoquinone

DFT.....density functional theory

DiFMUP.....6,8-difluoro-4-methylumbelliferyl phosphate

DMEDA.....*N*,*N*'-dimethylethylenediamine

DMF.....*N*,*N*-dimethylformamide

DMSO.....dimethylsulfoxide

DTT.....dithiothreitol

EDTA.....ethylenediaminetetraacetic acid

ELSD.....evaporating light scattering detector

Equiv.....equivalents

ESI.....electrospray ionization

Et.....ethyl

FAD.....flavin adenine dinucleotide

FCS .....fluorescence correlation spectroscopy

FDA.....United States Food and Drug Administration

FKBP.....FK506 binding protein

GC-MS.....gas chromatography-mass spectrometry

HDM2 .....human double minute 2

HFIP.....hexafluoroisopropanol

HIF .....hypoxia inducible factor

HOMO .....highest occupied molecular orbital

HRMS .....high-resolution mass spectrometry

HSQC.....heteronuclear single quantum coherence spectroscopy

IR.....infrared spectroscopy

LC/MS.....liquid chromatography/mass spectrometry

LUMO.....lowest unoccupied molecular orbital

Me .....methyl

mp .....melting point

mTOR .....mammalian target of rapamycin

NADH.....nicotinamide adenine dinucleotide (H)

NBS.....*N*-bromosuccinimide

NCI.....National Cancer Institute

NMR .....nuclear magnetic resonance

NSC.....National Service Center

OIDD.....Open Innovation Drug Discovery

PDGF(R).....platelet-derived growth factor (receptor)

Ph .....phenyl

PRL .....phosphatase of regenerating liver

PTP.....protein tyrosine phosphatase

RCC.....renal cell carcinoma

RITA .....reactivation of p53 and induction of tumor cell apoptosis

rt .....room temperature

SAR.....structure-activity relationship

sat .....saturated

sm.....starting material

t-BuXPhos Pd G1.....[2-(di-tert-butylphosphino)-2′,4′,6′-triisopropyl-1,1′-biphenyl][2-(2-aminoethyl)phenyl)]palladium(II) chloride

THF .....tetrahydrofuran

TLC.....thin layer chromatography

TMS .....trimethylsilyl

UV.....ultraviolet spectroscopy

VEGF(R).....vascular endothelial growth factor (receptor)

VHL .....von Hippel-Lindau protein

ACKNOWLEDGEMENTS

I would like to thank Professor Peter Wipf for presenting me with the opportunity to work in his lab and offering his guidance and support throughout my studies. His passion for chemistry coupled with his high work ethic and expectations are both inspiring and motivating for me to deliver my best. I acknowledge Professors Alexander Deiters, Kazunori Koide, and John Lazo for serving on my committee and for providing valuable advice for my projects. I thank Professor Nathan Yates and Dr. Steven Mullett for welcoming me into their lab and offering guidance on the mass spectrometry proteomics studies.

I am grateful to all Wipf group members past and present for their guidance, support, and various contributions to the projects. In particular, I would like to thank Pete Chambers and Taber Lewis for evaluating the purity of the final compounds before biological testing. The valuable contributions of Shelby Anderson, Dr. Christopher Rosenker, Dr. Erin Skoda, Dr. Kalyani Patil, and Dr. Steven Geib are presented in the main text.

I would like to acknowledge the University of Pittsburgh and the National Cancer Institute (F31 CA200145) for supporting my graduate studies. Finally, I thank our collaborators Christopher Beadle (Eli Lilly & Company) and Dr. Richard Gussio (National Cancer Institute) along with their colleagues.

1.0 HETEROCYCLIC TRIADS AS POTENTIAL CHEMOTHERAPEUTICS TARGETING RENAL CELL CARCINOMA

1.1 INTRODUCTION

1.1.1 Renal Cell Carcinoma and Therapeutic Challenges

Kidney and renal pelvis cancer will account for nearly 64,000 new cases and >14,000 deaths in the United States in 2017.[1] Renal cell carcinoma (RCC) encompasses a variety of highly vascularized heterogeneous solid tumors, creating a dependence on angiogenesis for tumor growth and progression.[2] Significant advances in the understanding of RCC biology led to the development of therapeutic agents targeting the von Hippel-Lindau (VHL)/hypoxia-inducible factor (HIF)/vascular endothelial growth factor (VEGF) pathway (Figure 1).[2-3] This pathway is a cellular response mechanism for low concentrations of molecular oxygen, O_2, also known as hypoxia.

Under normal O_2 concentrations, HIF is enzymatically hydroxylated on a proline residue by an O_2 dependent process. The hydroxyl group retards aggregation of HIF, which prevents its transcriptional role and enables higher recognition and binding affinity by VHL, an E3 ligase, which signals HIF for ubiquitination and proteasome mediated degradation. When hypoxia occurs, HIF is not hydroxylated/inactivated but aggregates into the active form leading to the

transcriptional activation of HIF target genes. The new proteins then target VEGFR and platelet-derived growth factor receptors (PDGFR), resulting in angiogenesis. To mimic this hypoxia response under normal O_2 concentrations, clear cell RCC typically has mutated or epigenetically inactivated VHL where HIF is no longer regulated, and thus leads to angiogenesis and tumor growth.[4] An alternate route to angiogenesis proceeds through the PI3K/Akt signaling pathway, which activates the mammalian target of rapamycin (mTOR). In addition to overlapping with the HIF pathway, the activation of mTOR leads to the production of Cyclin D1 and c-Myc, resulting in cancer cell growth and survival.[3b]

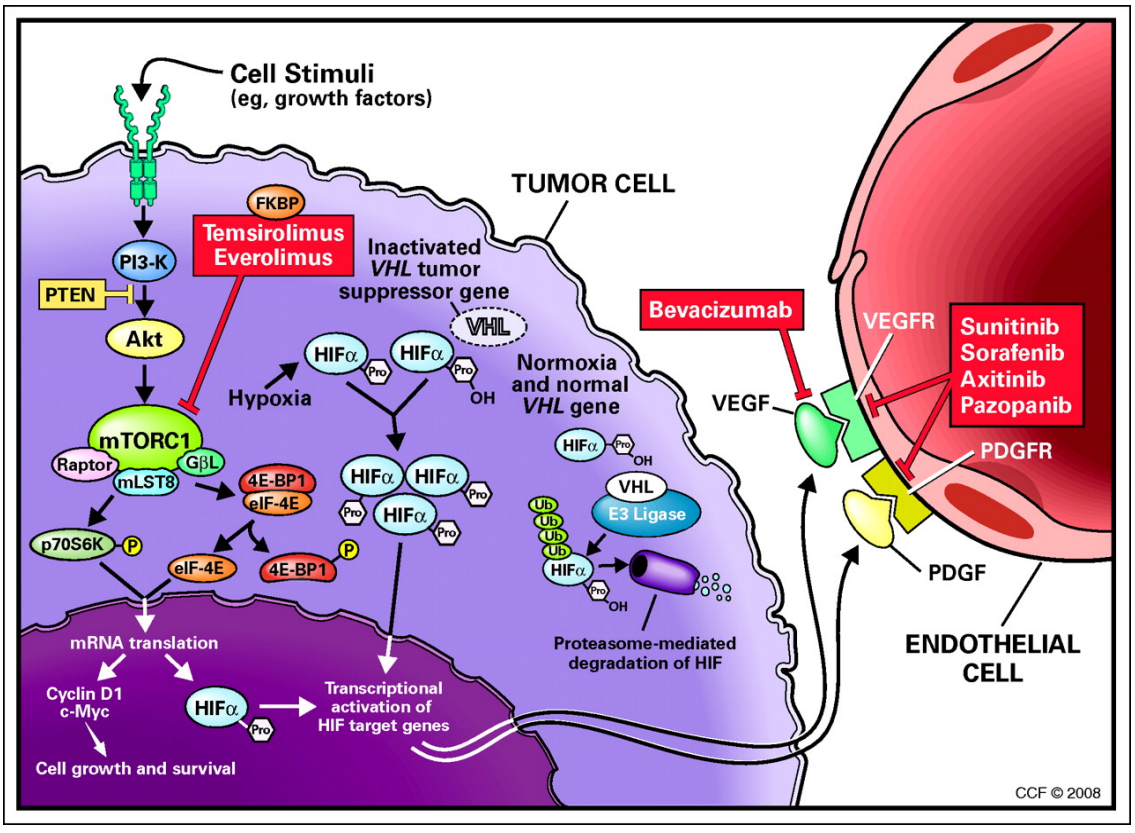

Figure 1. Illustration of the VHL/HIF/VEGF pathway. The red boxes indicate targets of FDA approved therapeutic agents.[3b] Reprinted with permission. © 2009 American Society of Clinical Oncology. All rights reserved.

There are a number of United States Food and Drug Administration (FDA) approved therapeutic agents that act on the VHL/HIF/VEGF pathway and mTOR (Figures 1 and 2).[2-4] The macrolides everolimus and temsirolimus share the same core as the natural product rapamycin and inhibit mTOR via hydrophobic interactions at the three conjugated π-bonds, preventing tumor proliferation.[5] Both macrolides also interact with the prolyl isomerase FK506 binding protein (FKBP), with the piperidine ring acting as a proline mimic. Bevacizumab is an anti-VGEF monoclonal antibody that is co-administered with interferon α.[2-4] The small molecules axitinib, cabozantinib, lenvatinib, pazopanib, sorafenib, and sunitinib are potent and selective protein tyrosine kinase inhibitors of growth factor receptors, including VEGFR and PDGFR.[2-4,6]

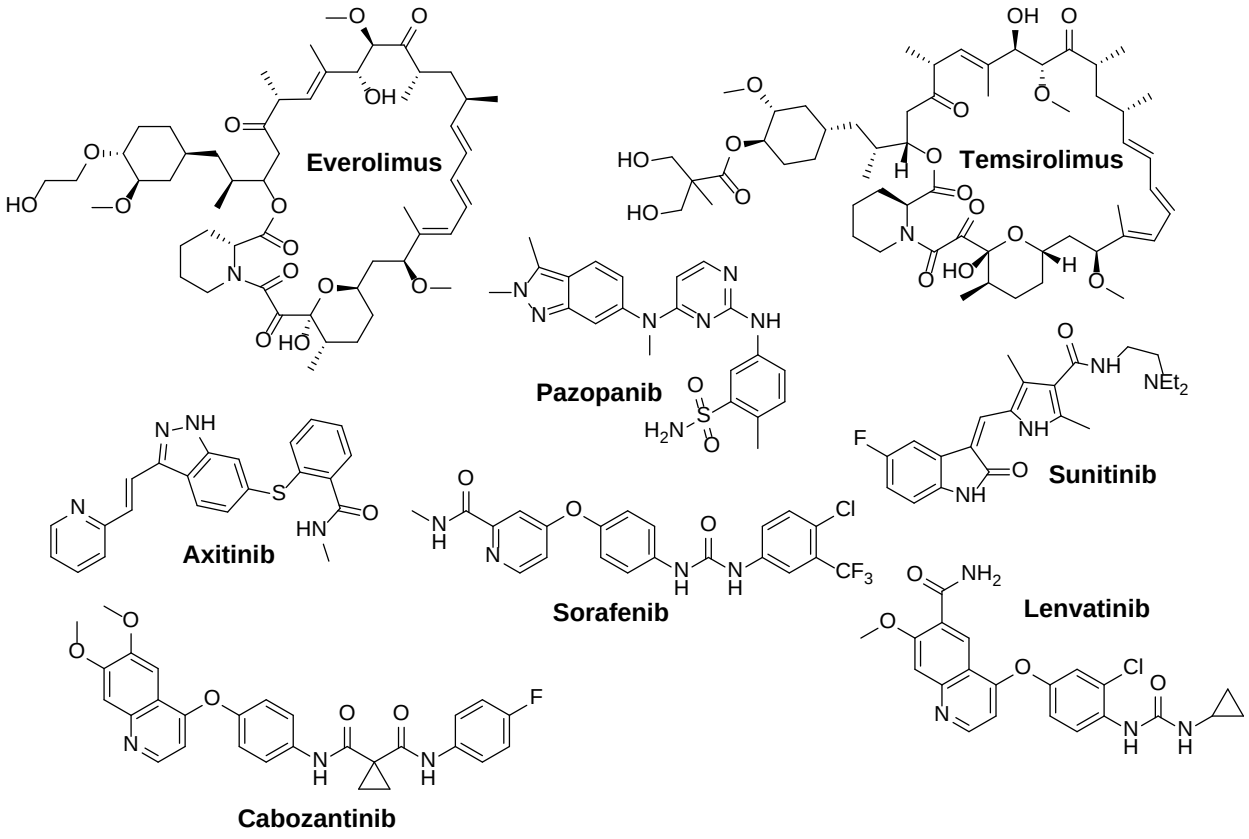

Figure 2. Chemical structures of therapeutic agents approved for kidney cancer treatment.[6]

Current therapeutics can provide patients with some initial relief as first or second treatment options, but positive response is often not sustained which results in relapse and eventual patient death from either RCC or drug induced toxicity.[2-4,7] Patients with advanced RCC have a 5-year survival rate of about 6%.[2,4] In many cases, tumor cells develop resistance to the kinase inhibitors through either inherent mechanisms such as low drug uptake, or acquired mechanisms such as activation of alternate pathways for tumor proliferation.[4] Combination therapies of the kinase and mTOR inhibitors have been attempted, but often led to unacceptable toxicity.[3c] Further optimization of these kinase inhibitors may not lead to more successful and safe therapies, especially with the high potency of current drugs. For example, axitinib is 50-450 times more potent than sunitinib, sorafenib, and pazopanib with subnanomolar IC_{50} values and better specificity, but it presents adverse effects similar to other treatment options.[2,8] Thus, discovery of antitumor molecules that involve mechanisms of action outside of the VHL/HIF/VEGF pathway would be clinically useful.

1.1.2 Heterocyclic Triads as Potent Inhibitors of Renal Carcinoma Cell Line A498

A common approach for drug discovery is the utilization of phenotypic screening to identify lead candidates before developing target oriented analog designs.[9] The National Cancer Institute (NCI) Anticancer Drug Screen was established in the late 1980s as an initiative for anticancer drug discovery.[10] This phenotypic screen, also known as NCI-60, consists of 60 well characterized tumor cell lines representing leukemia, non small-cell lung, colon, central nervous system, melanoma, ovarian, renal, prostate, and breast cancers. Approximately 2,500 compounds solicited from government, industrial, and academic labs are tested every year as part of a disease-oriented preclinical screening with about 2% of the screened compounds progressing to

mice studies. Testing is conducted with a 1- or 5-concentration colorimetric assay, most commonly utilizing sulphorhodamine B as the protein dye.[10-11] The NCI then utilizes a computer algorithm (COMPARE), which identifies similarities in the activity of screened compounds to well-known standards, in an effort to predict likely cellular targets and mechanisms of action.[12] The bioactivity profiles generated from the NCI-60 assay have enabled the elucidation of the mechanism of action of several compounds such as halichondrin B, a natural product that targets tubulin for mitotic inhibition and led to the FDA-approved analog eribulin for the treatment of breast cancer, and bortezomib, a proteasome inhibitor and FDA-approved drug for the treatment of myeloma.[10,13] Thus, the NCI-60 assay provides a widely accessible screening tool for the identification of potential novel therapeutic agents targeting cancers such as RCC.[14]

Among the compounds screened in the NCI-60 assay, Rivera and coworkers, in 1999, identified the growth inhibition of renal cell line A498 by a heterocyclic triad known as National Service Center (NSC) 652287 (**1-1**) (Figure 3).[15] The α-terheterocycle scaffold in **1-1** may be regarded as a structural alert by medicinal chemists due to the potential toxicity that can result from chemical reactivity and bioactivation of the electron-rich heterocycles.[16] Despite these concerns, five-membered heterocycles remain a privileged scaffold in medicine (Figure 3).[16b,17] For example, clopidogrel, a member of the thienopyridine class of antiplatelet agents, is a prodrug that requires bioactivation by CYP, which oxidizes the thiophene ring.[18] Tiotropium bromide, which features two thiophene rings, is a muscarinic receptor antagonist used in the management of chronic obstructive pulmonary disease.[19] Duloxetine is a serotonin-norepinephrine reuptake inhibitor that undergoes oxidation on the naphthyl ring rather than the thiophene[20] and rivaroxaban is an anticoagulant used to prevent blood clots by inhibiting direct factor Xa.[21] In addition to marketed drugs, naturally occurring and synthetic dithiophenes,

terthiophenes, and related analogs have been shown to have insecticidal, bactericidal, antifungal, antitumoral, and antiviral activity (Figure 3).[22] For example, α-terthiophene **1-2** and related alkyl substituted terthiophenes are naturally occurring phototoxic sensitizers of plant origin with useful insecticidal and bactericidal applications.[22a,b] Ether-substituted terthiophene **1-3**, isolated from the plant species *Eclipata prostrata*, has potent submicromolar antihyperglycemic activity against dipeptidyl peptidase IV,[22e] dialdehyde **1-4** is a potent protein kinase C inhibitor,[23] and diol **1-5** showed 100-fold higher cytotoxicity against wild-type human colon cancer cell line HCT-116 versus its p53 knockdown (HCT-116/p53$^{-/-}$).[22d] Additionally, oligothiophenes have been considered for use as possible fluorescent markers for biological applications due to their extended π-system.[24] Accordingly, terthiophenes and related triads provide a versatile scaffold with a wide range of bioactivities that are readily modulated by minor structural modifications. These observations warrant a more detailed exploration of this heterocyclic triad scaffold as a potential therapeutic agent against RCC.

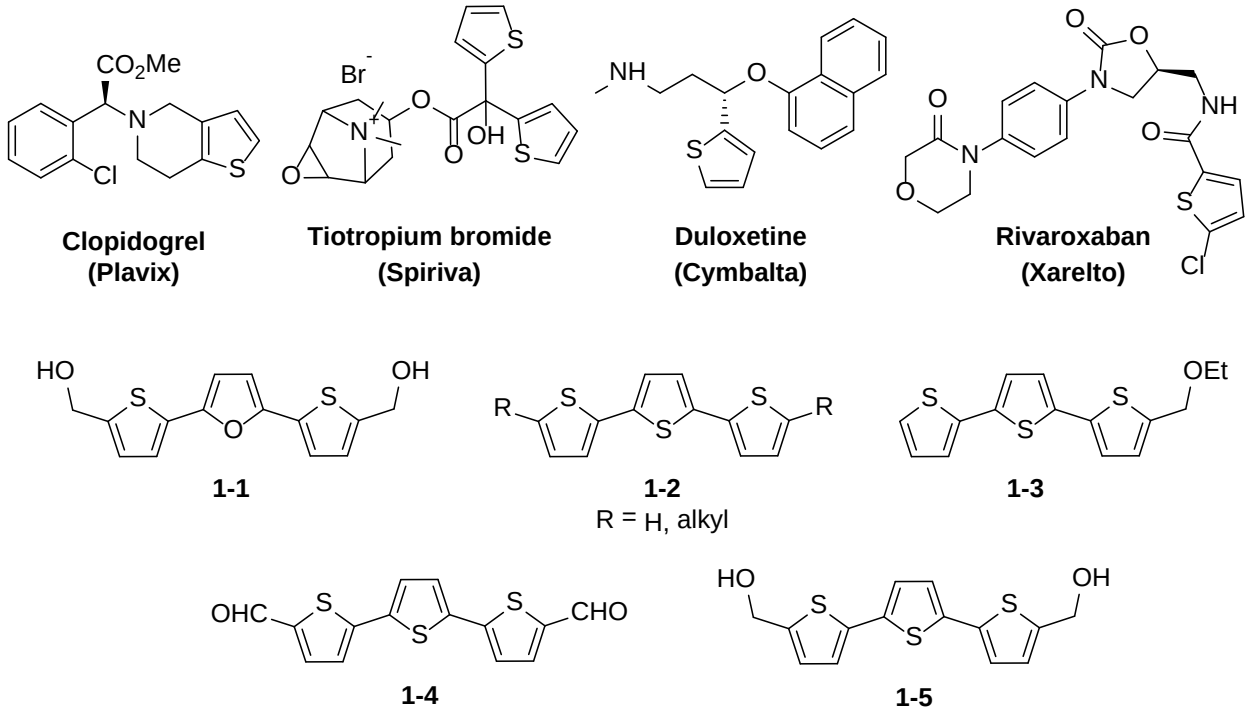

Figure 3. Structures of FDA-approved drugs featuring thiophenes, NSC 652287 (**1-1**), and closely related heterocyclic triads.

1.1.3 Reported Studies on the Mechanism of Action and Metabolism of NSC 652287

NSC 652287 (**1-1**) showed potent activity against a number of cancer cell lines with a GI_{50} value of about 0.02 μM in the renal cancer cell line A498.[15] More importantly, **1-1** did not impact all the cancer cell lines equally, indicating some selectivity. The COMPARE algorithm did not find any match for the observed activity, suggesting either a novel mechanism of action or multiple targets. In an effort to explain the selectivity seen in the phenotypic assay, the accumulation, retention, and metabolism of **1-1** were determined in renal cancer cells A498, TK-10, ACHN, and UO-31. Interestingly, lower GI_{50} concentrations correlated with higher accumulation, lower retention, and faster metabolism in the order of A498 > TK-10 >> ACHN ~

UO-31. The observation that a faster metabolism correlated with a more potent activity provided some early indication that the heterocyclic triad **1-1** may be a prodrug.

There are dozens of literature reports on potential mechanisms of action of **1-1**, but the most widely cited study associates **1-1** with binding to the antitumor protein p53, an essential defense tool for cells against uncontrolled growth,[25] leading to the renaming of the compound to RITA (reactivation of p53 and induction of tumor cell apoptosis).[26] A common approach for the activation of p53 involves targeting the regulatory protein human double minute 2 (HDM2), an E3 ligase that binds p53 and then signals it for ubiquitination and subsequent proteasome degradation. The discovery and development of the nutlin compounds by Hoffmann-La Roche has set the foundation for targeting the p53-HDM2 interaction for antitumor therapeutics.[27] Nultins bind to HDM2 in the same pocket as p53, preventing complex formation and ubiquitin-mediated degradation of p53.[28] Most importantly, they were more selective for cells that overexpress HDM2 over healthy cells. Many molecules targeting HDM2 have made it into clinical trials for cancer treatment.[29]

In contrast to the nutlin series, **1-1** is proposed to bind directly to p53, lending some criticism to the proposed activity.[26,30] Fluorescence correlation spectroscopy (FCS) showed a shift in the diffusion of **1-1** once combined with wild-type p53, indicating an interaction between the triad and the protein.[26] In contrast, heteronuclear single quantum coherence (HSQC) spectroscopy strongly suggested that there is no significant binding between **1-1** and p53 to prevent HDM2 binding.[30] In addition to targeting wild-type p53, **1-1** showed antitumor activity in tumor cells with mutant p53, making it a dual targeting molecule of both wild-type and mutant p53.[31] This activity was in part rationalized by claiming that mutated p53 undergoes a conformational change when **1-1** binds, thus restoring transcriptional activity. CRISPR-Cas9

based target validation techniques were used to compare the response of lung and colorectal cancer to the treatment with either nutlin or **1-1**.[32] They found that the activity of nutlin was strictly dependent on wild-type p53, whereas, **1-1** correlated with induction of DNA-damage and cells that were resistant to treatment with **1-1** were also resistant to cisplatin, a DNA crosslinking compound.

In 2011, Spitzer and co-workers looked at **1-1** as a potential DNA minor groove binder.[33] While the compound was a match in the computational model for a minor groove binder, testing with Dickerson-Drew dodecamer yielded disappointing results. Nonetheless, **1-1** was shown in previous studies to interact covalently with DNA. Studies conducted by the NCI with [^{14}C] labeled molecules suggested the formation of DNA-DNA and DNA-protein crosslinks, with the latter being more common.[15,34] Interestingly, the extent of crosslink formation correlates to the cancer cell line response in the NCI-60 assay where the most sensitive cell line A498 formed the most crosslinks. The observation that **1-1** does not crosslink purified DNA or proteins provided further support that the compound may be a prodrug and the identification of an active metabolite may provide important insight into the crosslink formation.[34]

Metabolic studies using gas chromatography-mass spectrometry (GC-MS) showed a 14 amu gain in mass of the bis-TMS protected derivative of **1-1** after incubation in dog liver S9 fractions.[35] Oxidation of one of the terminal alcohols of **1-1** to carboxylic acid **1-6** was suggested (Scheme 1). Addition of NADH significantly hindered metabolism, supporting an oxidative transformation. Another validation of oxidative transformation of the terminal hydroxymethyl groups came in a study by Fraaije and co-workers that showed quadruple oxidation of [5-(hydroxymethyl)furan-2-yl]methanol (**1-7**) by FAD-dependent 5-hydroxymethylfurfural oxidase to the dicarboxylic acid **1-8** (Scheme 1).[36] They also noted that the carbinol group is oxidized

significantly faster than the carbaldehyde derivative. They attributed the difference in oxidation to the necessity of hydrating aldehydes to diols before oxidation to the carboxylic acid. This observation is consistent with the phenotypic screening of related heterocyclic triads that showed the aldehyde derivatives of **1-1** to be less active.[14] Further studies with cell homogenates localized metabolism to cytosolic fractions of the cell and, to a much smaller extent, the nuclear and mitochondrial fractions.[35] P450 enzymes are not believed to have a significant impact on **1-1** despite their known metabolic activity on five membered heterocycles.[16a] While this is unexpected, there is precedence in many marketed drugs of mono- and di-substituted five-membered heterocycles, particularly thiophenes, that are not prone to P450 mediated bioactivation.[16b]

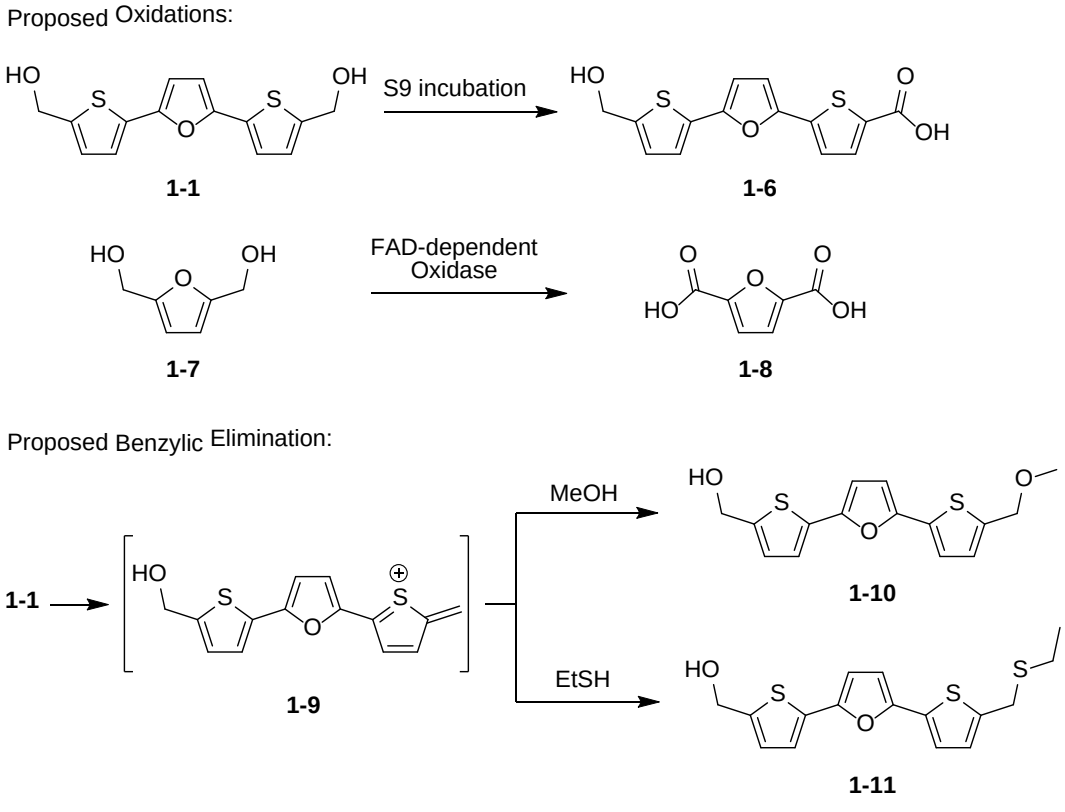

Scheme 1. Potential metabolites of **1-1**.

In addition to oxidation, it was noted that the terminal alcohol groups in **1-1** undergo benzylic elimination to produce **1-9** which contains a 2-(*exo*-methylene) on a terminal thiophene ring (Scheme 1).[35] The electrophilicity of the exocyclic double bond was demonstrated with the nucleophilic attack of methanol and ethanethiol, resulting in methyl ether **1-10** and ethyl thioether **1-11**, respectively. We believe this elimination may be responsible for the observed high-resolution mass spectrometry (HRMS) with the compound mass minus 17 amu, corresponding to elimination of a hydroxyl group (see Section 3.2 for specific examples). In a biological environment, the *exo*-methylene moiety may be attacked by a nucleophilic residue from DNA or protein resulting in a covalent bond. This is one possibility for the reported crosslinking.

In addition to DNA and p53, other direct or indirect targets have been suggested for **1-1**. These targets include N-myc,[31c] Chk2,[37] HIF-1α,[38] JNK/SAPK and p38,[39] SULT1A1,[40] and TrxR1.[41] The wide range of targets suggests that **1-1** is likely a non-specific protein binder. The broad activity highlights the challenge of preclinical target identification especially when measuring downstream phenotypic readouts such as cellular growth inhibition or p53-mediated apoptosis.[42]

1.1.4 Preclinical Development of NSC 652287

Even though the biological target of **1-1** is not confirmed, the triad underwent considerable development as a preclinical candidate for the treatment RCC.[43] The compound was highly efficacious in A498 xenograft studies in mice where tumor growth was greatly suppressed, as compared to the control group, with an excellent therapeutic index (see Figure 18 in the Appendix). Some mice were tumor free at the end of the study. Unfortunately, progression

of **1-1** into clinical trials was halted due to unacceptable pulmonary toxicity in more advanced mammals, dogs and monkeys. The dose-limiting toxicity occurred well below the *in vivo* efficacious dose in mice. Thus, there is an interest in designing analogs of **1-1** that address the toxicity concerns, but maintain or increase potency, and allow progression into clinical trials.

Phenotypic assays can be useful predictors of how a drug's preclinical evaluation translates into clinical performance.[44] For example, the NCI-60 panel consists of human-derived tumor cells, and designed compounds that have tissue specific activity (i.e. are potent against renal cells but inactive against lung cells) may help to overcome the undesired pulmonary toxicity of **1-1**. Therefore, we hypothesize that improving the cell-selectivity of **1-1** in the phenotypic assay by new analog designs may lead to a better therapeutic agent.

1.1.5 Analog Design and Rationale

Since the biological mechanism of action of these compounds is not well understood, target-oriented analog designs are not possible. Rather, the design was focused on the chemical structure and properties of the heterocyclic triads. Analogs for *in vivo* testing were prioritized based on the information gained from the NCI-60 assay, namely potency and cell-selectivity towards A498 cells.

A survey of compounds previously tested in the NCI-60 provided dozens of hits with structures related to **1-1**.[45] This information provided us with an initial structure-activity relationship (SAR) study to assist with the analog design (Figure 4). Our observation for the core, highlighted as zone 1, was that triads (3 rings) had better potency and selectivity profiles than diads (2 rings) or tetrads (4 rings). Compounds with two or more thiophene or selenophene rings showed very high and broad cytotoxicity across the 60 cell lines. While high potency is

desirable, the lack of selectivity was a cause for concern. For zone 2, the primary alcohol resulted in more desirable activity profiles than amines, carbonyls, carboxylates, and ethers. More specifically, two primary alcohols, one on each end of the molecule, outperformed analogs with one alcohol moiety. Therefore, from these observations, we decided to leave zone 2 unchanged, and focus our attention on zone 1.

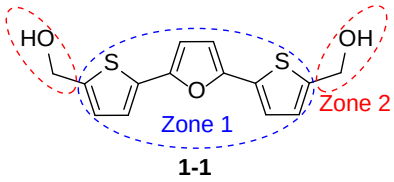

1-1

Figure 4. The highlighted zones reflect the focus of the SAR of **1-1** based on compounds screened in the NCI-60.

1.2 RESULTS AND DISCUSSION

1.2.1 Synthesis of Heterocyclic Triads

Heterocyclic triads such as **1-1** were previously synthesized by a lengthy stepwise approach featuring Suzuki-Miyaura[22d] or Stille cross-couplings[46] of halogenated heterocycles or by construction of the central ring via a Paal-Knorr condensation of substituted 1,4-diketones (Scheme 2).[22c,23,47] The terminal alcohols were, in many cases, accessed by formylation of the terminally unsubstituted α-heterocyclic triads.[23,47] We envisaged a more direct and efficient access to symmetrical triads by palladium catalyzed tandem cross-coupling of readily accessible di-halogenated heterocycles, followed by a reduction of the resulting aldehyde or ester to the

desired alcohol. This method provided a uniform route for a variety of analogs with high step economy from commercially available starting materials.[48]

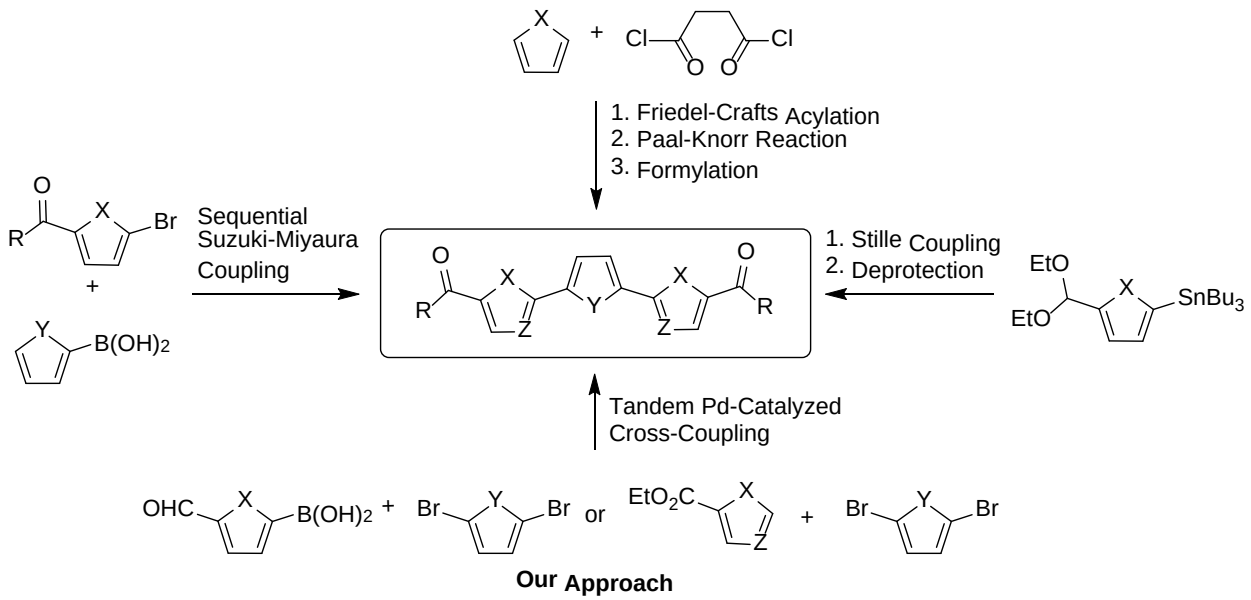

Scheme 2. Various approaches towards five-membered heterocyclic triads.

The Suzuki-Miyaura cross-coupling was utilized to form triads of five-membered heterocycles containing one heteroatom (Schemes 3 – 5).[48] Several Pd(0)/ligand combinations were screened and the combination $Pd_2(dba)_3$ and tri-*tert*-butylphosphine provided the best cross-coupling yield under microwave irradiation.[49] Other ligands such as JohnPhos,[50] triisopropyl phosphine, and tricyclohexylphosphine gave yields below 25% of **1-14a**. Mono-coupling was attempted by using an excess of halide **1-12a** with the ligand XPhos;[51] however, bis-coupled **1-14a** was the major product. In comparison, $Pd(PPh_3)_4$ with tetra-*N*-butylammonium bromide as an additive gave a mixture of mono-coupled (major) and bis-coupled (minor) products.[52]

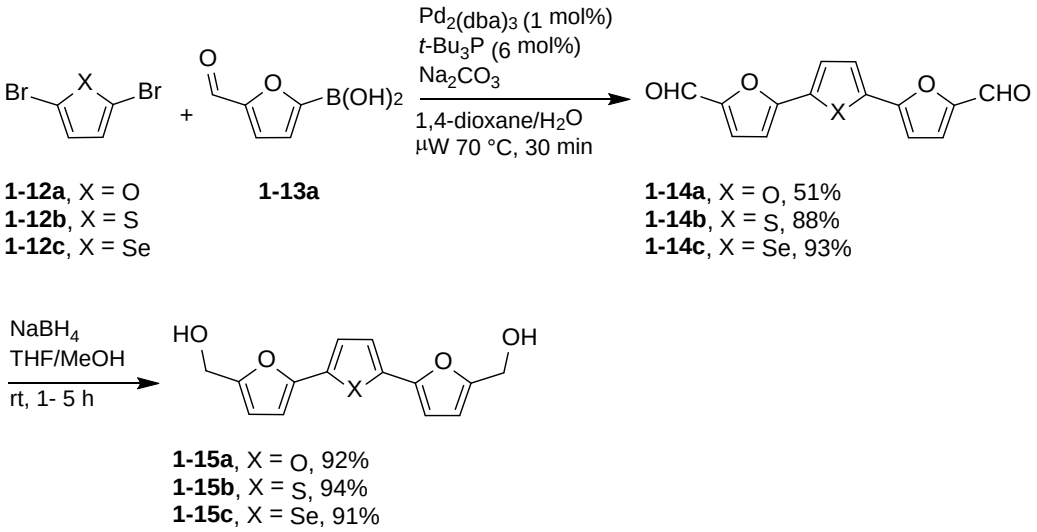

Scheme 3. Tandem Suzuki-Miyaura cross-coupling of 2,5-dibrominated furan, thiophene, and selenophene followed by reduction to diols.[48]

Commercially available boronic acid **1-13a** was coupled with readily accessible dibrominated heterocycles **1-12a–f** (Schemes 3 and 4).[48] Bis-coupling at the 2,5-positions of dibrominated furan **1-12a**, thiophene **1-12b**, and selenophene **1-12c** was achieved in good to excellent yields (Scheme 3). Interestingly, coupling products **1-14b** and **1-14c** were observed as yellow precipitates in the reaction mixture at room temperature immediately after addition of all reaction components, and when left stirring overnight at room temperature, aldehyde **1-14b** was obtained in >70% yield. While the reaction proceeds at room temperature, microwave conditions greatly expedited reaction completion without signs of decomposition. Finally, reduction of the aldehydes **1-14a–c** with $NaBH_4$ furnished the alcohols **1-15a–c** in excellent yields. These reactions were successfully scaled-up to multi-gram scale for producing quantities sufficient for *in vivo* studies (Section 1.2.5).

Similarly, regioisomeric analogs with 3,4- and 2,4-substitutions on the central heterocycle were obtained by bis-coupling of **1-13a** to 3,4-dibromothiophene (**1-14d**), 2,5-dimethyl-3,4-dibromothiophene (**1-14e**), and 2,4-dibromothiophene (**1-14f**) (Scheme 4).[48] Due to the lower

reactivity at C(3) of thiophene,[53] we increased the catalyst loadings and equivalents of boronic acid **1-13a** to facilitate conversion of **1-12d–f** to the bis-coupled products **1-14d–f** in moderate to excellent yields. Subsequent $NaBH_4$ reduction furnished the diols **1-15d–f** in excellent yields. Proton nuclear magnetic resonance (NMR) analysis of analog **1-15d** revealed decomposition in the form of additional aromatic and nonaromatic peaks upon mild heating to *ca.* 50 °C, presumably due to the high reactivity of the unsubstituted C(2) and C(5) on the central electron-rich thiophene ring. This observation signals a potential instability of the 3,4-substituted analogs.

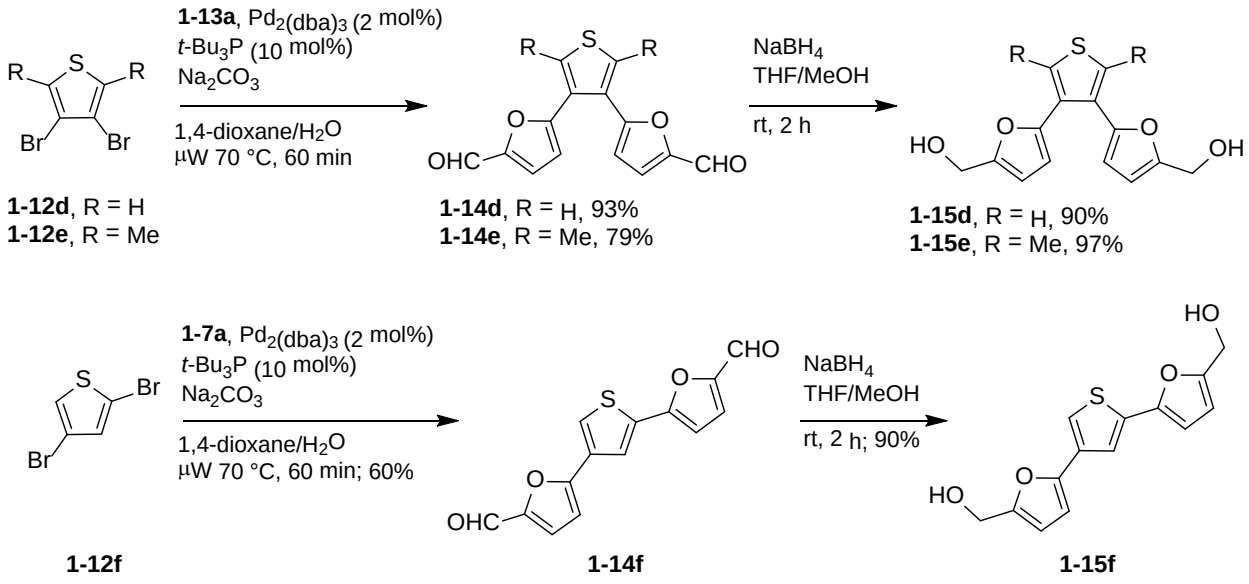

Scheme 4. Tandem Suzuki-Miyaura cross-coupling of 3,4- and 2,4-dibrominated thiophene followed by reduction to diols.[48]

The symmetrical analogs were rapidly constructed by bis cross-coupling of dihalogenated heterocycles. Even though selective mono-coupling of the 5-position of 2,3,5-tribromothiophene has been previously demonstrated,[54] it was difficult to prevent bis-coupling on the 2,5-dibromothiophene and a mixture of products was obtained. Therefore, desymmetrized analog **1-15g** was constructed in a complementary stepwise approach, using the optimized Suzuki-Miyaura conditions (Scheme 5).[48] Commercially available halide **1-12g** and boronic acid **1-13b**

were coupled, and the resulting product was subsequently brominated with *N*-bromosuccinimide and benzoyl peroxide[55] to yield **1-16** in 61% over the two steps. Aryl bromide **1-16** and boronic acid **1-13a** were coupled to yield **1-14g** in 78% yield, and reduction of the aldehyde functional groups with $NaBH_4$ provided diol **1-15g** in 90% yield.

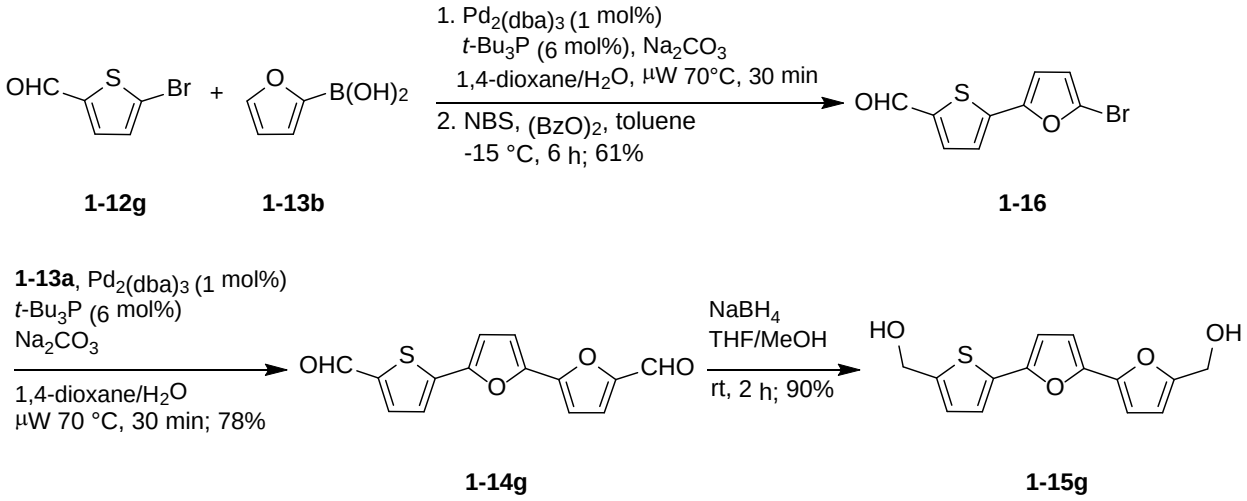

Scheme 5. Sequential Suzuki-Miyaura cross-couplings for the synthesis of desymmetrized analog **1-15g**.[48]

Since bromo-furans are highly unstable upon storage, we opted for the lengthier stepwise approach to synthesize **1-1** (Scheme 6). The synthesis of a tetrad analog was also attempted, using a similar route, featuring four thiophene rings all substituted in the 2,5-postions, but the solubility of this analog in organic and aqueous solvents was highly limited. It is therefore highly unlikely that this compound would perform well in bioassays.

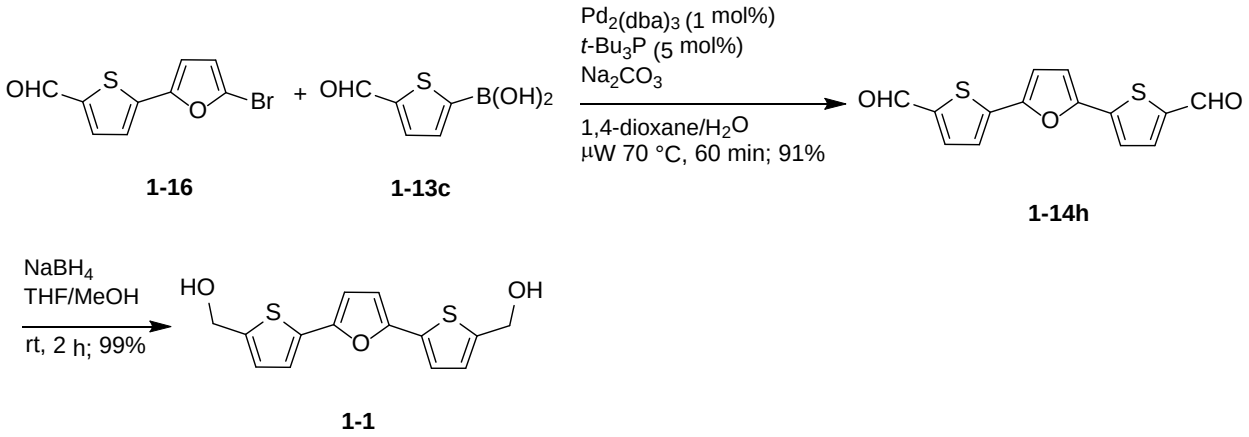

Scheme 6. Synthesis of NSC 652287 (**1-1**).

With diols **1-15a–g** in hand, we sought to diversify the analog library by incorporating an oxazole into the scaffold, ideally through a similar bis cross-coupling method (Scheme 7).[48] Ethyl 2-iodo-4-oxazole carboxylate (**1-17**) and the organozinc iodide **1-18** were prepared in order to attempt Suzuki and Negishi cross-couplings, respectively. These methods yielded only trace amounts of the desired bis coupled product **1-19a**.

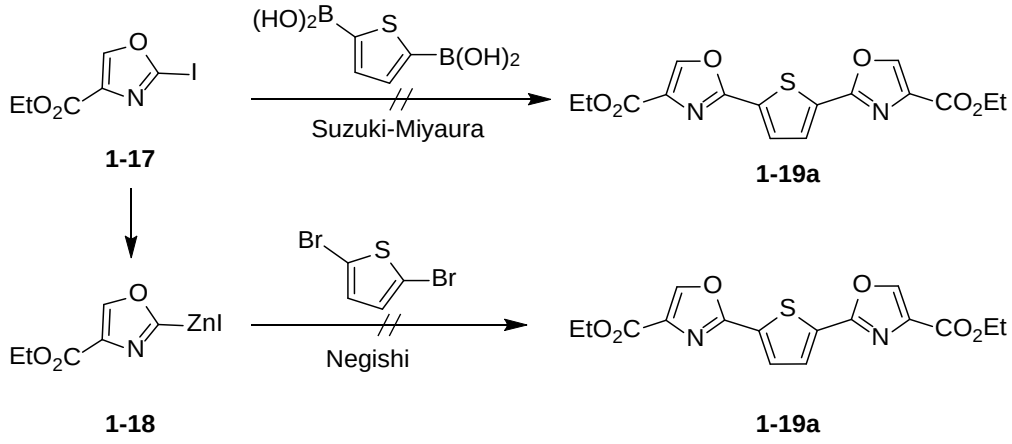

Scheme 7. Attempted cross-couplings on functionalized oxazoles.

The challenge of functionalizing and coupling oxazoles[56] was circumvented by expanding on a direct regioselective arylation strategy via C-H activation of commercially

available oxazole ester **1-20**. The Hoarau group reported the selective arylation of either the C(2) and C(5) positions of **1-20** using palladium catalysis.[57] The electron-withdrawing nature of the ester was reported to be important for the reactivity of the oxazole, particularly for the activation and deprotonation of C(2)-H.[58] Our attempts to couple the carbinol and aldehyde derivatives of **1-20** under the same conditions were unsuccessful. However, **1-20** underwent a C(2) selective dual C-H activation/cross-coupling with **1-12b–c** using Hoarau's conditions to furnish esters **1-19a–b** in good yields (Scheme 8).[48] Additionally, the position of the ester on the oxazole ring influences reactivity. When we attempted the coupling with ethyl-5-oxazole carboxylate under identical conditions, only 5% of the bis coupled product was isolated, reinforcing the need for electron withdrawing group at C(4). With **1-19a–b**, we extended the Hoarau methodology by applying a dihalogenated coupling partner and performing a tandem cross-coupling. Finally, $LiAlH_4$ reduction of the ester functionality provided access to the desired alcohols **1-21a–b** in good yields.

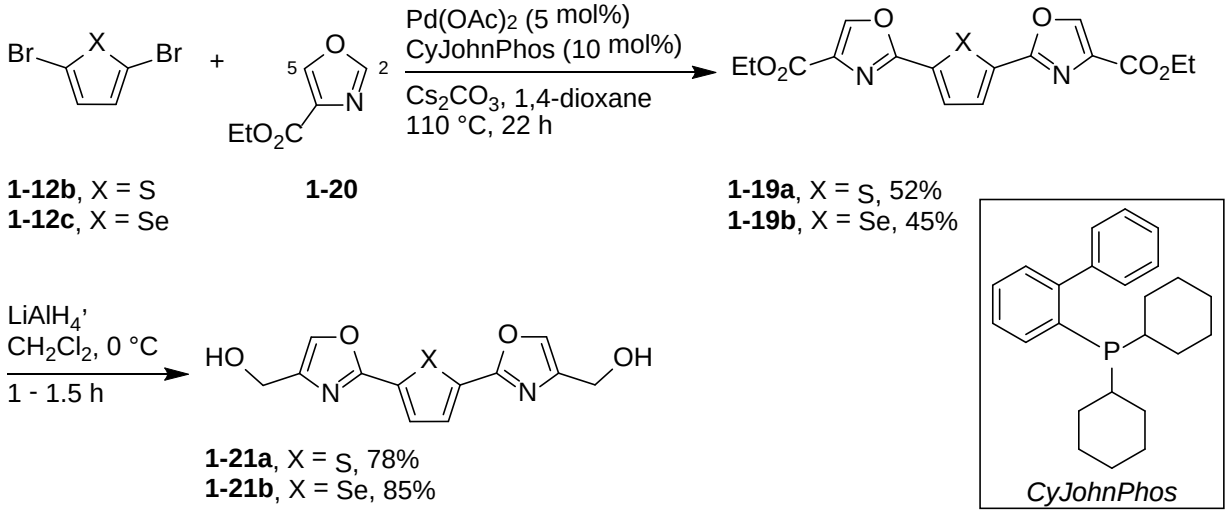

Scheme 8. Sequential Pd-catalyzed C-H bond activation/cross coupling of oxazoles with dibromothiophene and dibromoselenophene followed by reduction to diol.[48]

The central ring was further diversified by the incorporation of a triazole (Scheme 9). The reaction sequence began with the Fischer esterification of brominated furoic acid **1-22** with concentrated sulfuric acid in ethanol to yield ester **1-23** in 93%. Sonogashira coupling and subsequent TMS deprotection yielded alkyne **1-24** in 65% yield over two steps.[59] *In situ* formation of aryl azide on **1-23** followed by copper(I)-catalyzed azide/alkyne cycloaddition (CuAAC) with **1-24** gave 1,4-substituted 1,2,3-triazole **1-25** in 62% yield.[60] $LiAlH_4$ reduction gave access to diol **1-26** in 83%.

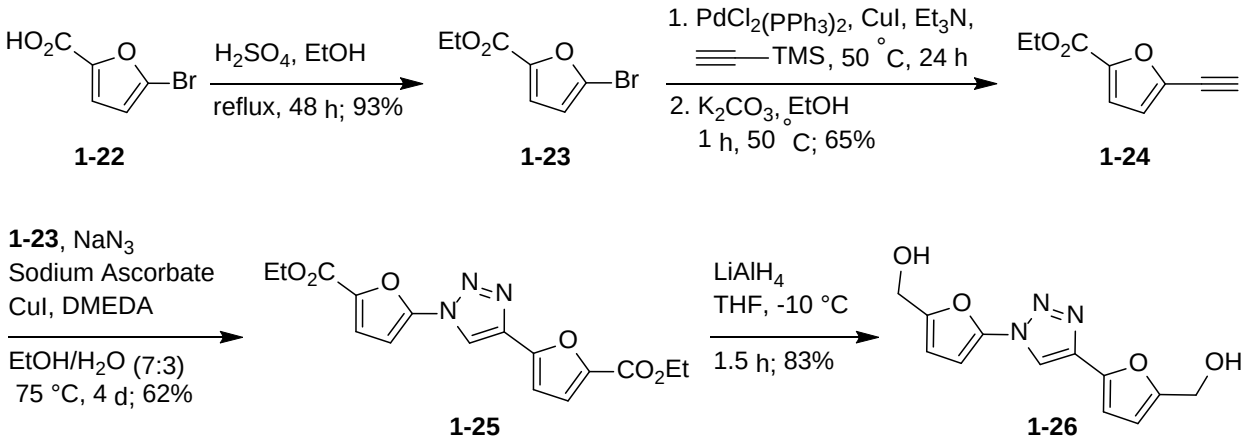

Scheme 9. Synthesis of 1,4-substituted 1,2,3-triazole by Cu-catalyzed azide-alkyne cycloaddition followed by reduction of ester groups to alcohols.

1.2.2 NCI-60 Cell Assay

Diols **1-15a–g**, **1-21a–b**, **1-26** and aldehyde **1-14c** were evaluated in the NCI-60 cell panel for anticancer activity. With the exception of triazole-containing analog **1-26** and oxazole-containing analogs **1-21a–b**, which provided no significant cell growth inhibition at 10 μM concentration, the heterocyclic triads were active and, in general, more selective towards the renal cell line A498 over other cell lines (Table 1).

NSC 652287 (**1-1**) showed a GI_{50} of about 15 nM with a hyperactive profile (Table 1, see the Appendix for the complete cell panel profiles of **1-1**, **1-15b**, **1-15c**, and **1-15f**). Replacing the terminal thiophenes in **1-1** with terminal furans in analogs **1-15a–c** resulted in a ten-fold reduction in potency but higher cell-selectivity. Aldehyde **1-14c** was nearly a hundred-fold less active than **1-1** and ten-fold less active than the reduced selenophene analog **1-15c**. Interestingly, analog **1-15g**, the sequence isomer of **1-15b**, placed a thiophene ring on one terminal end with a furan as the central ring and resulted in the same potency as **1-1**, also with low selectivity. Changing the triad geometry by altering the substitution positions on the central ring in **1-15d–e** retained the same potency and low selectivity as **1-1** and **1-15g** despite having terminal furans. However, the 2,4-substituted analog **1-15f** was equipotent to **1-1** but with the highest cell-selectivity of all analogs.

Table 1. Growth inhibition in renal (A498), lung (NCI-H226), kidney (CAKI-1), and breast (MDA-MB-468, MCF7) cancer cell lines in the NCI-60 cell assay.

entry	compd/NSC no.	GI_{50}[a] (μM)	GI_{50}[b] (μM)	Selectivity towards A498[c]
1	**1-1**, 652287	0.012 (CAKI-1)	0.015 (A498)	Low
2	**1-15a**, 672348	0.18 (A498)	0.58 (NCI-H226)	High
3	**1-15b**, 773097	0.13 (A498)	0.17 (MDA-MB-468)	High
4	**1-14c**, 773393	0.30 ± 6.1 (A498)	6.3 (MCF7)	High
5	**1-15c**, 773392	0.17 (A498)	0.22 (MDA-MB-468)	High
6	**1-15d**, 777422	0.015 (A498)	0.074 (MDA-MB-468)	Low
7	**1-15e**, 778301	0.016 (MDA-MB-468)	0.018 (A498)	Low
8	**1-15f**, 782846	0.020 (A498)	0.11 (MDA-MB-468)	High
9	**1-15g**, 777196	0.016 (A498)	0.018 (MDA-MB-468)	Low

[a]Most sensitive cell line; [b]Second most sensitive cell line; [c]High selectivity indicates that the GI_{50} values of ≤6 cell lines (≤10% of NCI-60 panel) were within 50x of the A498 GI_{50} value and low selectivity indicates that the GI_{50} values of >6 cell lines (>10% of NCI-60 panel) were within 50x of the A498 GI_{50} value.

The oxazole and triazole containing analogs were inactive, presumably due to the instability of the polyheteroatom-containing rings. The oxazole analog **1-21b** showed signs of decomposition by ^{1}H NMR when left overnight in a solution of deuterated dimethyl sulfoxide (DMSO). The aromatic peaks became complex and new nonaromatic peaks appeared, presumably from oxazole ring opening. Since the biological assay is conducted with the compounds dissolved in DMSO, it is likely that the analogs decomposed before testing. The triazole analog **1-26** formed reversible adducts with solvents, particularly methanol, as detected by ^{1}H NMR. We hypothesized the formation of the diazo/imine tautomer,[61] but no conclusive evidence of ring opening by infrared (IR) or ultraviolet (UV) spectroscopy was found.

1.2.3 Chemical and Metabolic Stability of Heterocyclic Triads

The SAR of **1-1** revealed that small changes in the triad structure can have significant impact on the potency and cell-selectivity in the NCI-60 assay. For example, analogs **1-15b** and **1-15g** only differ in the sequence of the heterocycles; **1-15b** has a central thiophene and **1-15g** has a terminal thiophene. Interestingly, the high potency but poor selectivity of **1-15g** resembles the profile of **1-1** whereas **1-15b** is less potent but more selective. This observation suggests that the sulfur atom in the terminal rings may play a role in the observed bioactivity. However, analog **1-15f** was equipotent to **1-1** and does not feature a terminal thiophene. Instead, **1-15f** differs from the less potent **1-15b** by the geometry of the substitution on the central ring. To gain a greater insight into the causes for the influence of the 2,4-geometry of **1-15f** and the 2,5-geometry of **1-1** and **1-15b** on activity, we studied the chemical stability of these triads.

We noticed considerable differences in the color of the three triads when dissolved in DMSO. Triad **1-1** formed a very bright yellow-green and slightly fluorescent solution. The

solution of analog **1-15b** in DMSO was also bright yellow, but **1-15f** was only pale yellow and formed a clear solution. These observations were supported by UV-Vis spectroscopy, since **1-1** and **1-15b** absorbed at higher wavelengths than **1-15f** (Table 2). The dialdehyde derivatives of the triads, **1-14f** and **1-14h** had an even higher absorption wavelength as would be expected with the added conjugation of the carbonyl groups. Triads **1-1** and **1-15b** are fully conjugated across the three rings, whereas **1-15f** has a cross-conjugation that prevents direct electron flow across all three rings (Figure 5). HOMO-LUMO gaps were calculated and showed that the gap in **1-15f** is *ca.* 10 kcal/mol greater than the gaps in the 2-5-substituted triads.

Table 2. Ultra-violet/visible light spectroscopy of heterocyclic triads in MeOH.

entry	Compound	λ_{max} (nm)
1	**1-1**	358.5, 264.5
2	**1-14h**	409.0, 291.0
3	**1-15b**	357.0, 245.0
4	**1-15f**	281.5
5	**1-14f**	330.5, 217.0

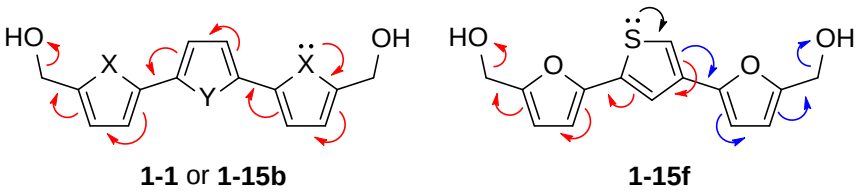

1-1 or **1-15b** **1-15f**

HOMO-LUMO Gap: **1-1,** 52.3 kcal/mol
1-15b, 51.6 kcal/mol
1-15f, 61.4 kcal/mol

Figure 5. The 2,5-substituted triads **1-1** and **1-15b** are fully conjugated across the three rings, whereas the 2,4-substituted triad **1-15f** has a cross-conjugation that prevents direct electron flow across all three rings. HOMO-LUMO gaps were computed from optimized structures at the DFT level of approximation using BIOVIA Materials DMol^3 (2016, v.16.1.0.21) using the PW91 functional.[62]

Given the known electron and optical properties of oligo-heterocycles[24,63] and the observed physical properties of the triads, we postulated that the triads may be prone to light mediated degradation. Solutions of **1-1** and **1-15f** in methanol were stirred at room temperature next to a 23 W compact fluorescent lamp (CFL) for 18 h. Analysis of the reaction mixtures revealed that **1-1** readily decomposed (<30% remaining) to form new oxidation products, whereas **1-15f** was significantly unchanged (>85% remaining) by ^{1}H NMR analysis.

For further studies, the solution stability of triads **1-1**, **1-15b**, and **1-15f** in DMSO-*d6*/D_2O at 1 mg/mL at room temperature under ambient light was monitored by ^{1}H NMR. Within one week, significant decomposition (>30%) of **1-1** and **1-15b** was observed. The degradation studies were scaled-up to 15 mg in 2 mL of DMSO-*d*6. Based on 1D and 2D NMR monitoring along with high resolution LC-MS, we assigned tentative structures for the main decomposition products of **1-1** (Figure 6). Both products arise from the oxidative ring opening of the central furan ring. Due to the symmetry of **1-27**, it was unclear whether the double bond was the *E*- or *Z*-isomer. The decomposition products of **1-15b** were not well defined, instead the NMR was very messy. In contrast, after two weeks in solution, **1-15f** remained >95% unchanged. To better understand the properties of these compounds in the biological assays, a mouse plasma stability assay was conducted (Table 3). Triads **1-1**, **1-15b**, and **1-15f** were mostly stable in plasma after incubation for 3 hours at 37 °C. A mouse liver microsome assay is planned for these compounds.

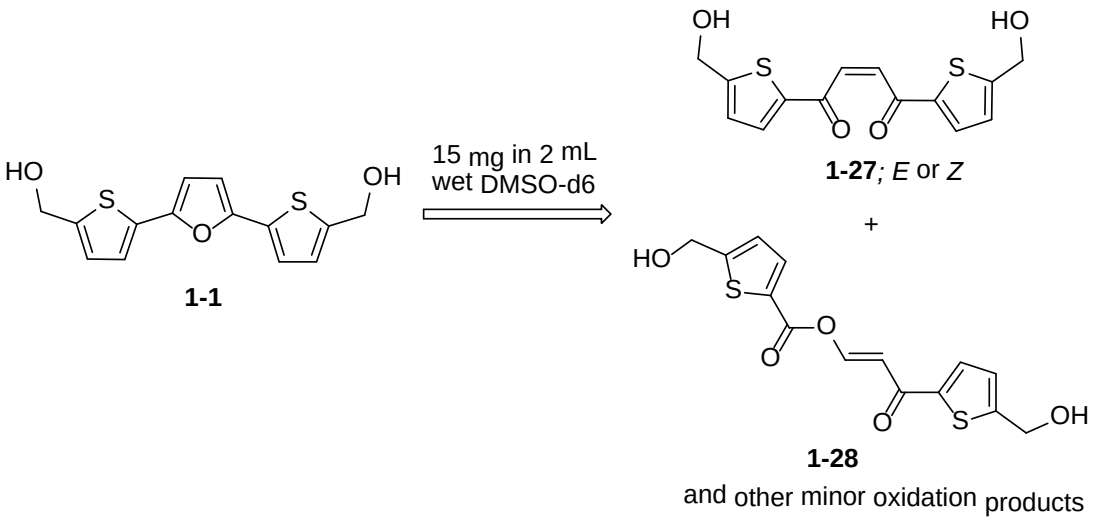

Figure 6. Tentative assignment of the major degradation products of **1-1**.

Table 3. Plasma stability assay with triads **1-1**, **1-15b**, and **1-15f**.

		amount remaining after specified incubation time with plasma[a]		
entry	compound	no incubation[b]	1.5 h	3 h
1	procaine (positive control)	100%	~ 5%	<5%
2	procainamide (negative control)	100%	>99%	>99%
3	**1-1**	100%	>90%	~90%
4	**1-15b**	100%	>99%	>95%
5	**1-15f**	100%	>99%	>99%

[a]Compounds were tested at 10 µM by incubating in a mixture of mouse plasma and PBS pH 7.4 (1:1) at 37 °C. The amount remaining was quantified using high-resolution LC/MS with an internal standard (caffeine); n = 3. [b]Samples were quenched immediately after addition of plasma.

The degradation products of **1-1** from our studies differ from the metabolites suggested in previous reports (Section 1.1.3, Scheme 1), and these compounds can potentially act as electrophilic Michael acceptors in a biological system. These observations highlight the complexity of studying the mechanism of action of this compound and may contribute to the fact

that a wide variety of biological targets have been postulated. Furthermore, it is remarkable that analog **1-15f** is equipotent to **1-1** without exhibiting similar degradation kinetics.

1.2.4 Thermal Shift Assay and Mass Spectrometry for Target Identification

Over the past three decades, a target-oriented approach to developing new anticancer therapeutic agents has emerged and resulted in many approved drugs.[64] When the biological target is known, the exact nature of the interaction between the target and the drug molecule can be studied in great detail with various analytical methods, such as NMR, X-ray crystallography, and cryo-electron microscopy.[65] In contrast, lead molecules identified via a phenotypic screen, such as the NCI-60 cell assay, are chosen without prior knowledge of the biological targets. Consequently, it is possible that each triad acts differently once it enters the cell. Based on the previous studies on **1-1** discussed in Section 1.1.3, we hypothesized that cell-active triads indeed bind to multiple biological targets.

Unknown drug interactions with biological targets can be identified by a variety of techniques such isotopic labeling, fluorescence imaging, affinity binding, and protein pull-down studies.[66] However, techniques that can avoid any cumbersome chemical modifications to the small molecules are more desirable since these modifications may impact the biological and physical properties of the test compounds. In recent years, the thermal shift assay has been developed where protein-ligand interactions can be surveyed in cell lysates and whole cells without the need of any chemical modification of the drug compounds.[67]

The non-covalent interaction of a ligand molecule with a protein is thermodynamically driven. In order for the interaction to be favorable in the cellular environment, the binding of the small molecule to a protein should alter its conformation into a more stable structure. The

thermal shift assay is predicated on the concept that applying heat to a pool of proteins will cause them to denature and precipitate out of solution (Figure 7). If a ligand molecule is bound to the protein, the extra stabilization gained from the binding will protect the protein from thermal denaturation and the protein will remain in solution at higher temperature. This increased stability can then be measured as an indication that the protein is a potential target for the small molecule.

Current methods use post-thermal assay labeling with tandem mass tags of analytes subjected to different temperatures followed by protein identification and quantification by LC-MS/MS[67b] or Western blots to compare the relative band intensity of drug-treated samples and the control.[67a] The Yates group at the University of Pittsburgh is developing a new approach that uses differential mass spectrometry to quantify the protein readouts following the thermal shift assay (Figure 7).[68] This approach is tag-free and does not require post-assay modification of the analyte mixtures. Proteins are separated by liquid chromatography and their identity determined by MS/MS techniques. The protein concentrations of the drug-treated group are compared to vehicle controls, under otherwise identical experimental conditions. Any proteins that undergo a statistically significant positive fold change in the treated samples (vs. control) are deemed of interest.

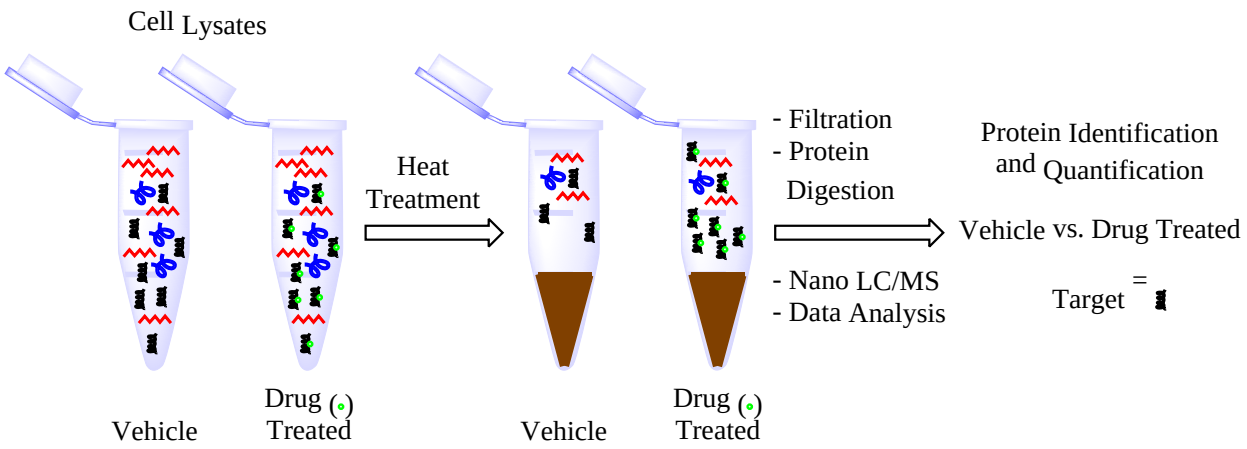

Figure 7. Overview of the thermal shift assay coupled with differential mass spectrometry.

The effects of compounds **1-1**, **1-15b**, and **1-15f** on the proteome were tested in the thermal shift assay on cell lysates derived from cultures of the renal cell carcinoma A498 (Figures 8-10).[68] After treatment with either a vehicle (DMSO) or test compound, the lysates were heated to 56 °C to induce thermal degradation of the proteins. The remaining soluble proteins in the supernatant were collected, purified, lysed with trypsin, and then measured by nanoLC-MS/MS. The analyte was identified by a computer platform (i.e. MaxQuant),[69] quantified, and subjected to rigorous statistical analysis to measure for significant positive fold change in protein amounts between the drug treated group and vehicle control (Figures 8-10). In Table 4, the top five protein hits are summarized for triads **1-1**, **1-15b**, and **1-15f** resulting from the thermal shift assay using the lysates from A498 cells. This preliminary data represents the potential that these compounds have many different targets. Most of these protein hits are typically located in the cytoplasm of cells. However, since this assay was conducted on cell lysates, the significance of the subcellular localization of the targeted proteins can't be determined. Currently, we are conducting the assay in whole cells to evaluate the localization of protein hits and to address the possibility of the triads being prodrugs. Furthermore, the thermal

assay is not conclusive on its own of the drug interaction with proteins. We will validate the protein hits with separate *in vitro* assays.

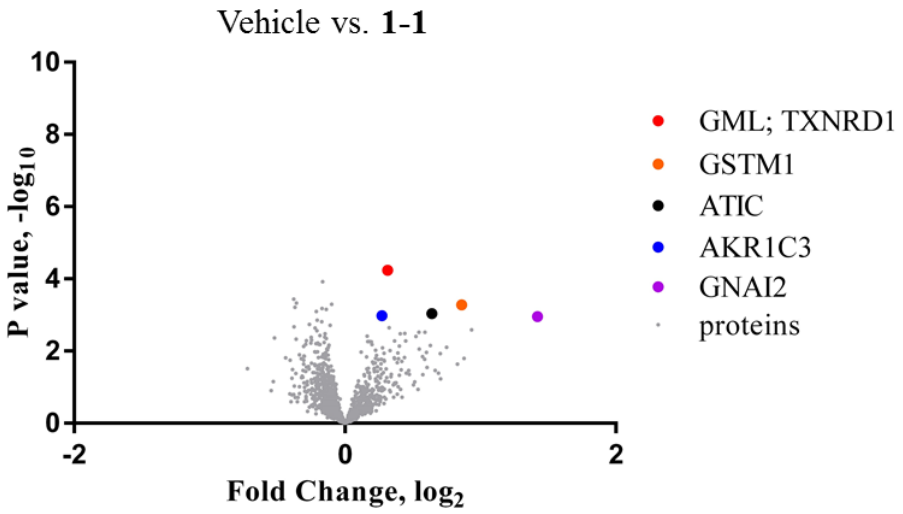

Figure 8. Comparison of the proteins remaining in solution between the vehicle control (DMSO) and **1-1** treated A498 cell lysate after the thermal shift assay at 56 °C.

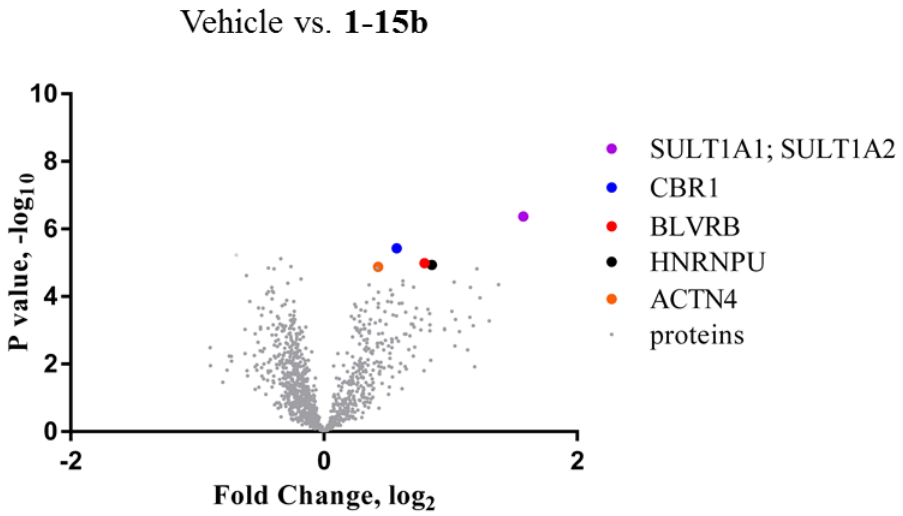

Figure 9. Comparison of the proteins remaining in solution between the vehicle control (DMSO) and **1-15b** treated A498 cell lysate after the thermal shift assay at 56 °C.

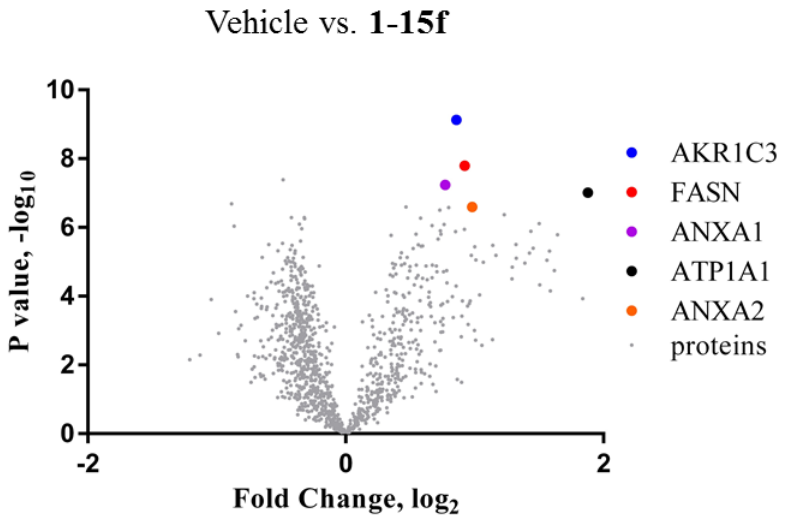

Figure 10. Comparison of the proteins remaining in solution between the vehicle control (DMSO) and **1-15f** treated A498 cell lysate after the thermal shift assay at 56 °C.

Table 4. Top five protein hits for compounds **1-1**, **1-15b**, and **1-15f** in the thermal shift assay using lysates derived from A498 cells.

protein rank	test compound: **1-1**	references
1a	Glycosyl-phosphatidylinositol-anchored molecule-like protein (GML)	70
1b	Thioredoxin reductase 1 (TXNRD1)[a]	41, 71
2	Glutathione S-transferase Mu 1 (GSTM1)	72
3	5-Aminoimidazole-4-carboxamide ribonucleotide formyltransferase/IMP cyclohydrolase (ATIC)	73
4	Aldo-keto reductase 1C3 (AKR1C3)	74
5	G-protein subunit alpha i2 (GNAI2)	75
protein rank	test compound: **1-15b**	references
1	Sulfotransferase 1A1 and 1A2 (SULT1A1; SULT1A2)[a]	40,76
2	Carbonyl reductase 1 (CBR1)	77
3	Heterogeneous nuclear ribonucleoprotein U (hnRNP U)	78
4	Biliverdin reductase B (BLVRB)	79
5	Actinin Alpha 4 (ACTN4)	80
protein rank	test compound: **1-15f**	references
1	AKR1C3	74
2	Fatty acid synthase (FASN)	81
3	Annexin A1 (ANXA1)	82
4	ATPase Na^+/K^+ transporting subunit alpha 1 (ATP1A1)	83
5	Annexin A2 (ANXA2)	82

[a]Previously linked to **1-1**.

1.2.5 A498 Xenograft Studies in Mice with 1-15b and 1-15c

The heterocyclic scaffold proved to be quite versatile in that changes to the identity and the geometry of the tricyclic core yielded significantly different activity and cell-selectivity in the NCI-60 assay. We saw different combinations of potency and degree of cell-selectivity,

however, the renal cell line A498 was a constant target for all active analogs (1.2.2). We are interested in determining whether increased cell-selectivity translates to a better therapeutic index in *in vivo* studies and a predictor of toxicity. All biological studies were conducted by the NCI Developmental Therapeutics Program.[45]

NSC 652287 (**1-1**) has been previously tested in A498 cell line xenograft models where it showed significant inhibition of tumor growth as compared to a DMSO-treated control group with treatment doses ranging from 27 mg/kg/dose to 90 mg/kg/dose (see Appendix; Figure 18). Two lead compounds **1-15b** and **1-15c** were selected as representatives of cell-selective activity profiles for testing in a A498 cell line mouse xenograft models to enable comparison with the broadly cytotoxic **1-1**. The complete NCI-60 cell panel for **1-1**, **1-15b**, and **1-15c** are shown in Appendix A (Figures 20 – 23). At the time, we were unaware of the NCI-60 activity of **1-15f**, therefore the compound was not selected for testing in animal models (although these tests are planned).

Triads **1-15b** and **1-15c** were tested in A498 xenograft studies in mice under identical experimental conditions (Figure 11 and Figure 12). The activity was compared to a control group consisting of 16 mice treated with only DMSO. There were 8 mice in each compound-treated group and the compounds were delivered by intraperitoneal injections (IP). Due to the lower potency seen in the cell assay, the treatment dose was set at 200 mg/kg/dose. Tumor size was monitored during treatment (days 17-21 post-implant) and for ca. 60 days after treatment delivery was completed.

Treatment with compound **1-15b** showed impressive inhibition of tumor growth that persisted for ca. 45 days post-treatment (Figure 11). The net mouse body weight showed a slight average decrease in weight, *ca.* 2-3 g, when the treatment was administered; however, the net

mouse body weight quickly recovered once the treatment was completed (Figure 12). Notably, there were no drug-related deaths and one mouse was found to be tumor free at the end of the study.

Results for the selenophene analog **1-15c** were nearly identical to the related thiophene analogue **1-15b** during treatment (Figure 11). Likewise, there were no drug-related deaths and significant tumor growth suppression was observed while treatment was administered. However, significant tumor growth resumed after ca. 20 days after treatment was completed, compared to ca. 45 days with compounds **1-1** and **1-15b**. Overall, while tumor growth was suppressed, near the end of the study it appeared that the positive effects of the treatment were diminishing and tumor growth was returning, highlighting the difficulty of treating RCC as discussed earlier (Section 1.1.1).

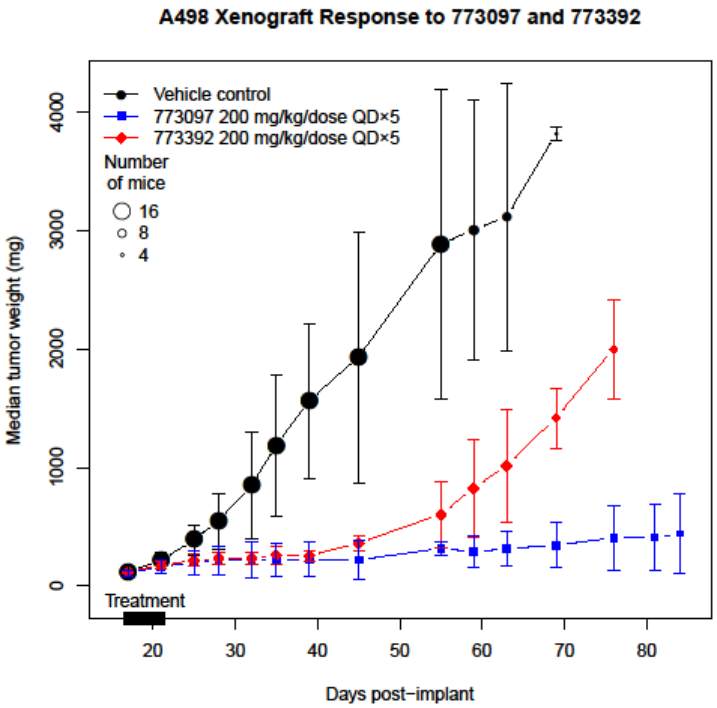

Figure 11. A498 cell line xenograft study with NSC 773097 (**1-15b**) and 773392 (**1-15c**). Mice were treated by intraperitoneal injections on days 17-21 post implant. Bars reflect ± scaled median absolute deviation.[45]

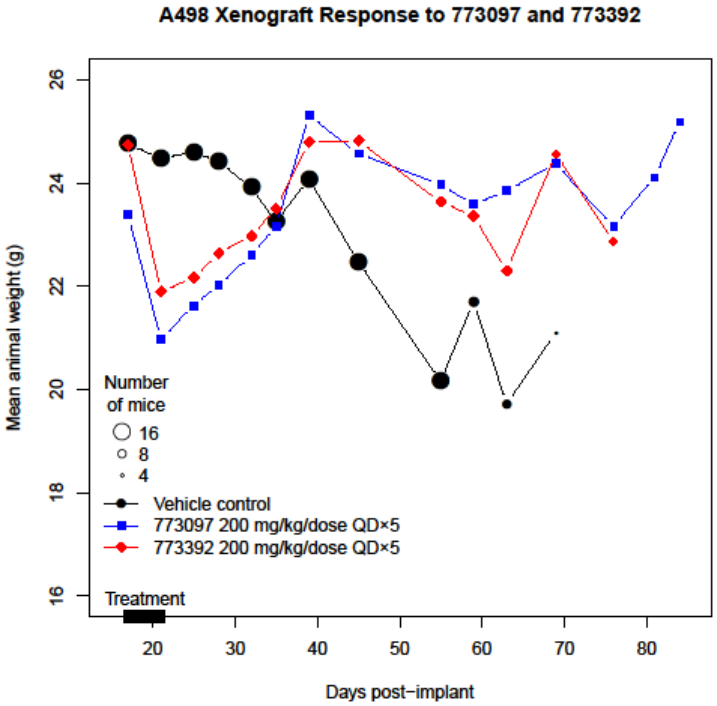

Figure 12. Mean mouse weight response to **1-15b** and **1-15c** in A498 xenograft study.[45]

A selective activity profile is often desired in therapeutic agents to minimize off-target effects and toxicity. The *in vivo* tumor suppression profiles for **1-15b** and **1-1** are nearly identical. The main difference is that the tested dose for **1-15b** is 2-7 times greater than for **1-1**. Since the efficacious dose is the main variable in determining the therapeutic index, more extensive toxicology studies are necessary in order to better judge the connection of the NCI-60 assay cell-selectivity and the therapeutic index.

1.3 CONCLUSION

Five-membered heterocycles offer a privileged scaffold in medicinal chemistry where wide variations in electron density, structural geometry, and physical properties are accessible. The broadly cytotoxic triad **1-1**, consisting of three linked five-membered heterocycles, showed significant tumor inhibition without any drug related deaths in A498 xenograft studies in mice over the course of 75 days. However, studies with **1-1** were halted after discovery of severe toxicity in larger mammals. The tunability of heterocycles enabled the design and synthesis of novel analogs of **1-1** with improved cell-selectivity in the NCI-60 assay.

Our studies have shown that the activity and potency of **1-1** can be altered by replacing the terminal thiophenes with furans and changing the substitution pattern on the central ring, thus limiting the accessibility of the sulfur atoms to oxidative pathways. Interestingly, changing the triad geometry from 2,5-substitution pattern on the central thiophene of **1-15b** to the 2,4-substitution in **1-15f** improved both the potency and cell-selectivity towards A498 in the NCI-60 assay. Moreover, chemical stability studies showed that the 2,4-substitution in **1-15f** made the compound more stable than the 2,5-substituted **1-15b** and **1-1**. Preliminary results from the

thermal shift assay for target identification revealed that the triads likely bind many biological targets. Xenograft studies with **1-15b** showed that a tumor growth suppression comparable to **1-1** can be achieved by using a higher drug dose. Xenograft studies with **1-15f** are planned for the near future. The initial assessment of these compounds shows promise for their use for the treatment of renal cell carcinoma. However, additional studies are needed to determine if high cell-selectivity in the NCI-60 assay translate to an improved therapeutic index.

2.0 SMALL MOLECULE MODULATORS OF PROTEIN TYROSINE PHOSPHATASE 4A3 ACTIVITY

2.1 INTRODUCTION

2.1.1 Protein Tyrosine Phosphatase 4A3 as a Therapeutic Target

The reversible phosphorylation of the hydroxylated moieties of serine, threonine, and tyrosine residues is a key mechanism for eukaryotic cells to regulate enzymatic activity, respond to extracellular signals, and manage various pathways.[84] This reversibility is managed by kinases and phosphatases, which create an essential balance of activating and deactivating substrates. The human genome encodes for >500 protein kinases and >125 protein phosphatases.[84b,85] Historically, targeted drug discovery efforts have been biased towards kinase inhibition resulting in >35 FDA-approved drugs.[86] Meanwhile, targeting phosphatases in drug discovery remains largely underdeveloped with no approved drugs. Recent studies have revealed that protein tyrosine phosphatases are highly regulated by protein oligomerization, redox control, and allosteric modulation allowing for specific control of cellular signaling pathways.[87] When these pathways are associated with human diseases, targeting phosphates provides an opportunity for novel discoveries of selective inhibitors and expansion of current therapeutic options.[86a,88]

Protein tyrosine phosphatases 4A (PTP4A), formerly known as phosphatases of regenerating liver (PRL), have garnered interest in recent years as anticancer targets. There are a number of comprehensive reviews detailing the validation of PTP4A as biomarkers and therapeutic targets in cancer.[89] Three proteins in this family have been identified: PTP4A1, PTP4A2, and PTP4A3. From this family of phosphatases, PTP4A3 is of particular interest as it has a higher rate of overexpression in cancer cells than other phosphatases, including PTP4A1 and PTP4A2. Comparison of gene expression profiles in colon cancers which metastasized to the liver showed that, among 144 upregulated genes, only PTP4A3 was overexpressed in all the colon cancer metastases studied.[90] Additionally, PTP4A3 is also overexpressed in breast, lung, cervical, ovarian, and gastric cancers.[89c] PTP4A3 was validated as anticancer target *in vivo* where PTP4A3-deficient mice showed decreased clonogenicity and tumor-initiation ability without gross histological abnormalities in normal tissues.[91] Furthermore, there was decreased tumor driven angiogenesis, VEGF-dependent endothelial cell motility, and vascular permeability. Overall, PTP4A3 seems to play a larger role in tumor cells than in normal cells. Consequently, targeting PTP4A3 in cancer therapy may have limited untoward effects. Even though no endogenous substrates of PTP4A3 have been confirmed, several downstream signaling pathways that may have serious implications in cancer have been linked to PTP4A3 including PI3K/AKT,[92] Rho GTPases,[93] ERK1/2,[94] and Src.[95] Therefore, the discovery of small molecule modulators of PTP4A3 will enable the detailed exploration of these pathways and elucidation of its biological role in cancer tumorigenesis and metastasis.[96]

2.1.2 Structural Features of the Protein Tyrosine Phosphatase 4A Family

There is considerable conservation of sequence identity between the PTP4A proteins (Figure 13). PTP4A1 shares 86% identity with PTP4A2 and 78% with PTP4A3.[89a] Notably, there is a conserved C49 residue (C46 in PTP4A2), WPD loop, and a $C(X)_5R$ active site phosphatase domain.

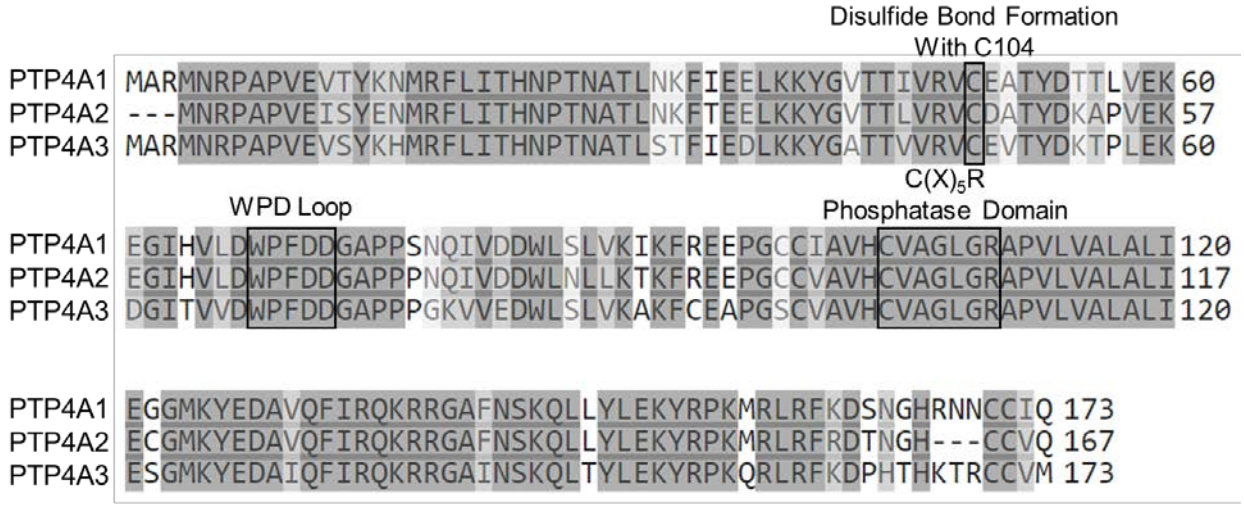

Figure 13. Aligned sequences of the PTP4A family showing sequence similarities including identical WDP loop and $C(X)_5R$ active site domain.[89]

Even though there is no X-ray crystal structure for these proteins with a native or drug substrate in the active site, the crystal structure of PTP4A1 and the NMR solution structure of PTP4A3 provide meaningful insights into the role of the conserved residues in the activity of the PTP4A family (Figure 14).[89a,89c,97] The C49 (C46 in PTP4A2) residue plays a key role in regulating the activity of PTP4A by forming a disulfide bond with C104 (C101 in PTP4A2) of the $C(X)_5R$ domain. Redox driven dissociation and formation of the disulfide bond can regulate the activity of the proteins by, respectively, opening and closing the active site pocket. The proline residue in the WPD loop can provide the shape and size flexibility needed to form the

other end of the active site. One proposed difference in the structures of PTP4A1 and PTP4A3 is the orientation of the C104 and R110 side chains. In PTP4A3, these chains seem to point away from the active site.[89a] Since the two structures do not have any substrates in the active site, any structural observation is somewhat uncertain.

The proposed mechanism of dephosphorylation involves the $C(X)_5R$ and WPD domains (Figure 14).[89c] R110 (R107 in PTP4A2) in the $C(X)_5R$ domain plays a role in stabilizing the incoming negative charge(s) on the substrate, positioning the substrate in the pocket, and increasing the electrophilicity of the phosphorous atom in the phosphate group. Then, C104 can act as a nucleophile and attack the phosphorous resulting in the release of a phenoxide anion that is quickly protonated by D72 of the WPD loop. The resulting thiophosphate group can then be hydrolyzed to regenerate the cysteine residue and a phosphate group.

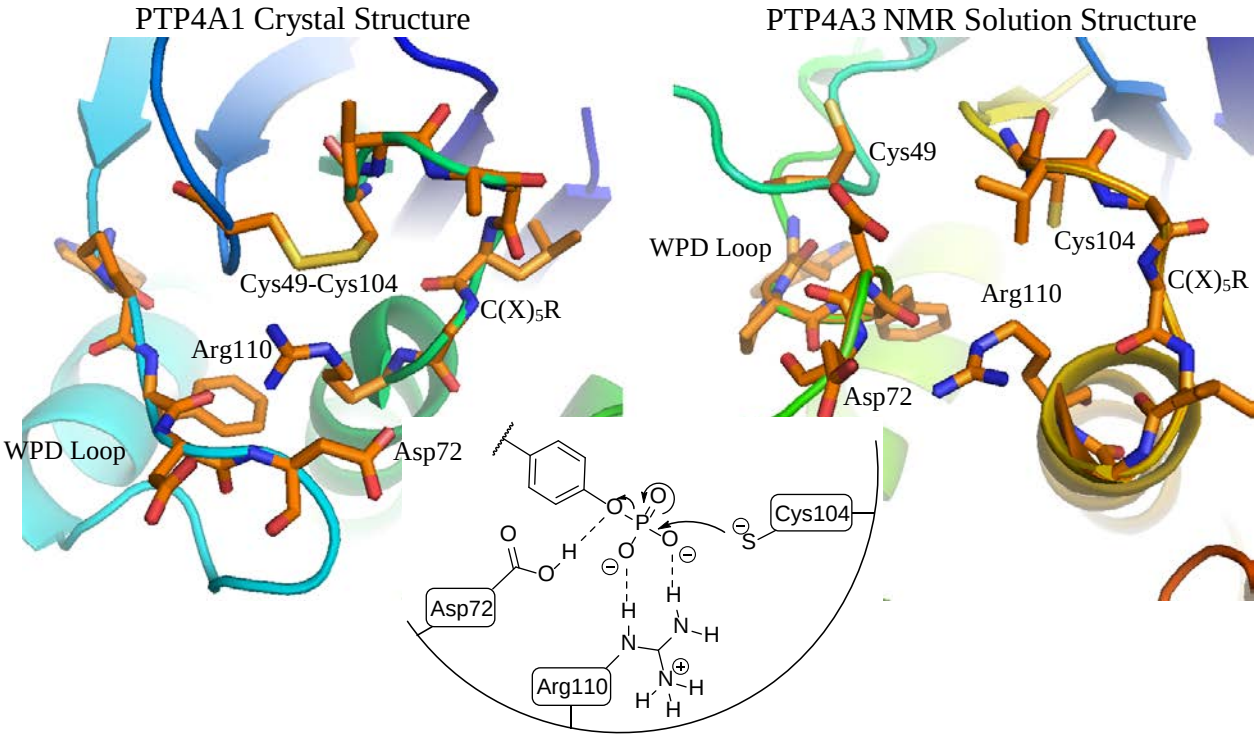

Figure 14. Active site of PTP4A family based on the crystal structure of PTP4A1 (top left, pdb code 1X24), NMR solution structure of PTP4A3 (top right, pdb code 2MBC), and proposed mechanism of dephosphorylating a tyrosine containing substrate (bottom).

The phenotypic importance of PTP4A3 is well known, but the exact details of its activity is not well understood. There are many known inhibitors of PTP4A that were highlighted in a recent review by Sharlow et al. (Figure 15).[89c] Even though some of these inhibitors are sub-micromolar active, they contain many undesired structural features such as quinones, phenols, and Michael acceptors. These structural liabilities may contribute to alkylative binding, which presents possible selectivity, irreversible inhibition, and toxicity issues *in vivo*. Ideally, a novel inhibitor should improve on the potency and selectivity of known inhibitors while eliminating the potential for nonspecific covalent interactions.

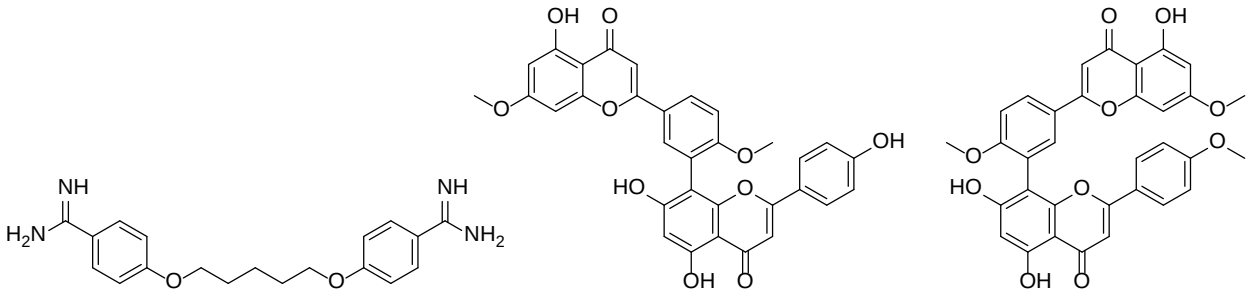

Pentamidine
PTP4A1: ~ 0.3 μM
PTP4A2: ~ 0.3 μM
PTP4A3: ~ 0.3 μM

Ginkgetin
PTP4A1: - μM
PTP4A2: - μM
PTP4A3: 26 μM

Sciadopitysin
PTP4A1: - μM
PTP4A2: - μM
PTP4A3: 46 μM

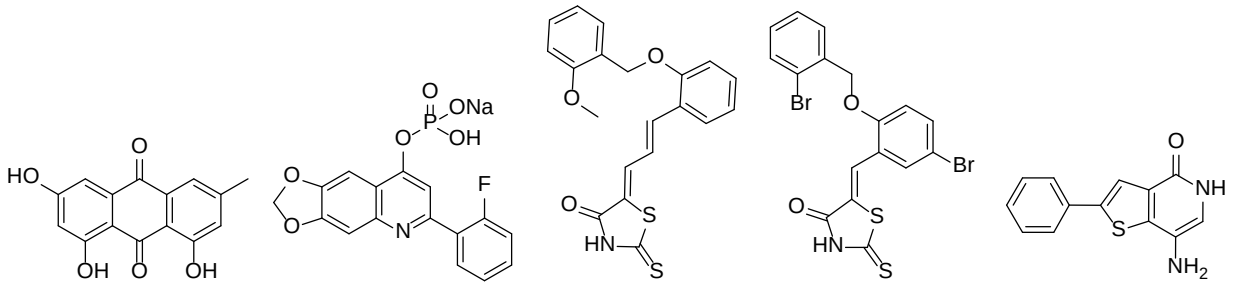

Emodin
PTP4A1: - μM
PTP4A2: - μM
PTP4A3: 3.5 μM

CHM-1-P-Na
PTP4A1: 0.68 μM
PTP4A2: 0.31 μM
PTP4A3: 4.9 μM

CG-707
PTP4A1: - μM
PTP4A2: - μM
PTP4A3: 0.8 μM

BR-1 (2-1)
PTP4A1: - μM
PTP4A2: - μM
PTP4A3: 0.9 μM

Thienopyridone (2-2)
PTP4A1: 0.17 μM
PTP4A2: 0.28 μM
PTP4A3: 0.13 μM

Figure 15. A selection of known PTP4A inhibitors with *in vitro* IC_{50} (μM).

Pentamidine is a pan inhibitor of PTP4A at submicromolar concentrations.[98] However, it, as well as structurally similar amidines, lacks specificity due to binding to DNA and RNA polynucleotides, likely through hydrogen bonding between the protonated terminal amidine functionalities and nucleotides in the minor groove.[99] Two naturally occurring bioflavonoids, ginkgetin and sciadopitysin, have double digit micromolar activity against PTP4A3.[100] The large molecular weight, multiple phenolic hydroxyl groups,[101] and Michael acceptors[102] cause concern for further development due to potential toxicity and irreversible binding. Emodin, likewise, suffers from quinone and polyphenolic features.[103] CHM-1-P-Na shows an interesting selectivity with 10-fold higher potency towards PTP4A1 and PTP4A2 over PTP4A3.[104] While this compound may be further optimized, PTP4A3 is a more attractive therapeutic target, as noted in section 2.1.1, therefore this selectivity is undesired. For CG-707 and BR-1 (**2-1**), there is an ongoing debate about the usefulness of rhodanines in medicinal chemistry.[105] Rhodanines are known to participate in an alkylation mechanism of action and aggregate in cells leading to disruption of cellular processes. Furthermore, CG-707 and **2-1** contain a potential Michael acceptor with an *exo*-methylene group. Nonetheless, these rhodanine-containing compounds provide attractive potency and a promising starting point for designing a new scaffold. Finally, thienopyridone **2-2** showed the best reported potency to date against PTP4A3. One drawback of this compound is the potential for hydroquinone/quinone type redox activity.

2.1.3 Analog design based on BR-1 and Thienopyridone

Small molecule modulators of protein activity can be highly useful tools in elucidating signaling pathways, protein substrates, and cellular responses.[88e,106] The modulator must be potent but also selective for the target protein. For the molecule design, we considered building

on the existing scaffolds of **2-1** and **2-2**. From a synthetic point of view, **2-1** was chosen over CG-707 because of simpler structural features. The orientation and extension of the aromatic rings that is provided by the additional alkene in CG-707 does not seem to contribute to activity.

High throughput screening of the Korean Chemical Bank identified the rhodanine scaffolds as potential inhibitors of PTP4A3.[107] After SAR studies, **2-1** was identified as a lead inhibitor.[107-108] PTP4A3 was confirmed as target of **2-1** by the recovery of phosphorylated ezrin and cytokeratin 8, putative substrates of PTP4A3.[108] Selectivity toward PTP4A3 was demonstrated against 10 other phosphatases. Additional studies showed the inhibition of migration and invasion activity of PTP4A3 overexpressing colon cancer cells (DLD-1 (PRL-3)) without exhibiting cytotoxicity or inhibiting proliferation.[108]

A hypothesis was offered for the mode by which **2-1** binds to the active site of PTP4A3.[107] It was suggested that the nitrogen in the rhodanine ring is deprotonated and the resulting negative charge is stabilized by the positive charge of the Arg residue in the active site. This observation was further supported when the *N*-methylated derivative of **2-1** showed no activity. However, this hypothesis does not consider the possibility of alkylative binding. It is possible that deprotonated **2-1** acts as a nucleophile and forms an irreversible covalent bond with an electrophile. The alkylative mechanism is equally supported by the observation of no activity with the *N*-methylated **2-1**. It is also possible that the true mechanism of action may involve some balance of alkylative and non-alkylative activity. Further, SAR studies on **2-1** revealed that the thione in the rhodanine ring is essential for activity.[108] When the sulfur atom was replaced with an oxygen atom, the activity significantly decreased.

Thienopyridone **2-2** was the most potent known inhibitor at the time (IC_{50} PTP4A3 = 0.13 μM).[109] It was shown to be selective for the PTP4A family over 11 other phosphatases.

Significant inhibition of tumor cell anchorage-independent growth, induction of p130Cas cleavage, and apoptosis that is not related to increased levels of p53 were observed. The main concern with this compound is the potential for hydroquinone/quinone type redox activity resulting from the high electron density of the fused thiophene and aniline-like amino substituent on the pyridinone ring. Quinones and quinone-imines, derived from phenols and anilines, have been shown to be bioactivation metabolites responsible for many idiosyncratic drug toxicities in marketed drugs.[110]

2.2 RESULTS AND DISCUSSION

2.2.1 Synthesis of Thienopyridone 2-2

The synthesis of **2-2** was targeted since it was the most potent inhibitor known at the time and could be used as a control to validate our protein assays. The synthetic route towards **2-2** has not been previously disclosed but the construction of the bicyclic thienopyridone scaffold via a tandem Curtius-rearrangement/cyclization is a well-known strategy and was used in our first approach towards **2-2** (Scheme 10).[111]

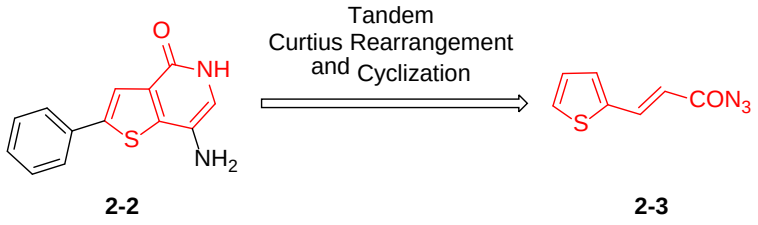

2-2 **2-3**

Scheme 10. Synthetic approach towards thienopyridone **2-2** using the tandem rearrangement and cyclization.

The route began with a Suzuki-Miyaura coupling of commercially available phenyl boronic acid and brominated thiophene **2-4** to yield aldehyde **2-5** in excellent yield (Scheme 11).[111d] Regioselective bromination under acidic conditions yielded **2-6** in 98%. The regioselectivity arises from the unfavorable formation of the carbocation alpha to the aldehyde during the electrophilic aromatic substitution. The halogen offers a synthetic handle for structural diversification. Knoevenagel condensation onto aldehyde **2-6** produced the carboxylic acid **2-7** in a high yield. The three step sequence of acid chloride formation and azidation, followed by heating for the tandem Curtius rearrangement/cyclization gave pyridone **2-9** only in poor yield (ca. 23% over 3 steps) with limited scalability (<50 mg). We were interested in whether the high temperature was needed for the Curtius rearrangement or for the cyclization (Scheme 12). The reaction is thought to require three transformations: (1) the acyl azide rearranges to the vinyl isocyanate; (2) the *trans* double bond must isomerize prior to cyclization (it is possible that the isomerization occurs before the rearrangement); and (3) intramolecular cyclization. We thought that it may be more practical and safer to form the isocyanate at lower temperatures and then heat to 250 °C for the cyclization. However, all our attempts at low temperatures failed to produce any rearrangement products. Nonetheless, the synthesis of **2-2** was completed by nitration and then hydrogenation to yield the desired product in 9%.[112]

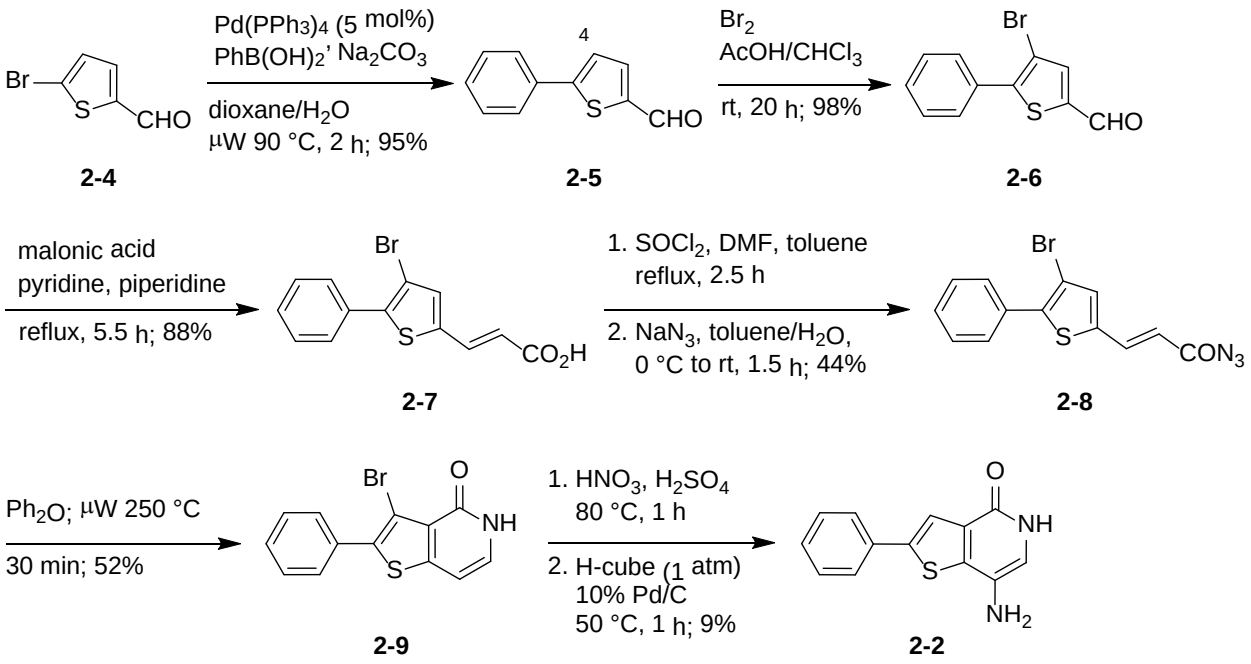

Scheme 11. Synthesis thienopyridone based on an established strategy.[111d]

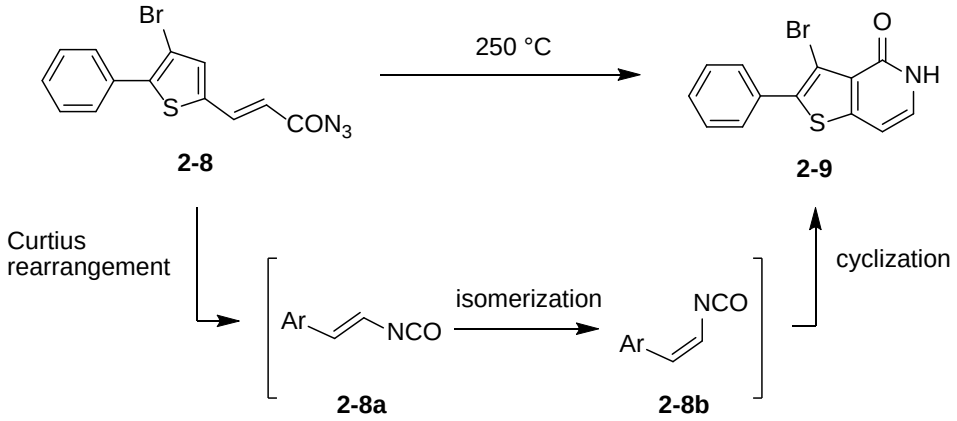

Scheme 12. The intramolecular cyclization of **2-8** to construct the bicyclic scaffold of **2-2** proceeds via a Curtius rearrangement, double bond isomerization, and cyclization.

Since we could not affect the rearrangement of the acyl azide at lower temperatures, we searched for an alternative precursor for the isocyanate. Previous reports indicate that isocyanates can also be accessed from the thermal decomposition of carbamates.[113] We modified the reaction sequence to include the formation of ethyl carbamate intermediate **2-11** (Scheme

13). With aldehyde **2-5** in hand, we carried out a Takai olefination to yield a 10:1 *E*/*Z* mixture of **2-10**.[114] Purification of the olefination product proved to be difficult since iodoform and vinyl iodide **2-10** have similar polarities. When **2-10** was used crude in the amination reaction, the iodoform seemed to react and the desired product was not obtained. To address this concern, we switched to the Stork-Wittig olefination with phosphonium salt **2-14** and aldehyde **2-5** to give vinyl iodide **2-10** in 52% as an *E*/*Z* isomeric mixture of 1:1.[115] The isomeric mixture is not a concern for the cyclization since under the high temperatures the olefin can isomerize. Amination attempts on purified **2-10** failed to cleanly yield vinyl carbamate **2-11**. The reactions generally yielded a complex mixture of compounds.

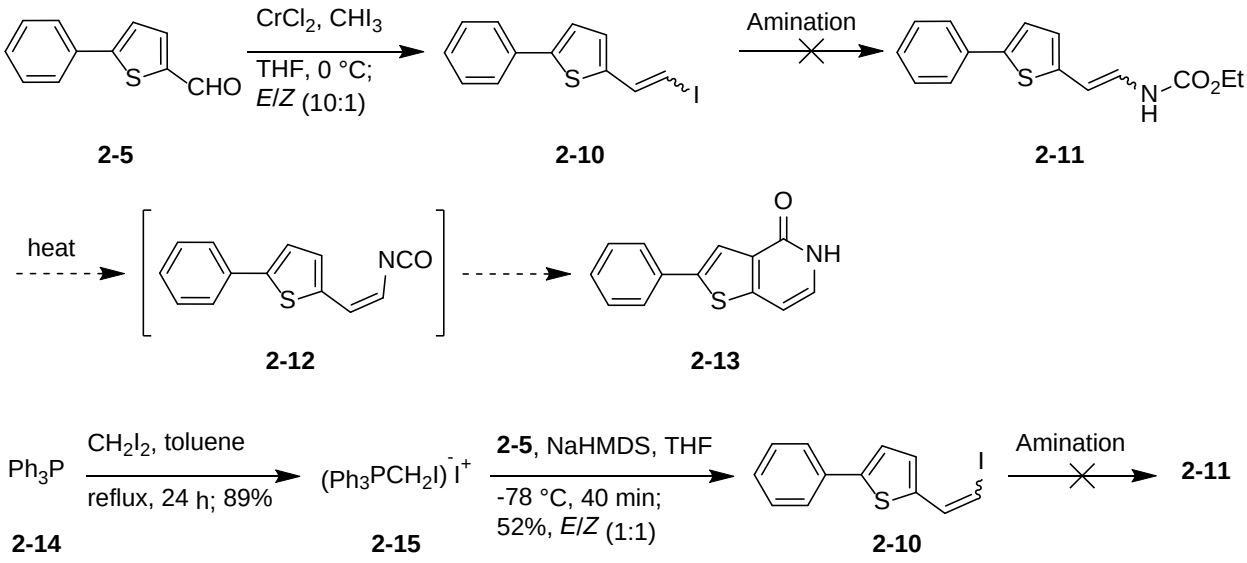

Scheme 13. Modified synthetic route towards **2-2** without the use of azides.

To overcome the bottleneck of synthesizing an isocyanate precursor, we decided to directly form the isocyanate via the primary amine **2-16** (Scheme 14).[111d] Additionally, not having a double bond in **2-16** obviated the need for the alkene isomerization at high temperatures. Reacting **2-16** with triphosgene formed the requisite isocyanate which underwent a Friedel-Crafts intramolecular cyclization with $FeCl_3$ acting as a Lewis acid to yield lactam **2-17**

in 71% over the two steps. The thiophene in **2-17** was brominated and then a Suzuki-Miyaura cross-coupling installed the phenyl ring followed by a DDQ mediated aromatization to yield thienopyridone **2-13**. Analogous to the first route, the synthesis was completed with a nitration and then hydrogenation to yield **2-2** in 19%. Overall, this route is more conducive to analog synthesis as it allows for late-stage variations of the phenyl ring and *N*-substitutions (Section 2.2.5).

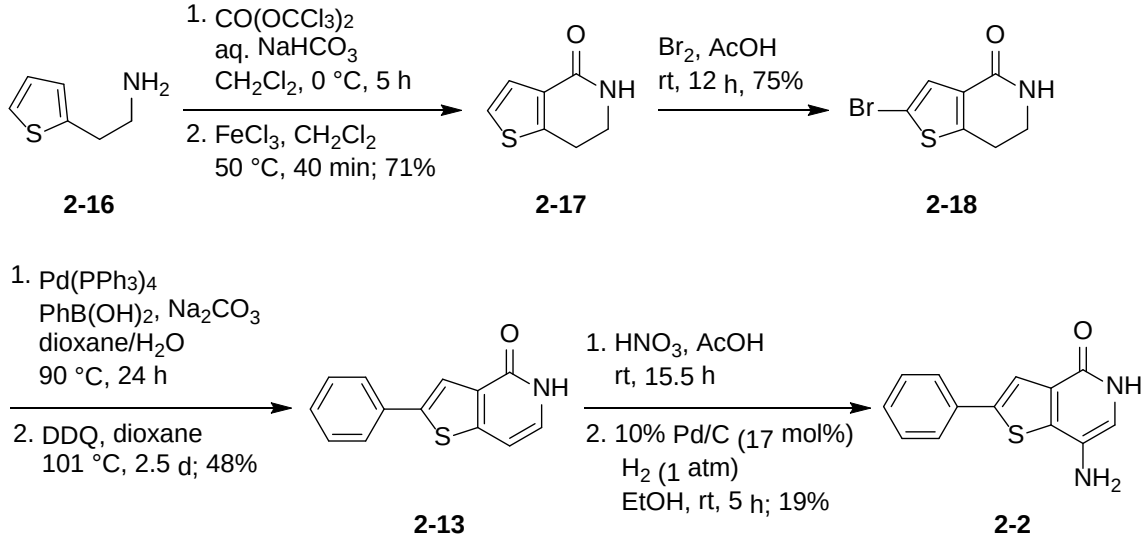

Scheme 14. Second-generation synthesis of thienopyridone **2-2**.[111d]

2.2.2 Design and Synthesis of a Hybrid Analog of 2-1 and 2-2

While the exact binding modes of BR-1 (**2-1**) and thienopyridone **2-2** are unknown, a structural overlay of the two structures showed structural similarities, suggesting some key interactions (Figure 16). Aligning the two carbonyl functionalities of **2-1** and **2-2** positions the phenyl groups in nearly identical spatial arrangements. The carbonyl groups can participate as hydrogen bond acceptors and the phenyl groups may be responsible for key hydrophobic interactions in the active site of PTP4A3. Switching the main heterocycle to a pyrimidine dione

scaffold in **2-19** provided a similar positioning of hydrogen bond donors and acceptors as the rhodanine ring, while also removing the amino group of thienopyridone and consequentially reducing the electron-density and potential for redox activity.

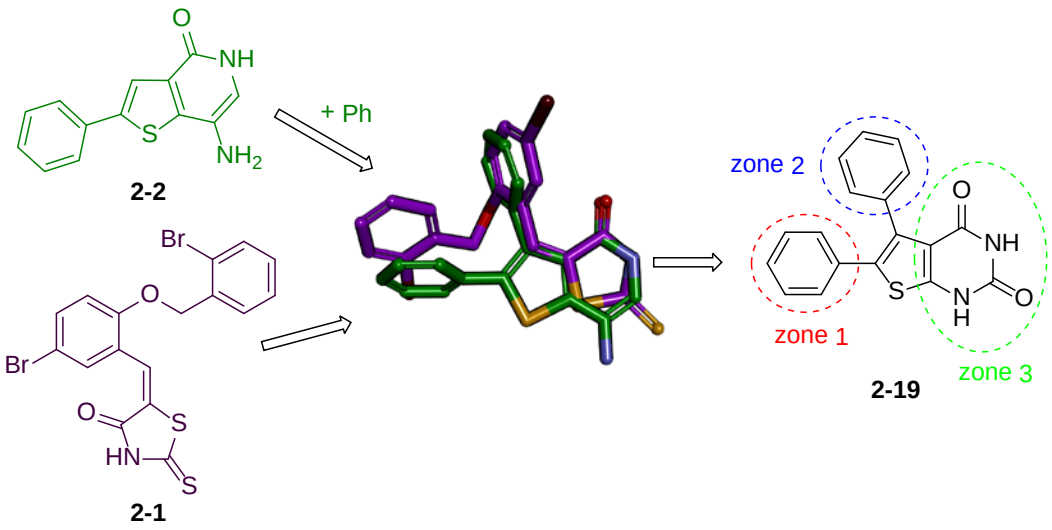

Figure 16. Overlay of BR-1 (**2-1**) and thienopyridone **2-2** for the design of the hybrid analog. The colored zones are planned areas of modification for SAR studies. 3D overlap modeled with Biovia Discovery Studio (v.16.1.0.15350).

SAR studies were focused on changes to zones 1–3 (Figure 16) to modulate physical properties and biological activity. The phenyl rings in zones 1 and 2 can be modified to improve the hydrophobic interactions and/or solubility of the analogs. For zone 3, the dione scaffold can modulated and a thioxo derivative is accessible by replacing one of the oxygen atoms with sulfur, similar to **2-1**.

For the hybrid analog, we envisaged constructing the amino thiophene core **2-21** via a Gewald reaction (Scheme 15).[116] The requisite aldehyde **2-20** for the Gewald reaction would also introduce the desired substitution for zone 1 in **2-19**. The pyrimidine dione ring **2-22** can be constructed by the addition of amino thiophene **2-21** to an isocyanate followed by base mediated cyclization and quenching with acid to establish zone 3. Subsequent bromination of the thienyl

pyrimidine dione **2-22** would allow for a late stage cross-coupling of **2-23** to introduce the desired substitution in zone 2 of **2-19**.

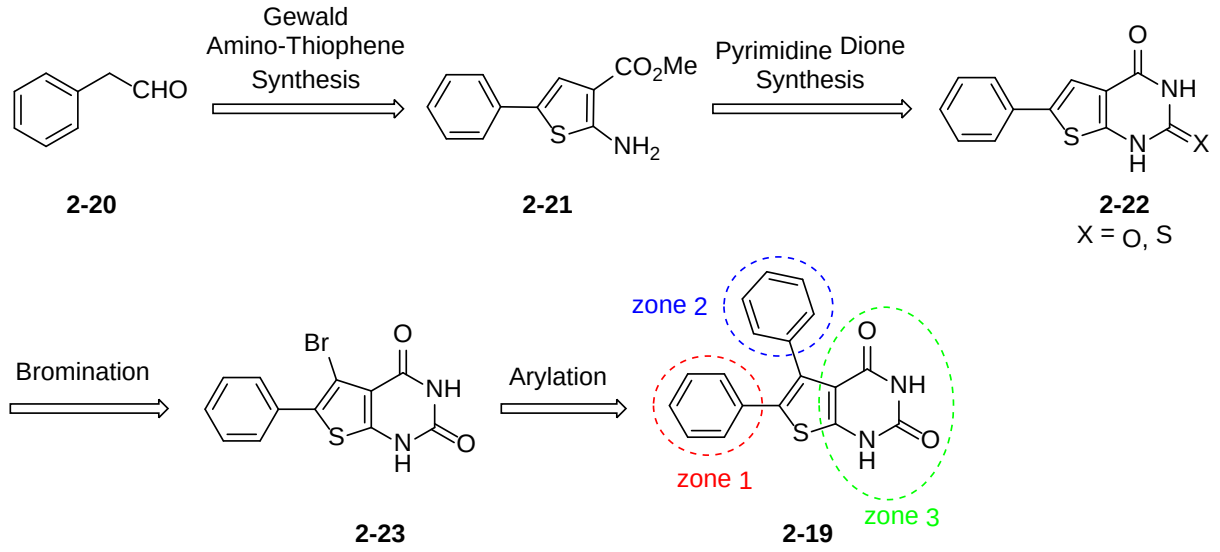

Scheme 15. Synthetic strategy towards pyrimidine dione scaffold of hybrid analog design.

Gewald thiophene synthesis with phenyl acetaldehyde (**2-20**) and methyl cyanoacetate (**2-24**) gave amino thiophene **2-21** in 90% (Scheme 16).[111d] Formation of the urea adduct on the amino group of **2-21** with chlorosulfonylisocyanate and then cyclization under basic conditions followed by quenching with acid gave the cyclized product **2-22** in 57%. Once the pyrimidine dione ring was formed, various bromination conditions failed to provide the desired brominated analog **2-23** and starting material was recovered. A directed lithiation/bromination also failed. The difficulty of brominating the thiophene may be attributed in part due to the electron-withdrawing nature of the fused pyrimidine dione ring as well as possible bromination of the nitrogen atoms. The thiophene ring in **2-22** is considerably deactivated with respect to electrophilic aromatic substitution. We thought that the precursor **2-21** may be a better candidate for bromination since the thiophene should be less deactivated.

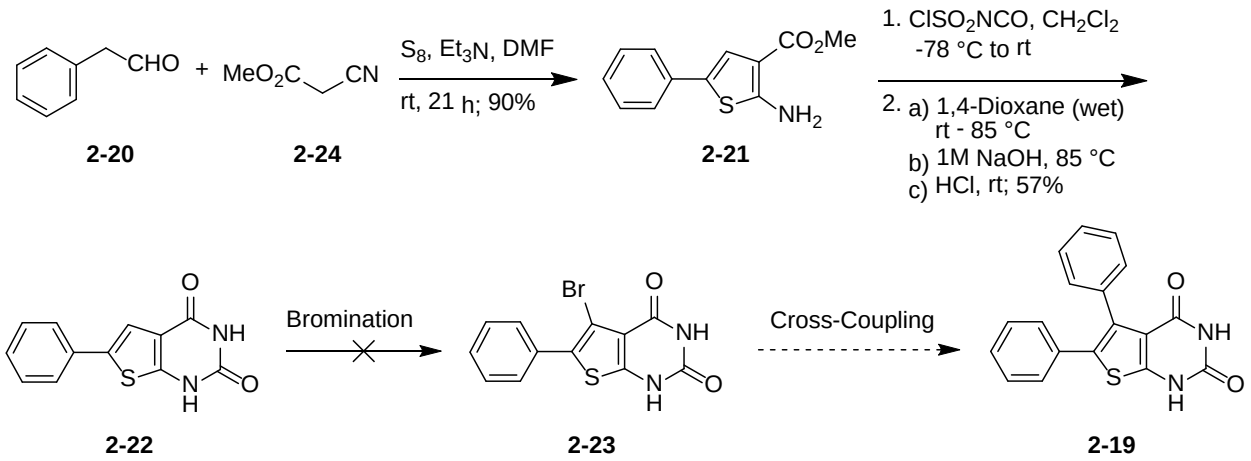

Scheme 16. Attempted synthesis of pyrimidine dione analog **2-19**.

Unfortunately, attempted bromination on **2-21**, with or without protecting the amino group, also failed. The thiophene ring was also sufficiently deactivated by the electron-withdrawing ester functional group and the Boc group when the amino functionality is protected. Under mild conditions, starting material was recovered. Using stronger brominating agents or heat resulted in either para bromination of the phenyl ring or decomposition of the thiophene ring. The lone pair of the amino group is not conjugated with the C(4) of thiophene, but instead would delocalize to the phenyl substituent. Thus, the para position on the benzene ring was more activate towards the electrophilic substitution. As result, we decided to modify the route to eliminate the need for bromination.

Deoxybenzoin (**2-25**) provides both the zone 1 and 2 substituents (Scheme 17). The ketone was not sufficiently reactive for a one-pot Gewald reaction. To address the lower reactivity, the Knoevenagel product with **2-24** was formed via Lewis acid activation of **2-25** followed by thiophene synthesis to yield **2-26** in 87% over two steps. The combination of morpholine and acetic acid aids in isomerizing the Knoevenagel condensation intermediate from **2-26int1** to **2-26int2**.[117] The cyano and the benzylic methylene groups in the condensation adduct need to be *syn* for the thiophene synthesis to proceed. Amino thiophene **2-26** can be

cyclized analogously to compound **2-22**. However, this compound was not pursued any further once the PTP4A3 assay revealed that this series of analogs to be inactive (Section 2.2.4).

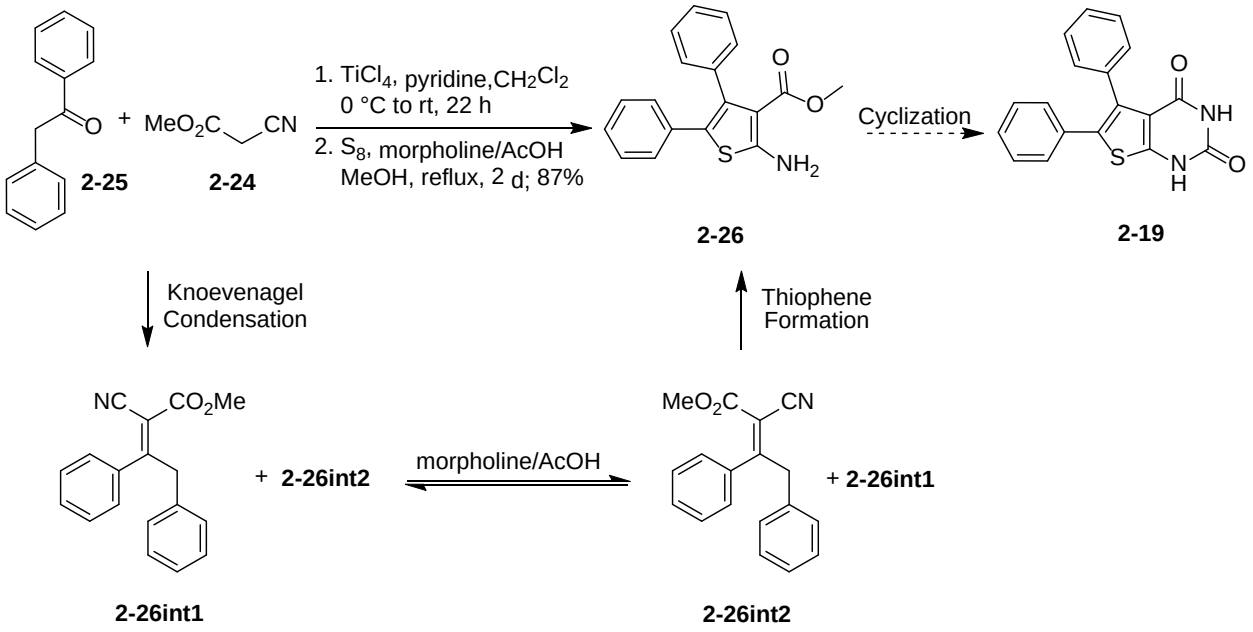

Scheme 17. Modified approach towards analog **2-19**.

In addition to the thieno pyrimidine dione core, we also synthesized analogs with a 2-thioxo thieno pyrimidin-4(1*H*)-one core to investigate the effect of the sulfur atom on bioactivity (Scheme 18).[111d] Amino thiophenes **2-21** and **2-27** were cyclized first by addition of acylated isothiocyanate to give intermediates **2-28** and **2-29** in modest yield, then base-mediated cyclization followed by acidic treatment yielded analogs **2-30** and **2-31** in 49% and 57% respectively.

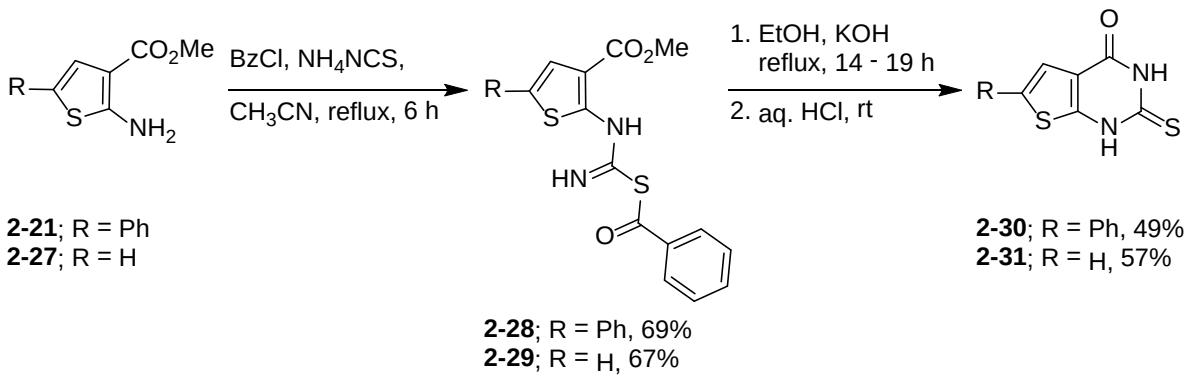

Scheme 18. Synthesis of analogs with the 2-thioxo thieno pyrimidin-4(1*H*)-one core.[111d]

2.2.3 Photooxygenation of Thienopyridone 2-2

The amino-thienopyridone in **2-2** is highly electron-rich and can be a potential redox-liability in a biological system.[110] In order to decrease the electron-density in the heterocyclic scaffold of **2-2**, we explored photooxygenation conditions for the possibility of oxidation by selectively introducing an oxygen atom. While currently underutilized, photooxygenation offers a useful synthetic strategy to generate novel structural motifs from electron-rich moieties.[118]

Recent reports demonstrated light-driven reactions in the absence of a photocatalyst or an additional photosensitizer. Instead, the reaction substrate itself acts a photosensitizer that is excited by light and drives reaction. *N*-heterocycles such as quinolinones and pyridones has been shown to be sensitive to visible light and upon excitation they can generate singlet oxygen.[119] Also, pyridones are known to trap singlet oxygen by a [4+2] cycloaddition to form pyridone endoperoxides.[120] Thienopyridone **2-2** is bicyclic like quinolinones and contains a pyridone ring. Additionally, the thiophene ring and amino substituent add high electron-density, therefore, we had reason to believe that **2-2** was prone to photo-excitation.

We monitored a solution of **2-2** in methanol under ambient laboratory light and we discovered the novel 7-iminothieno-[3,2-*c*]pyridine-4,6(5*H*,7*H*)-dione **2-32**, but the conversion

was incomplete with a significant amount of **2-2** left after 2 days stirring at room temperature (Table 5, entry 1).[111d] The photooxygenation under ambient light was also attempted in hexafluoroisopropanol (HFIP), but only a trace amount of **2-32** was observed (Table 5, entry 2). In order to accelerate the reaction, we placed a 23 W CFL at a distance of 15 cm away from the borosilicate reaction flask and observed complete conversion within 23 h and an isolated yield of 85% (Table 5, entry 3). This transformation was accomplished without the use of any catalysts or additives, and, due to its poor solubility in methanol, the isolation of **2-32** was achieved by a simple filtration of the reaction precipitate. The high yield is particularly noteworthy due to the potential for different oxidation pathways including oxidation of the thiophene ring and a ring-contraction rearrangement of the pyridone ring.[121] Compound **2-32** precipitated from the reaction mixture as an amorphous brown powder, but crystalline **2-32** was obtained by the slow evaporation of a solution in acetonitrile. The structure was confirmed by X-ray crystallography (Scheme 19). Larger scale synthesis required longer reaction times, presumably due to poor light penetration in the larger solvent volume (Table 5, entry 4). We are currently also exploring flow methods for this photochemical process.

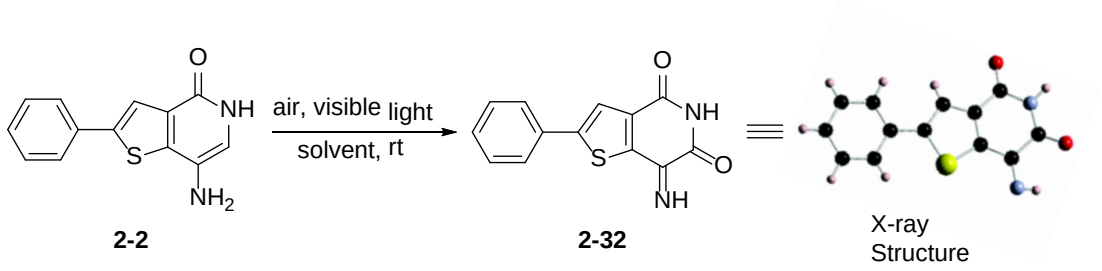

2-2 **2-32**

Scheme 19. Photooxygenation of **2-2**.[111d]

Table 5. Screening reaction conditions for the photooxygenation of **2-2** to **2-32**.[111d]

entry	solvent	reaction scale[a]	light source	conversion time[b] (isolated yield)
1	MeOH	<10 mg	ambient light	>2 d partial conversion
2	HFIP	<10 mg	ambient light	1 d trace conversion
3	MeOH	<10 mg	23 W CFL[c]	23 h (85%)
4	MeOH	32.5 mg	23 W CFL[c]	2.5 d (77%)

[a]Reaction concentration was 1-1.1 mg/mL; [b]Conversion was monitored by high resolution LC/MS for the disappearance of **2-2**; [c]Compact fluorescent lamp (CFL) at a distance of 15 cm.

To the best of our knowledge, the oxidized thiophene-containing scaffold has not previously been reported. Two literature studies of related imino-isoquinolinediones are shown in Scheme 20. While studying the synthesis of spiro heterocyclic compounds, the Otomasu group noted the spontaneous oxidation of **2-36** to **2-34** after the hydrogenation of the nitrosodione **2-36** to the amine. The Henry group was interested in the synthesis and fluorescence properties of 2-methyl-1-isoquinolones and found that 4-amino-2-methyl-1-isoquinolone (**2-33**), in contrast to analogous 5- or 7-amino derivatives, was converted *in situ* to pyridazine **2-35**. They postulated that the dimer resulted from the condensation of **2-33** and air oxidized **2-34**.

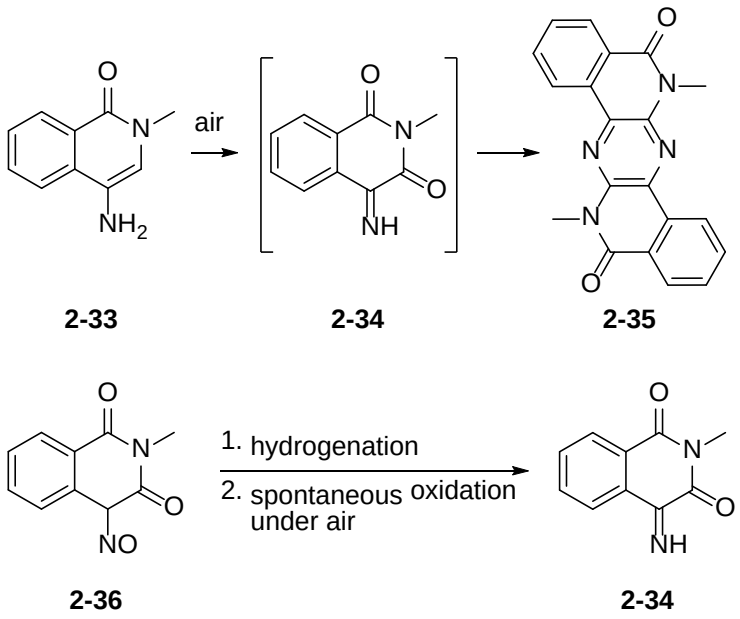

2-33 **2-34** **2-35**

2-36 **2-34**

Scheme 20. Previously reported spontaneous oxidations of aminoquinolines, analogous to the transformation of **2-2** to **2-32**.[122]

2.2.4 Biological Evaluation of Analogs

The biochemical activity of thienopyridone **2-2** and related analogs was evaluated in an *in vitro* assay with recombinant human PTP4A3, which was overexpressed in *E. coli* using His_6-tag fusion and then purified by a metal affinity column.[111d] The phosphatase activity was monitored using the artificial substrate 6,8-difluoro-4-methylumbelliferyl phosphate (DiFMUP) for 30 min at 25 °C in 40 mM Tris-HCl (pH 7.0), 2 mM EDTA, 4 mM DTT, and 75 mM NaCl buffer solution. The fluorescence was measured and used to calculate the percent inhibition relative to the maximal enzyme activity in the absence of an inhibitor and maximal inhibition in the presence of 2 mM Na_3VO_4 (Table 6). All biological evaluations were conducted by Kelley McQueeney, Dr. Elizabeth Sharlow, and Professor John S. Lazo at the University of Virginia (Charlottesville, VA).

Table 6. *In vitro* inhibition of PTP4A3 activity.[111d]

entry	compound	IC_{50} [μM ± S.D.][a]
1	**2-2**	0.132 ± 0.003
2	**2-13**	>80
3	**2-22**	>240
4	**2-30**	>100
5	**2-31**	>100
6	**2-32**	0.018 ± 0.014

[a]n = 3.

The inhibitory action of **2-2** was comparable to previously reported value (Table 6).[109] The desamino analog **2-13** was ineffective at concentrations up to 80 μM, highlighting the significance of the 7-amino substituent. The hybrid scaffold in **2-22**, **2-30**, and **2-31** showed no inhibitory activity and these analogs can serve as negative controls in future assays. Interestingly, the novel analog **2-32** was nearly 10x more potent than **2-2** with an IC_{50} of 18 nM, making this imino-pyridinedione the most potent inhibitor of PTP4A3.

Thienopyridone **2-2** and the oxidized analog **2-32** were screened against a limited panel of phosphatases, including members of the PTP4A family (Table 7).[111d] Compound **2-32** was *ca.* 3x more selective towards PTP4A3 *vs.* PTP4A1 and PTP4A2. Moreover, the compounds showed little to no inhibition of other phosphatases, PTP1B and PP2A, and was significantly less potent towards CDC25B. Since **2-2** readily oxidizes to **2-32** (Section 2.2.3), we were interested in whether the thienopyridone **2-2** was oxidized in the *in vitro* assay. We tested the stability of **2-2** in the assay mixture for 90 min in the presence or absence of DTT, and we did not detect by LC-MS any quantifiable spontaneous oxidation (>5%) of **2-2** to **2-32**.

Table 7. *In vitro* inhibition of the activity of a phosphatase panel by **2-2** and **2-32**.[111d]

		IC_{50} (μM ± S.D.)	
entry	Phosphatase	**2-2**	**2-32**
1	PTP4A3	0.132 ± 0.003	0.018 ± 0.014
2	PTP1B	>80	>80
3	CDC25B	22 ± 16	2.6 ± 1.2
4	PP2A	>80	>80
5	PTP4A1	n.d.	0.050
6	PTP4A2	n.d.	0.52

n.d. = not determined.

The activity of **2-2** and **2-32** in ovarian cancer cells lines were compared to the PTP4A3 inhibitor BR-1 (**2-1**), the inactive analog **2-22**, and cisplatin (Table 8).[123] The human ovarian cancer cells were seeded, treated with a vehicle control or test compound, and incubated at 37 °C for 44 h. Then, the cells were incubated with alamar blue for 4 h and the cell count was measured. Compound **2-32** was significantly more potent than the other PTP4A3 inhibitors **2-1** and **2-2**, as well as cisplatin. Potent activity was also seen in the cisplatin resistant cell line (entry 5).

Table 8. Compound activity against ovarian cancer cells.[123]

		EC_{50} (μM ± S.D.)				
entry	cell line	**2-1**	**2-2**	**2-32**	**2-22**	Cisplatin
1	SKOV3	48.3 ± 9.1	28.8 ± 2.2	4.3 ± 1.1	>50	>100
2	OVCAR-4	48.5 ± 7.9	15.5 ± 2.4	1.5 ± 0.3	>50	30.3 ± 4.4
3	HEYA8	>50	8.5 ± 1.3	3.2 ± 0.06	>50	n.d.
4	A2780CW (drug sensitive)	26.4 ± 1.0	4.5 ± 0.6	0.6 ± 0.2	>50	20.7 ± 1.0
5	A2780CP20 (cisplatin resistant)	17.3 ± 2	13.1 ± 0.6	1.1 ± 0.04	>50	>100

n.d. = not determined.

2.2.5 Progress towards the Automated Synthesis of Thienopyridone Analogs

Machine-assisted organic synthesis is an emerging field in the divergent synthesis of small molecules.[124] In some cases, the synthesis of compounds, purification, and *in vitro* biological evaluation is automated in sequence to allow for the rapid screening of compounds for biological activity.[125] However, relative to conventional synthesis, automated synthesis remains in its infancy with regard to reaction efficiency, scope, and scale. As a result, this field provides a vast opportunity for development of new methods and expansion of its application in small molecule synthesis.

We are interested in expanding the SAR of both **2-2** and **2-32** to gain a better understanding of the physical attributes responsible for the observed bioactivity and to expand on the reaction scope of the photooxygenation. The thienopyridone scaffold of **2-2** allows for a divergent multi-step synthesis of analogs featuring a variety of useful transformations such as cross-couplings, halogenations, and alkylations that would be suitable for automated synthesis (Scheme 21). Therefore, we pursued a collaboration with Lilly and their Open Innovation Drug Discovery (OIDD) program and were granted access to their Automated Synthesis Lab (ASL).[126] The program features a globally accessible, remote-controlled automated chemical synthesis lab that allows for real-time monitoring and manipulation of reaction parameters by remote users. Among its many features, the system is enabled with conventional and microwave heating, liquid-handling abilities, workup stations, cameras for visual inspection, LC/MS for reaction monitoring, and solvent evaporation.

The synthetic route was modeled on the improved synthesis of **2-2** (Scheme 14). Starting with the bicyclic **2-18**, a Suzuki-Miyaura or Sonogashira cross-coupling attaches the cyclic or alkynyl substituent in the R_1 position of **2-38**. Then, *N*-alkylation provides the R_2 substitution in

2-39 followed by aromatization with DDQ to yield thienopyridone **2-40**. Unlike the previous synthetic routes (Section 2.2.1), the use of corrosive nitric acid is avoided on the automated system. Instead, halogenation of **2-40** provides **2-41**, the precursor for the transition-metal catalyzed amination reactions. Once the synthesis of **2-37** is completed, the analogs will be subjected to the photooxygenation conditions to explore the scope of the transformation. Mainly, we want to explore the impact of the R_3 and R_4 substitutions on the oxidation of **2-37** to the **2-32** imine dione scaffold.

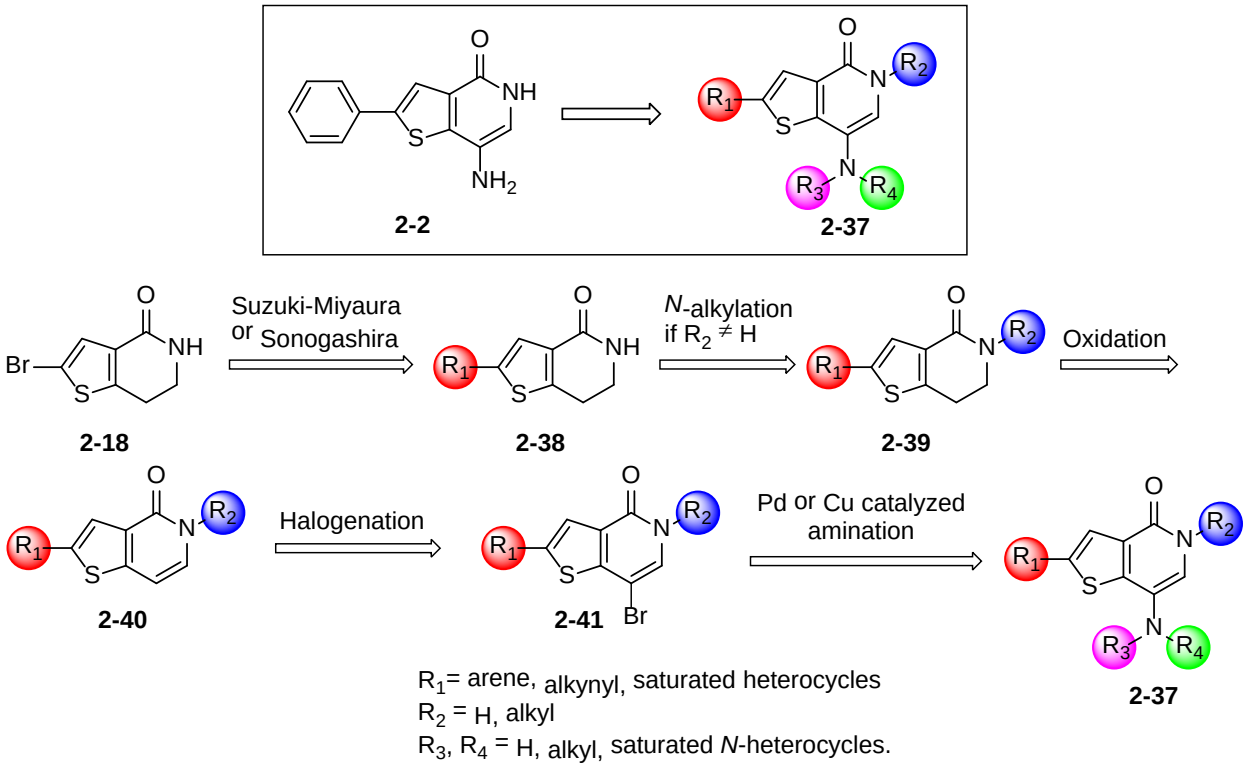

Scheme 21. Synthetic route for the automated synthesis of thienopyridone **2-37**.

Procedural workflows were designed for each transformation providing step-by-step instructions to the robot (Figure 17). Once the reaction instructions were submitted, a chemist weighed out the requested reactants, reagents, and solvents into a reaction vessel. Deoxygenation with an inert gas such as argon and nitrogen was conducted upon request for air sensitive

reactions involving transition metals. The reaction vessel was then placed on the automated system and the robot started to carry out the instructions. Cameras equipped on the system provided snapshots of the vessels for visual inspection. The vessel was placed in incubation under the requested temperature for a defined amount of time on either a conventional heating plate or in a microwave reactor. Reaction progress was monitored by periodic sampling of the crude reaction mixture for LC/MS analysis. Then, the crude mixture was quenched as needed and filtered. Volatile components were evaporated and the crude weight was measured. Based on the crude LC/MS result, the sample was either sent for additional purification via mass-guided HPLC in the Automated Purification Lab (APL) or sent to storage for use in the next reaction.

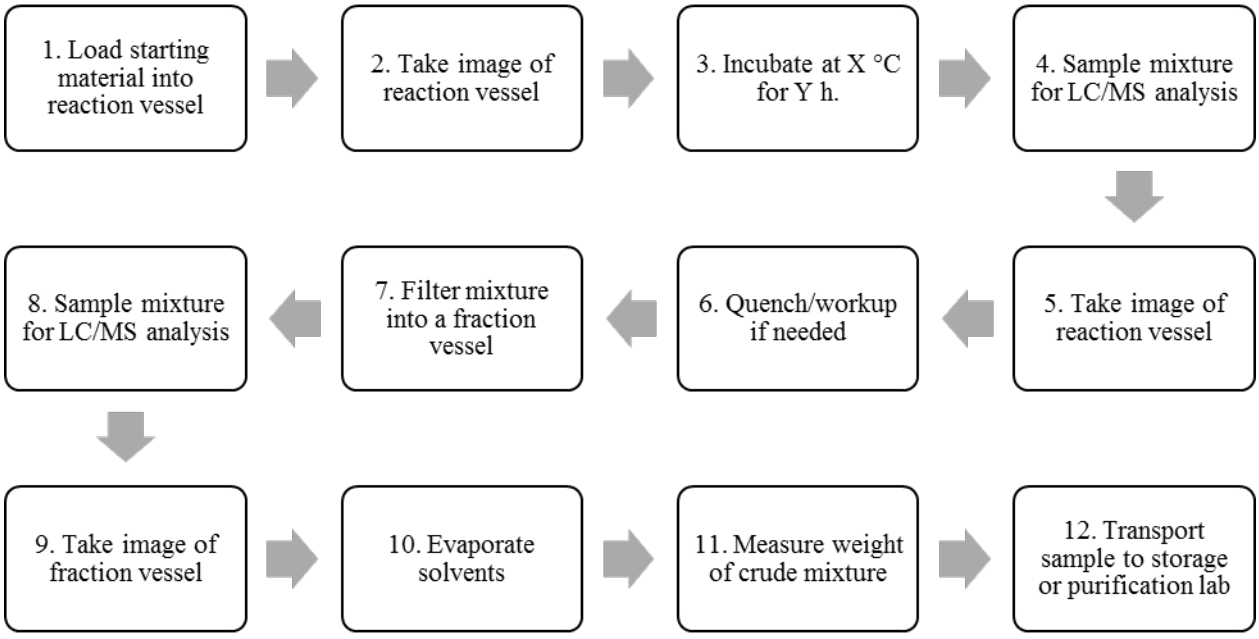

Figure 17. An abbreviated representative of the workflow instructions for the automated synthesis of analogs.[127]

The reaction workflows were tailored based on our procedures for the synthesis of **2-2** (Scheme 14), to first provide cross-coupling product **2-38** which was used crude in the oxidation

step to yield **2-40** in modest yield over two steps (Scheme 22 and 24). In automated systems, the reaction components must remain in solution to allow for the flow of the mixtures from one station to another, such as moving from the incubation station to the quench station. This requirement proved especially challenging for compounds **2-40** due to their poor solubility in common organic solvents. The low solubility may have in part contributed to the modest isolated yields (26-45%), despite complete conversion of reactants to products as observed by LC/MS. Bromination of **2-13** and **2-40e** gave access to halides **2-41a,e** for the subsequent transition-metal catalyzed amination reactions (Table 9).

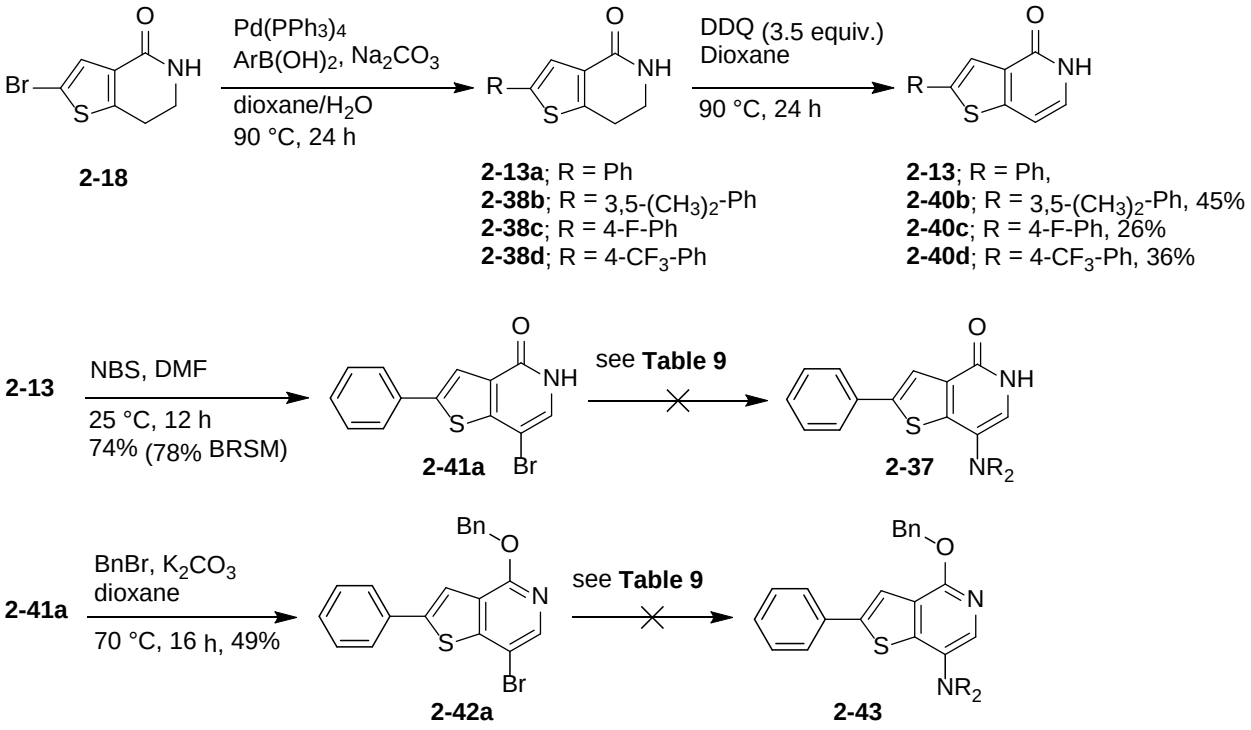

Scheme 22. Progress towards the automated synthesis of thienopyridone analogs **2-37**.

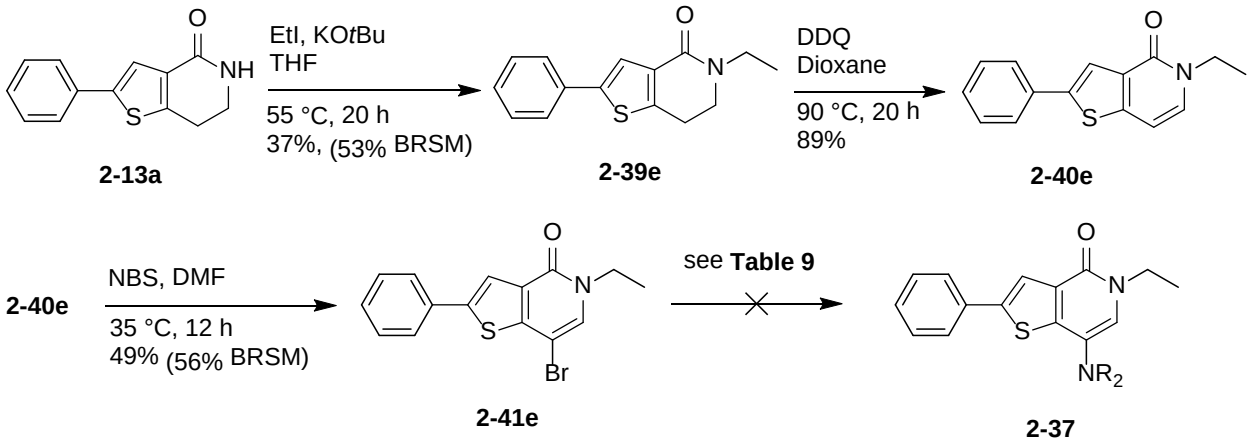

Scheme 23. Progress towards the automated synthesis of *N*-alkylated thienopyridone analogs **2-37**.

Our initial attempts to install the amines by Pd and Cu catalysis were unsuccessful (Table 9). In most cases, starting material or dehalogenated starting material was recovered. We considered the possibility that the pyridone moiety and the sulfur atom in the thiophene ring may deactivate the transition metals. To mask the pyridone moiety, **2-41a** was protected with a benzyl group to yield **2-42a** in 49% (Scheme 22) but the coupling attempts were still unsuccessful (entries 5 and 6)). We are currently screening more coupling conditions to troubleshoot this final reaction and complete the synthesis of **2-37**.

Table 9. Attempted amination reaction in the Lilly automated synthesis lab.

entry	halide	amine (equiv.)	reaction conditions (equiv.)	Result[a]
1	**2-41a**	piperidine (1.5)	Pd_2dba_3 (3 mol%) Davephos (9 mol%), NaO*t*-Bu (3) toluene, 100 °C, 20 h	No pdt. found
2	**2-41a**	CF_3CONH_2 (1.5)	CuI (5 mol%) Dimethylethylenediamine (10 mol%) K_2CO_3 (4) dioxane, μW 125 °C, 2 h	RSM
3	**2-41a**	CF_3CONH_2 (1.5)	CuI (10 mol%) Dimethylcyclohexyldiamine (20 mol%) K_2CO_3 (4) dioxane/H_2O, μW 125 °C, 2 h	des-Br SM
4	**2-41a**	CF_3CONH_2 (1.5)	CuI (10 mol%) Dimethylcyclohexyldiamine (20 mol%) K_2CO_3 (4) dioxane, 90 °C, 16 h	No pdt. found
5	**2-42a**	piperidine (1.5)	Pd-175 (5 mol%) Brettphos (5 mol%), NaO*t*-Bu (2) THF, 80 °C, 12 h	SM + des-Br SM
6	**2-42a**	CF_3CONH_2 (3)	CuI (20 mol%) Dimethylcyclohexyldiamine (40 mol%) KO*t*-Bu (4) toluene, 100 °C, 20 h	RSM
7	**2-41e**	$(CH_3)_2NH$ (1.5)	*t*-BuXPhos Pd G1 (2 mol%) LiHMDS (1.5) THF, rt, 3 h	SM

2.3 CONCLUSION

Phosphatases provide an opportunity for the development of novel inhibitors. With the propensity of malignancies to develop resistance to kinase inhibitors, phosphatases can offer options for alternative therapies. The current inhibitors of PTP4A are limited by selectivity, potency, and structural alerts. We designed a hybrid scaffold based on the structural features of

known PTP4A3 inhibitors, BR-1 (**2-1**) and thienopyridone **2-2**. Unfortunately, this scaffold proved ineffective against PTP4A3. Interestingly, photooxygenation of **2-2** yielded the novel imino-pyridine dione **2-32** that was a more potent inhibitor of PTP4A3. This compound showed selectivity towards PTP4A3 over other phosphatases and was active against human ovarian cancer cells. We are currently completing the automated synthesis of relevant analogs to explore the SAR of **2-2** and **2-32** and expand on the scope of the photooxygenation of amino-thienopyridones.

3.0 EXPERIMENTAL PART

3.1 GENERAL EXPERIMENTAL

All air-sensitive reactions were performed under an N_2 or Ar atmosphere. Reactions carried out at temperatures above rt employed an oil bath, Lab Armor Beads^{TM} (SKU # 42370), or a microwave reactor, as indicated. All microwave reactions were performed in sealed vials in a Biotage Initiator reactor (power range: 0 – 400 W from a magnetron at 2.45 GHz, temperature range: 40 – 250 °C, and pressure range: 0 – 20 bar). EtOH was stored over 4Å molecular sieves. 1,4-Dioxane and H_2O were deoxygenated by the freeze-pump-thaw technique or by sparging with Ar for 20 – 60 min immediately before use. THF was distilled over sodium/benzophenone ketyl. Et_3N was stored over KOH. All commercial reagents were used as received. Concentrating under reduced pressure refers to removing solvents by the use of a rotary evaporator connected to a PIAB Lab Vac H40.

Reactions were monitored by thin layer chromatography analysis (EMD, pre-coated silica gel 60 F_{254} plates, 250 μm layer thickness) and visualization was accomplished with a 254 nm or 365 nm UV light and by staining with a $KMnO_4$ solution (3 g of $KMnO_4$ and 4 g of K_2CO_3 in 200 mL of a 5% NaOH solution) when needed. Flash chromatography on SiO_2 (Silicycle, Silia-P Flash, or SiliaFlash® P60; 40-63 μm) was used to purify the crude reaction mixtures where

indicated. All products were placed under high vacuum (0.5 – 4 mmHg) to remove trace solvents.

Melting points were determined using Laboratory Devices Mel-Temp II in open capillary tubes and are uncorrected. Infrared spectra were obtained from neat solids or oils on a Perkin Elmer® Spectrum 100 FT-IR or Smiths Detection IdentifyIR FT-IR spectrometer. High-resolution mass spectra were obtained on a Micromass UK Limited, Q-TOF Ultima API or a Thermo Scientific Exactive Orbitrap LC-MS. Purities of final products were determined sing Agilent Technologies 385-ELSD. ELSD conditions: evaporator and nebulizer set at 45 °C; gas flow set at 1.80 standard liter / min; X Bridge BEH C18 2.5 µM; 2.1 x 50 mm XP column.

^{1}H NMR spectra were obtained on a Bruker Avance at 300 MHz, 400 MHz, 500 MHz, or 600 MHz in $CDCl_3$, $(CD_3)_2SO$, THF-*d8*, or CD_3OD. Chemical shifts (δ) were reported in parts per million with the residual solvent peak used as an internal standard δ ^{1}H / ^{13}C (solvent): 7.26/77.16 ($CDCl_3$); 2.50/39.52 ($(CD_3)_2SO$); 1.72 and 3.58 / 67.21 and 25.31 (THF-*d8*); 3.31/49.00 (CD_3OD). ^{1}H NMR spectra were obtained and are tabulated as follows: chemical shift, multiplicity (s = singlet, d = doublet, t = triplet, q = quartet, m = multiplet, bs = broad singlet), number of protons, and coupling constant(s). ^{13}C NMR spectra were recorded using a proton-decoupled pulse sequence run at 100 MHz, 125 MHz, or 150 MHz and are tabulated by observed peaks.

Supercritical fluid chromatography (SFC) semi-prep purification used a Mettler Toledo AG - Berger SFC™ MiniGram instrument. Sample preparation involved dissolving the analyte (10 mg/mL) in HPLC-grade MeOH and filtering with a 13 mm Millex® Syringe Filter (0.45 µm pore size). Separation was accomplished with a SiO_2 column (250 x 10 mm) at 100 bar pressure

with a detection wavelength of 220 nm, an oven temp. of 35 °C, an evaporator temp. of 27 °C, a trimmer temp. of 27 °C and using MeOH as a modifier under isocratic conditions.

3.2 CHAPTER 1 EXPERIMENTAL PART

Suzuki-Miyaura Cross-Coupling[48]

General Procedure A. Brominated heterocycle (1 equiv.) was added to a stirred mixture of boronic acid (2.1 – 2.3 equiv.), Pd_2dba_3 (1 mol%), *t*-Bu_3P (6 mol%), and Na_2CO_3 (2.3 equiv.) in deoxygenated 1,4-dioxane/H_2O (2:1, 0.1 M – 0.2 M) in a microwave vial under N_2 or Ar. The reaction mixture was sealed and heated to 70 °C for 30 min or 60 min in a microwave reactor. Upon completion, the reaction mixture was allowed to cool to rt and purified as indicated.

General Procedure B. Brominated heterocycle (1 equiv.) was added to a stirred mixture of boronic acid (3.5 equiv.), Pd_2dba_3 (2 mol%), *t*-Bu_3P (10 mol%), and Na_2CO_3 (2.3 equiv.) in deoxygenated 1,4-dioxane/H_2O (2:1, 0.1 M – 0.2 M) in a microwave vial under N_2 or Ar. The reaction mixture was sealed and heated to 70 °C for 60 min in a microwave reactor. Upon completion, the reaction mixture was allowed to cool to rt and purified as indicated.

C-H Activation / Cross-Coupling[48]

General Procedure C. Brominated heterocycle (1 equiv.) was added to a stirred mixture of ethyl oxazole-4-carboxylate (**1-20**) (2.1 equiv.), $Pd(OAc)_2$ (5 mol%), CyJohnPhos (10 mol%), and Cs_2CO_3 (3.5 equiv.) in 1,4-dioxane (2 mL) in a vial. The solution was flushed with Ar, sealed, and stirred at 110 °C in an oil bath for 22 h. The reaction mixture was allowed to cool to rt and purified as indicated.

Aldehyde and Ester Reduction[48]

General Procedure D. $NaBH_4$ (3 – 4 equiv.) was added to a suspension of aldehyde (1 equiv.) in THF/MeOH (4:1, 0.1 M – 0.2 M). The reaction mixture was stirred at rt until TLC analysis indicated the complete consumption of starting material. The solution was concentrated under

reduced pressure, diluted with water, and extracted with EtOAc. The combined organic layers were dried ($MgSO_4$ or Na_2SO_4), filtered, and concentrated under reduced pressure.

General Procedure E. $LiAlH_4$ in diethyl ether (1 M solution, 2 equiv.) was added slowly to a stirred solution of ester (1 equiv.) in CH_2Cl_2 (0.1 – 0.2 M) at 0 °C under N_2 or Ar. The reaction mixture was stirred for 1 h – 1.5 h at the same temperature, quenched and purified as indicated.

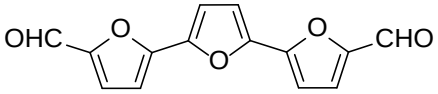

1-14a

[2,2':5',2''-Terfuran]-5,5''-dicarbaldehyde (1-14a).[46b,47a,48] Prepared by general procedure A with 2,5-dibromofuran (**1-12a**) (0.48 mmol) and (5-formylfuran-2-yl)boronic acid (**1-13a**). The reaction mixture was diluted with water and the precipitate was filtered. The crude precipitate was purified by chromatography on SiO_2 (2 – 5% MeOH/CH_2Cl_2) to yield **1-14a** (0.062 g, 51%) as an orange solid: Mp > 215 °C (dec., acetone); IR (ATR) 3141, 3115, 2835, 1661, 1473, 1265, 958, 767 cm^{-1}; ^1H NMR ($(CD_3)_2SO$, 400 MHz) δ 9.64 (s, 2 H), 7.70 (d, 2 H, *J* = 4.0 Hz), 7.30 (s, 2 H), 7.20 (d, 2 H, *J* = 3.6 Hz) ; ^{13}C NMR ($(CD_3)_2SO$, 100 MHz, 60 °C) δ 177.3, 151.7, 148.6, 144.9, 124.1, 111.9, 109.3; HRMS (ESI+) *m/z* calcd for $C_{14}H_9O_5$ $(M+H)^+$ 257.0444, found 257.0436.

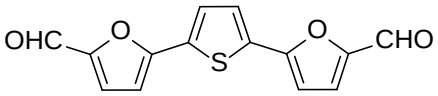

1-14b

5,5'-(Thiophene-2,5-diyl)bis(furan-2-carbaldehyde) (1-14b).[46b,48] Prepared by general procedure A with 2,5-dibromothiophene (**1-12b**) (1.8 mmol) and **1-13a**. The precipitate was

filtered, and the residue was rinsed with water (2 x 15 mL) and washed with diethyl ether (2 x 15 mL) to yield **1-14b** (0.427 g, 88%) as a yellow solid: Mp > 250 °C (dec., acetone); IR (ATR) 3115, 3075, 2850, 1655, 1477, 1394, 1263, 1027 cm^{-1}; ^{1}H NMR ($(CD_3)_2SO$, 400 MHz) δ 9.60 (s, 2 H), 7.78 (s, 2 H), 7.69 (d, 2 H, *J* = 3.6 Hz), 7.27 (d, 2 H, *J* = 4.0 Hz); ^{13}C NMR ($(CD_3)_2SO$, 125 MHz, 60 °C) δ 177.1, 152.4, 151.4, 132.0, 127.5, 124.5, 109.2; HRMS (ESI+) *m/z* calcd for $C_{14}H_9O_4S$ $(M+H)^+$ 273.0216, found 273.0212.

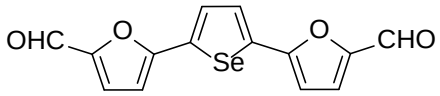

1-14c

5,5'-(Selenophene-2,5-diyl)bis(furan-2-carbaldehyde) (1-14c).[47b,48] Prepared by general procedure A with 2,5-dibromoselenophene (**1-12c**) (0.580 mmol) and **1-13a**. The precipitate was filtered, and the residue was rinsed with water (2 x 15 mL) and washed with diethyl ether (2 x 10 mL) to yield **1-14c** (0.172 g, 93%) as a yellow solid: Mp > 215 °C (dec., MeOH); IR (ATR) 3114, 3049, 2842, 1655, 1478, 1391, 1261, 1025 cm^{-1}; ^{1}H NMR ($(CD_3)_2SO$, 400 MHz) δ 9.58 (s, 2 H), 7.93 (s, 2 H), 7.67 (d, 2 H, *J* = 3.6 Hz), 7.27 (d, 2 H, *J* = 3.6 Hz); ^{13}C NMR ($(CD_3)_2SO$, 125 MHz, 60 °C) δ 177.1, 154.4, 151.4, 136.6, 129.5, 124.7, 109.0; HRMS (ESI+) *m/z* calcd for $C_{14}H_9O_4Se$ $(M+H)^+$ 320.9661, found 320.9652. ELSD purity = 100%.

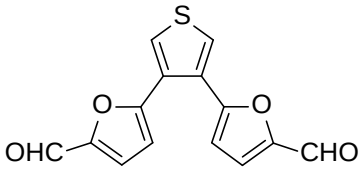

1-14d

5,5'-(Thiophene-3,4-diyl)bis(furan-2-carbaldehyde) (1-14d).[48] Prepared by general procedure B with 3,4-dibromothiophene (**1-12d**) (0.54 mmol) and **1-13a**. The precipitate was filtered, rinsed with water, and purified by chromatography on SiO_2 (1% MeOH/CH_2Cl_2) to yield **1-14d** (0.138 g, 93%) as a pale yellow solid: Mp 144-147 °C (CH_2Cl_2); IR (ATR) 3130, 3083, 2851, 1658, 1525 cm^{-1}; ^1H NMR ($CDCl_3$, 500 MHz) δ 9.63 (s, 2 H), 7.80 (s, 2 H), 7.29 (d, 2H, *J* = 3.5 Hz), 6.60 (d, 2 H, *J* = 3.5 Hz); ^{13}C NMR ($CDCl_3$, 100 MHz) δ 177.3, 154.2, 152.0, 129.0, 128.2, 123.1, 110.7; HRMS (ESI+) *m/z* calcd for $C_{14}H_8O_4NaS$ $(M+Na)^+$ 295.0036, found 295.0034.

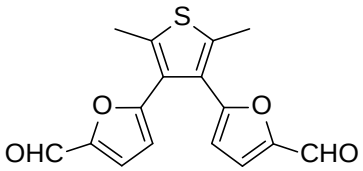

1-14e

5,5'-(2,5-Dimethylthiophene-3,4-diyl)bis(furan-2-carbaldehyde) (1-14e).[48] Prepared by general procedure B with 2,5-dimethyl-3,4-dibromothiophene (**1-12e**) (0.741 mmol) and **1-13a.** The reaction mixture was allowed to cool to rt and diluted with water (5 mL). The precipitate was filtered through Celite and washed with water (30 mL). The residue was dissolved in CH_2Cl_2, filtered, concentrated, and purified by chromatography on SiO_2 (0 – 50% EtOAc/hexanes) to yield **1-14e** (0.176 g, 79%) as a light orange solid: Mp 140.1-141.2 °C (EtOAc); IR (ATR) 3113, 2848, 1659, 1526, 1387, 1029, 969, 749 cm^{-1}; ^1H NMR ($(CD_3)_2SO$, 500 MHz) δ 9.50 (s, 2 H), 7.58 (d, 2 H, *J* = 4.0 Hz), 6.57 (d, 2 H, *J* = 3.5 Hz), 2.48 (s, 6 H); ^{13}C

NMR ($(CD_3)_2SO$, 125 MHz) δ 177.7, 153.3, 151.3, 137.8, 125.7, 124.1, 111.9, 14.1; HRMS (ESI+) *m/z* calcd for $C_{16}H_{12}O_4NaS$ $(M+Na)^+$ 323.0349, found 323.0345.

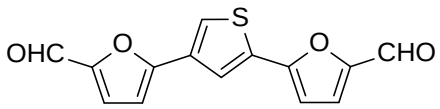

1-14f

5,5'-(Thiophene-2,4-diyl)bis(furan-2-carbaldehyde) (1-14f).[48] Prepared by general procedure B with 2,4-dibromothiophene (**1-12f**) (0.89 mmol) and **1-13a**. The reaction mixture was diluted with water (5 mL) and the precipitate was collected on Celite, rinsed with water (20 mL), washed off the filter with CH_2Cl_2, and concentrated under reduced pressure. The residue was purified by chromatography on SiO_2 (0 – 20% CH_2Cl_2/EtOAc then EtOAc) to yield **1-14f** (0.146 g, 60%) as a light orange solid: Mp >170 °C (dec., CH_2Cl_2); IR (ATR) 3074, 2816, 1663, 1465, 768 cm^{-1}; ^1H NMR ($CDCl_3$, 400 MHz) δ 9.65 (2s, 2 H), 7.83 (d, 1 H, *J* = 1.6 Hz), 7.81 (d, 1 H, *J* = 1.2 Hz), 7.32 (d, 1 H, *J* = 3.6 Hz), 7.31 (d, 1 H, *J* = 3.6 Hz), 6.76 (d, 1 H, *J* = 3.6 Hz), 6.74 (d, 1 H, *J* = 3.6 Hz); ^{13}C NMR ($(CD_3)_2SO$, 100 MHz, 60 °C) δ 177.3 (2 C), 153.9, 152.6, 151.3, 151.2, 132.4, 131.2, 125.3, 124.7, 124.6, 123.7, 108.9, 108.8; HRMS (ESI+) *m/z* calcd for $C_{14}H_9O_4S$ $(M+H)^+$ 273.0216, found 273.0213.

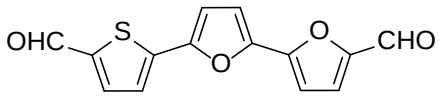

1-14g

5'-(5-Formylthiophen-2-yl)-[2,2'-bifuran]-5-carbaldehyde (1-14g).[22d] Prepared by general procedure A with **1-16** (0.36 mmol) and **1-13a**. The precipitate was filtered and the residue was rinsed with water (10 mL), washed with diethyl ether (10 mL), and dried (Na_2SO_4) to yield **1-14g**

(0.081 g, 78% (>95% purity by ^{1}H NMR)) as a dark brown solid: ^{1}H NMR ($CDCl_3$, 400 MHz) δ 9.91 (s, 1 H), 9.66 (s, 1 H), 7.72 (d, 1 H, *J* = 4.0 Hz), 7.43 (d, 1 H, *J* = 4.0 Hz), 7.34 (d, 1 H, *J* = 4.0 Hz), 7.01 (d, 1 H, *J* = 3.6 Hz), 6.88-6.85 (m, 2 H). The product was passed through a SiO_2 plug using EtOAc before reduction to **1-15g**.

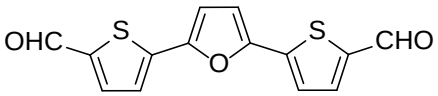

1-14h

5,5'-(Furan-2,5-diyl)bis(thiophene-2-carbaldehyde) (1-14h).[22d] Prepared by general procedure A with **1-16** (0.408 mmol) and **1-13c**. The reaction mixture was diluted with water (10 mL) and the precipitate was filtered. The residue was rinsed with water (25 mL) to yield **1-14h** (0.107 g, 91%) as a brown glossy solid: ^{1}H NMR ($(CD_3)_2SO$, 300 MHz) δ 9.93 (s, 2 H), 8.05 (d, 2 H, *J* = 4.2 Hz), 7.71 (d, 2 H, *J* = 4.2 Hz), 7.34 (s, 2 H).

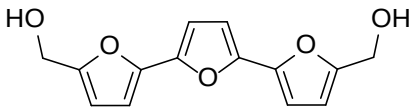

1-15a

[2,2':5',2''-Terfuran]-5,5''-diyldimethanol (1-15a).[22d,46b,47a,48] Prepared by general procedure D with **1-14a** (0.11 mmol) to yield **1-15a** (0.028 g, 92%) as a tan solid: Mp > 155 °C (dec., acetone); IR (ATR) 3283, 2915 1457, 1211, 999, 776 cm^{-1}; ^{1}H NMR (CD_3OD, 500 MHz) δ 6.66 (s, 2 H), 6.60 (d, 2 H, *J* = 3.0 Hz), 6.41 (d, 2 H, *J* = 3.5 Hz), 4.56 (s, 4 H); ^{13}C NMR (CD_3OD, 100 MHz) δ 155.8, 147.2, 147.0, 110.4, 107.8, 107.1, 57.3; HRMS (ESI+) *m/z* calcd for $C_{14}H_{11}O_4$ $(M\text{-}OH)^+$ 243.0652, found 243.0645.

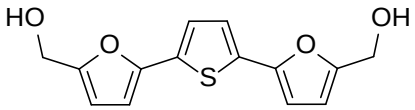

1-15b

(Thiophene-2,5-diylbis(furan-5,2-diyl))dimethanol (1-15b).[22d,46b,48] Prepared by general procedure D with **1-14b** (1.57 mmol) to yield **1-15b** (0.400 g, 94%) as a tan solid: Mp 102-104 °C (EtOAc); IR (ATR) 3276, 2924, 1441, 1062, 991, 783 cm^{-1}; ^{1}H NMR ($(CD_3)_2SO$, 300 MHz) δ 7.29 (s, 2 H), 6.72 (d, 2 H, *J* = 3.3 Hz), 6.41 (d, 2 H, *J* = 3.0 Hz), 5.29 (t, 2 H, *J* = 5.1 Hz), 4.42 (d, 4 H, *J* = 5.7 Hz); ^{13}C NMR ($(CD_3)_2SO$, 125 MHz) δ 155.2, 147.4, 131.2, 123.3, 109.4, 106.6, 55.6; HRMS (ESI+) *m/z* calcd for $C_{14}H_{11}O_3S$ $(M\text{-}OH)^+$ 259.0423, found 259.0420. ELSD purity = 99%.

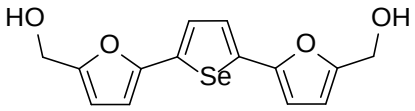

1-15c

(Selenophene-2,5-diylbis(furan-5,2-diyl))dimethanol (1-15c).[47b,48] Prepared by general procedure D with **1-14c** (1.50 mmol) to yield **1-15c** (0.441 g, 91%) as a yellow solid: Mp > 108 °C (dec., EtOAc); IR (ATR) 3327, 2925, 1450, 1183, 1051, 1015, 988 cm^{-1}; ^{1}H NMR ($(CD_3)_2SO$, 300 MHz) δ 7.44 (s, 2 H), 6.74 (d, 2 H, *J* = 3.0 Hz), 6.40 (d, 2 H, *J* = 3.3 Hz), 5.29 (t, 2 H, *J* = 5.7 Hz), 4.41 (d, 4 H, *J* = 5.7 Hz); ^{13}C NMR ($(CD_3)_2SO$, 125 MHz) δ 155.3, 149.4, 135.5, 125.1, 109.7, 106.5, 55.6; HRMS (ESI+) *m/z* calcd for $C_{14}H_{11}O_3Se$ $(M\text{-}OH)^+$ 306.9868, found 306.9864. ELSD purity = 99%.

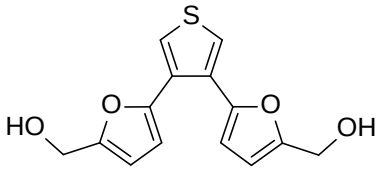

1-15d

(Thiophene-3,4-diylbis(furan-5,2-diyl))dimethanol (1-15d).[48] Prepared by general procedure D with **1-14d** (0.429 mmol). Extraction gave a crude oil that was purified by chromatography on SiO_2 (CH_2Cl_2 then EtOAc). The oil was dissolved in CH_2Cl_2 (1 mL), dried (Na_2SO_4), and concentrated to yield **1-15d** (0.107 g, 90%) as a yellow viscous oil: IR (ATR) 3323, 2934, 1602, 1450, 1007, 788 cm^{-1}; ^1H NMR ($(CD_3)_2SO$, 400 MHz) δ 7.73 (s, 2 H), 6.33 (d, 2 H, *J* = 2.8 Hz), 6.25 (d, 2 H, *J* = 3.2 Hz), 5.26 (t, 2 H, *J* = 5.6 Hz), 4.41 (d, 4 H, *J* = 5.2 Hz); ^{13}C NMR ($CDCl_3$, 100 MHz) δ 153.4, 149.6, 130.5, 124.5, 109.6, 108.4, 57.6; HRMS (ESI+) *m/z* calcd for $C_{14}H_{11}O_3S$ $(M\text{-}OH)^+$ 259.0423, found 259.0423. ELSD purity = 100%.

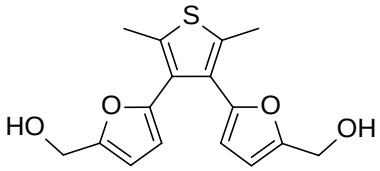

1-15e

((2,5-Dimethylthiophene-3,4-diyl)bis(furan-5,2-diyl))dimethanol (1-15e).[48] Prepared by general procedure D with **1-14e** (0.390 mmol) to yield **1-15e** (0.115 g, 97%) as a viscous yellow oil: IR (ATR) 3374, 2934, 1007, 790, 727 cm^{-1}; ^1H NMR ($CDCl_3$, 400 MHz) δ 6.30 (d, 2 H, *J* = 3.2 Hz), 6.16 (d, 2 H, *J* = 3.2 Hz), 4.47 (s, 4 H), 2.68 (br s, 2 H), 2.44 (s, 6 H); ^{13}C NMR ($CDCl_3$, 100 MHz) δ 152.9, 149.4, 134.4, 127.9, 109.4, 109.1, 57.3, 14.4; HRMS (ESI+) *m/z* calcd for $C_{16}H_{15}O_3S$ $(M\text{-}OH)^+$ 287.0736, found 287.0736. ELSD purity = 99%.

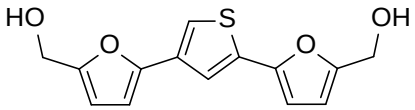

1-15f

(Thiophene-2,4-diylbis(furan-5,2-diyl))dimethanol (1-15f).[48] Prepared by general procedure D with **1-14f** (0.441 mmol) to yield **1-15f** (0.110 g, 90%) as a light yellow solid: Mp 108.2-109.6 °C (EtOAc); IR (ATR) 3379, 3256, 2934, 1441, 1007, 788 cm^{-1}; ^{1}H NMR (CD_3OD, 400 MHz) δ 7.53 (d, 1 H, *J* = 1.2 Hz), 7.46 (d, 1 H, *J* = 1.6 Hz), 6.59 (d, 1 H, *J* = 3.2 Hz), 6.56 (d, 1 H, *J* = 3.2 Hz), 6.39 (d, 1 H, *J* = 3.2 Hz), 6.37 (d, 1 H, *J* = 3.2 Hz), 4.55 (s, 4 H); ^{13}C NMR (CD_3OD, 100 MHz) δ 155.6, 155.1, 151.7, 150.1, 135.7, 134.4, 120.7, 118.4, 110.7, 110.3, 107.2, 106.9, 57.5, 57.4; HRMS (ESI+) *m/z* calcd for $C_{14}H_{11}O_3S$ $(M\text{-}OH)^+$ 259.0423, found 259.0420. ELSD purity = 100%.

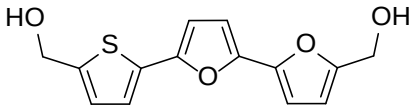

1-15g

(5-(5'-(Hydroxymethyl)-[2,2'-bifuran]-5-yl)thiophen-2-yl)methanol (1-15g).[22d,48] Prepared by general procedure D with **1-14g** (0.173 mmol) to yield **1-15g** (0.043 g, 90%) as a brown solid: Mp 105.5-107.8 °C (EtOAc); IR (ATR) 3341, 2933, 1450, 1003, 768 cm^{-1}; ^{1}H NMR (CD_3OD, 400 MHz) δ 7.19 (d, 1 H, *J* = 3.6 Hz), 6.95 (d, 1 H, *J* = 3.6 Hz), 6.64-6.62 (m, 2 H), 6.59 (d, 1 H, *J* = 3.2 Hz), 6.41 (d, 1 H, *J* = 3.2 Hz), 4.74 (s, 2 H), 4.56 (s, 2 H); ^{13}C NMR (CD_3OD, 100 MHz) δ 155.8, 150.2, 147.2, 146.8, 145.7, 134.0, 126.8, 123.5, 110.4, 108.2, 107.7, 107.0, 60.0, 57.3; HRMS (ESI+) *m/z* calcd for $C_{14}H_{11}O_3S$ $(M\text{-}OH)^+$ 259.0423, found 259.0415. ELSD purity = 100%.

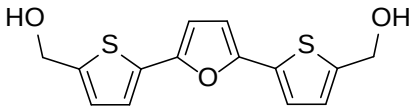

1-1

(Furan-2,5-diylbis(thiophene-5,2-diyl))dimethanol (1-1).[22d] Prepared by general procedure D with **1-14h** (0.100 mmol), under modified purification conditions. After the reaction was completed, the mixture was concentrated, diluted with water (15 mL), and extracted with EtOAc (15 mL). The organic layer was sequentially washed with a solution of cysteine (0.750 g in 15 mL water), a solution of cysteine and $Na_2S_2O_3$ pentahydrate (0.750 g of each solid in 15 mL water), and water (15 mL). The organic layer was then dried (Na_2SO_4) and concentrated to yield **1-1** (0.030 g, 99%) as a yellow solid: ^{1}H NMR ($(CD_3)_2SO$, 400 MHz) δ 7.23 (d, 2 H, *J* = 3.6 Hz), 6.95 (d, 2 H, *J* = 3.6 Hz), 6.78 (s, 2 H), 5.55 (t, 2 H, *J* = 5.6 Hz), 4.64 (d, 4 H, *J* = 5.6 Hz); ^{13}C NMR ($(CD_3)_2SO$, 100 MHz) δ 147.9, 146.0, 131.1, 124.8, 122.6, 107.4, 58.3.

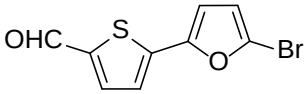

1-16

5-(5-Bromofuran-2-yl)thiophene-2-carbaldehyde (1-16).[22d,48] Intermediate 5-(furan-2-yl)thiophene-2-carbaldehyde was prepared by general procedure A with 5-bromothiophene-2-carbaldehyde (**1-12g**) (0.925 mmol) and furan-2-ylboronic acid (**1-13b**). The reaction mixture was diluted with water (10 mL) and extracted with EtOAc (3 x 15 mL). The combined organic layers were dried ($MgSO_4$), filtered, and concentrated under reduced pressure to yield a red oil. The oil was passed through a short SiO_2 column (CH_2Cl_2) to yield crude 5-(furan-2-yl)thiophene-2-carbaldehyde (0.165 g) as a red oil. NBS (0.304 g, 1.71 mmol) was added slowly at -15 °C to a stirred solution of benzoyl peroxide (0.044 g, 0.18 mmol) and crude aldehyde

(0.165 g) in toluene (5 mL). The solution was stirred for 4 h at -15 °C. More NBS (0.125 g) was added and the reaction mixture was stirred for an additional 2 h at -15 °C. The reaction mixture was purified by chromatography on SiO_2 (0 – 20% CH_2Cl_2/hexanes) to yield **1-16** (0.145 g, 61% over two steps) as a bright yellow solid: ^{1}H NMR ($CDCl_3$, 300 MHz) δ 9.89 (s, 1 H), 7.68 (d, 1 H, *J* = 4.2 Hz), 7.32 (d, 1 H, *J* = 3.9 Hz), 6.69 (d, 1 H, *J* = 3.6 Hz), 6.43 (d, 1 H, *J* = 3.6 Hz).

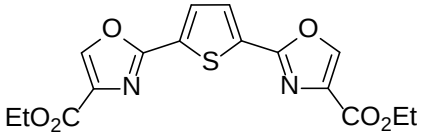

1-19a

Diethyl 2,2'-(thiophene-2,5-diyl)bis(oxazole-4-carboxylate) (1-19a).[48] Prepared by general procedure C with **1-12b** (1.06 mmol). The reaction mixture was diluted with CH_2Cl_2, and filtered through a pad of Celite. The filtrate was concentrated under reduced pressure, washed with hexanes, and filtered to yield a rust colored solid. The solid was dissolved in EtOAc (30 mL) and washed with aq. 10% sodium acetate. The organic layer was dried ($MgSO_4$) and concentrated. The residue was passed through a SiO_2 plug with CH_2Cl_2 followed by EtOAc to yield **1-19a** (0.198 g, 52%) as a bright orange solid: Mp 204.3-206.1 °C (CH_2Cl_2/EtOAc); IR (ATR) 3133, 2934, 1722, 1588, 1146 cm^{-1}; ^{1}H NMR ($CDCl_3$, 300 MHz) δ 8.25 (s, 2 H), 7.79 (s, 2 H), 4.43 (q, 4 H, *J* = 7.2 Hz), 1.41 (t, 6 H, *J* = 6.9 Hz); ^{13}C NMR ($CDCl_3$, 125 MHz) δ 161.0, 157.7, 143.7, 135.2, 131.8, 129.8, 61.6, 14.4; HRMS (ESI+) *m/z* calcd for $C_{16}H_{15}O_6N_2S$ $(M+H)^+$ 363.0645, found 363.0644.

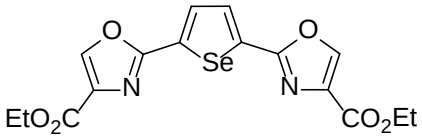

1-19b

Diethyl 2,2'-(selenophene-2,5-diyl)bis(oxazole-4-carboxylate) (1-19b).[48] Prepared by general procedure C with **1-12c** (0.837 mmol). The reaction mixture was diluted with CH_2Cl_2 and filtered through a pad of Celite. The filtrate was concentrated under reduced pressure, triturated with hexanes (3 x 15 mL), and filtered to yield **1-19b** (0.153 g, 45%) as a brown solid: Mp 171.5-173.5 °C (MeOH); IR (ATR) 3131, 2975, 2934, 1720, 1312, 1141, 1105 cm^{-1}; ^1H NMR ($CDCl_3$, 500 MHz) δ 8.23 (s, 2 H), 7.97 (s, 2 H), 4.43 (q, 4 H, *J* = 7.0 Hz), 1.41 (t, 6H , *J* = 7.0 Hz); ^{13}C NMR ($CDCl_3$, 125 MHz) δ 161.1, 159.4, 143.8, 136.5, 135.4, 131.9, 61.7, 14.5; HRMS (ESI+) *m/z* calcd for $C_{16}H_{15}O_6N_2Se$ $(M+H)^+$ 411.0090, found 411.0087.

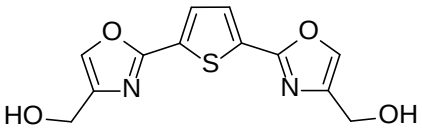

1-21a

(Thiophene-2,5-diylbis(oxazole-2,4-diyl))dimethanol (1-21a).[48] Prepared by general procedure E with **1-19a** (0.20 mmol). Saturated aqueous Rochelle's salt (1 mL) was added to the reaction solution and the mixture was stirred for 1 h at 0 ºC and extracted with CH_2Cl_2/isopropanol (3:1). The organic layers were combined, dried ($MgSO_4$), and concentrated. The residue was filtered through Celite with MeOH and concentrated to yield **1-21a** (0.044 g, 78%) as a yellow solid: Mp > 175 °C (dec., MeOH); IR (ATR) 3314, 3090, 2464, 1590, 1372, 982 cm^{-1}; ^1H NMR (CD_3OD, 500 MHz) δ 7.86 (t, 2 H, *J* = 1.0 Hz), 7.71 (s, 2 H), 4.57 (d, 4 H, *J* = 1.0 Hz); ^{13}C NMR (CD_3OD,

125 MHz) δ 158.5, 144.0, 137.4, 133.0, 129.8, 57.1; HRMS (ESI+) *m/z* calcd for $C_{12}H_{11}O_4N_2S$ $(M+H)^+$ 279.0434, found 279.0428. ELSD purity = 100%.

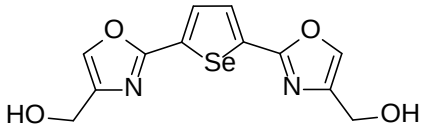

1-21b

(Selenophene-2,5-diylbis(oxazole-2,4-diyl))dimethanol (1-21b).[48] Prepared by general procedure E with **1-19b** (0.575 mmol). Water (44 μL), 15% NaOH solution (44 μL), and water (136 μL) were added sequentially to the reaction mixture at 0 ºC. The mixture was stirred for 1 h, dried ($MgSO_4$) and filtered through Celite. The filter cake was washed with CH_2Cl_2 (3 x 10 mL). The filter cake was rinsed with MeOH (3 x 15 mL) and the solvent was removed under reduced pressure. The crude product was dissolved in a minimal amount of EtOH and concentrated to yield a mixture of **1-21b** and EtOH (3 : 1) (0.159 g, 85%) as an orange powder: Mp > 225 °C (dec., EtOH); IR (ATR, EtOH) 3307, 1594, 1103, 982 cm^{-1}; ^1H NMR (CD_3OD, 500 MHz) δ 7.89 (s, 2 H), 7.85 (t, 2 H, *J* = 1.0 Hz), 4.56 (d, 4 H, *J* = 1.0 Hz); ^{13}C NMR (CD_3OD, 125 MHz) δ 160.2, 144.1, 137.5, 137.4, 131.9, 57.1; HRMS (ESI+) *m/z* calcd for $C_{12}H_{11}O_4N_2Se$ $(M+H)^+$ 326.9879, found 326.9868. ELSD purity = 98%.

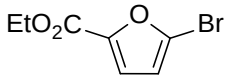

1-23

Ethyl 5-bromofuran-2-carboxylate (1-23).[128] A solution of 5-bromofuran-2-carboxylic acid (**1-22**) (2.00 g, 10.3 mmol) and H_2SO_4 (2 mL) in EtOH (50 mL) was stirred at reflux for 48 h under N_2. After the first 36 h, Na_2SO_4 (1.00 g) was added to the solution. The volatiles were removed

under reduced pressure. The residue was poured into water (200 mL) and extracted with EtOAc (3 x 50 mL). The combined organic layers were washed with brine (50 mL), dried (Na_2SO_4), and concentrated to yield **1-17** (2.11 g, 93%) as an orange liquid: ^{1}H NMR ($CDCl_3$, 400 MHz) δ 7.12 (d, 1 H, *J* = 3.2 Hz), 6.45 (d, 1 H, *J* = 3.6 Hz), 4.36 (q, 2 H, *J* = 7.2 Hz), 1.37 (t, 3 H, *J* = 7.2 Hz).

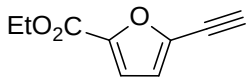

1-24

Ethyl 5-ethynylfuran-2-carboxylate (1-24). To a stirring solution of **1-23** (0.300 g, 1.37 mmol), CuI (0.006 g, 0.03 mmol), $PdCl_2(PPh_3)_2$ (0.020 g, 0.028 mmol) in Et_3N (3 mL) was added ethynyltrimethylsilane (0.40 mL, 2.8 mmol). The reaction solution was flushed with N_2, sealed, and stirred at 50 °C in an oil bath for 24 h. The reaction mixture was filtered through Celite and rinsed with hexanes (50 mL). The filtrate was concentrated to yield a dark red liquid. The crude liquid was dissolved in EtOH (3 mL) and K_2CO_3 (0.170 g, 1.23 mmol) was added. The mixture was stirred at 50 °C for 1 h. The solvent was removed under reduced pressure and the residue was purified by chromatography on SiO_2 (gradient: 0 – 4 % EtOAc/hexanes) to yield **1-24** (0.154 g, 65%) as a yellow oil: IR (ATR) 3282, 2975, 1717, 1292 cm^{-1}; ^{1}H NMR ($CDCl_3$, 300 MHz) δ 7.13 (d, 1 H, *J* = 3.6 Hz), 6.70 (d, 1 H, *J* = 3.6 Hz), 4.37 (q, 2 H, *J* = 7.2 Hz) , 3.43 (s, 1 H), 1.38 (t, 3 H, *J* = 7.2 Hz); ^{13}C NMR ($CDCl_3$, 100 MHz) δ 158.1, 145.2, 139.2, 118.3, 117.6, 83.6, 73.1, 61.5, 14.4; HRMS (ESI+) *m/z* calcd for $C_9H_9O_3$ (M^++H) 165.0546, found 165.0546.

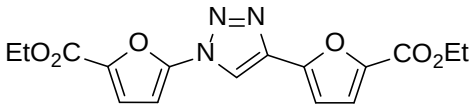

1-25

Diethyl 5,5'-(1*H*-1,2,3-triazole-1,4-diyl)bis(furan-2-carboxylate) (1-25). Alkyne **1-24** (0.175 g, 1.07 mmol), bromo-furan **1-23** (0.467 g, 2.13 mmol), sodium azide (0.278 g, 4.28 mmol), sodium ascorbate (0.042 g, 0.21 mmol), DMEDA (46 µL, 0.43 mmol), and CuI (0.042 g, 0.22 mmol) were dissolved in deoxygenated EtOH/H_2O (10 mL, 7:3). The reaction vial was flushed with Ar, sealed, and stirred at 75 °C for 4 d. The reaction solution was allowed to cool to rt and poured into ice-water (50 mL). To the beige aqueous solution was added NH_4OH (10 mL, 28-30% purity). The aqueous solution was extracted with EtOAc (3 x 50 mL). The combined organic layers were dried (Na_2SO_4) and concentrated. The residue was purified by chromatography on SiO_2 (gradient: 0 – 50% EtOAc/hexanes) to yield **1-25** (0.228 g, 62%) as a light yellow solid: Mp 152.5 – 152.9 °C (CH_2Cl_2); IR (ATR) 3124, 1713, 1294, 1137 cm^{-1}; ^1H NMR ($CDCl_3$, 300 MHz) δ 8.54 (s, 1 H), 7.32 (d, 1 H, *J* = 3.6 Hz), 7.28 (d, 1 H, *J* = 3.6 Hz), 7.07 (d, 1 H, *J* = 3.6 Hz), 6.86 (d, 1 H, *J* = 3.6 Hz), 4.42 (q, 2 H, *J* = 7.2 Hz), 4.40 (q, 2 H, *J* = 7.2 Hz), 1.42 (t, 3 H, *J* = 7.2 Hz), 1.41 (t, 3 H, *J* = 7.2 Hz); ^{13}C NMR ($CDCl_3$, 100 MHz) δ 158.7, 158.0, 148.6, 145.6, 144.7, 142.0, 139.9, 119.9, 119.6, 118.4, 109.6, 100.4, 61.7, 61.3, 14.50, 14.46; HRMS (ESI+) *m/z* calcd for $C_{16}H_{16}N_3O_6$ (M^++H) 346.1034, found 346.1032.

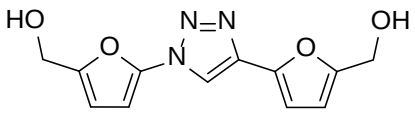

1-26

((1*H*-1,2,3-Triazole-1,4-diyl)bis(furan-5,2-diyl))dimethanol (1-26). $LiAlH_4$ in diethyl ether (0.6 mL, 1M) was added slowly to a stirring solution of **1-25** (0.120 g, 0.348 mmol) in THF (1.7 mL, 0.2 M) at -10 °C (MeOH/ice). The solution was stirred for 1.5 h at the same temperature. Sequentially, water (25 µL), 15% NaOH solution (25 µL), and then water (80 µL) were added to the reaction mixture. The mixture was stirred for 1 hr. The reaction mixture was dried (Na_2SO_4), diluted with *i*-PrOH (5 mL), and filtered through Celite. The filter cake was washed with IPA:MeOH (1:1) and the filtrate was concentrated to yield **1-26** (0.075 g, 83%) as a dark yellow solid: Mp >80 °C (dec., MeOH); IR (ATR) 3359, 3233, 3107, 2932, 2841, 1629, 1450, 1014, 798 cm^{-1}; ^1H NMR ($(CD_3)_2SO$, 300 MHz) δ 8.89 (s, 1 H), 6.84 (d, 1 H, *J* = 3.3 Hz), 6.80 (d, 1 H, *J* = 3.3 Hz), 6.55 (d, 1 H, *J* = 3.6 Hz), 6.45 (d, 1 H, *J* = 3.3 Hz), 4.47 (s, 2 H), 4.46 (s, 2 H); ^{13}C NMR (CD_3OD, 125 MHz) δ 156.7, 154.8, 146.0, 144.0, 141.4, 110.5, 110.3, 109.3, 101.7, 57.4, 57.2; HRMS (ESI+) *m/z* calcd for $C_{12}H_{12}N_3O_4$ $(M+H)^+$ 262.0822, found 262.0816; ELSD purity 100%.

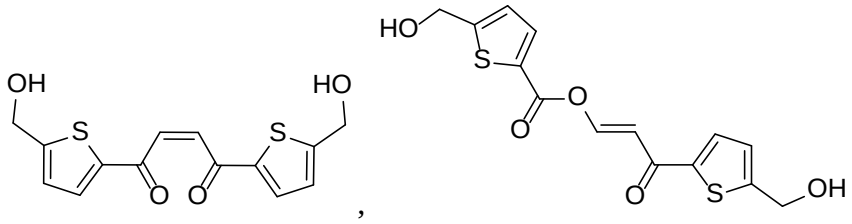

1-27, **1-28**
(tentative structural assignments)

A solution of **1-1** in DMSO at a concentration of 15 mg/mL was allowed to sit benchtop for five weeks. Then, the crude mixture was analyzed by ^{1}H, ^{13}C, COSY, HSQC, and HMBC NMR and high-resolution LC/MS. Due to its symmetry, the geometry of the double bond in **1-27** could not be assigned. The compound may be *E* or *Z*.

1,4-Bis(5-(hydroxymethyl)thiophen-2-yl)but-2-ene-1,4-dione (1-27): ^{1}H NMR ($(CD_3)_2SO$, 600 MHz) δ 7.76 (d, 2 H, *J* = 4.2 Hz), 7.25 (s, 2 H), 7.06 (d, 2 H, *J* = 4.2 Hz), 4.68 (s, 4 H) [-OH peaks not identified]; ^{13}C NMR ($(CD_3)_2SO$, 150 MHz) δ 184.3, 158.1, 141.3, 134.8, 134.3, 125.0, 58.7; HRMS (ESI+) *m/z* calcd for $C_{14}H_{13}O_4S_2$ $(M+H)^+$ 309.0250, found 309.0247.

(*E*)-3-(5-(Hydroxymethyl)thiophen-2-yl)-3-oxoprop-1-en-1-yl 5-(hydroxymethyl)thiophene-2-carboxylate (1-28): ^{1}H NMR ($(CD_3)_2SO$, 600 MHz) δ 8.32 (d, 1 H, *J* = 12 Hz), 8.03 (d, 1 H, *J* = 4.2 Hz), 7.93 (d, 1 H, *J* = 3.6 Hz), 7.23 (d, 1 H, *J* = 12 Hz), 7.15 (d, 1 H, *J* = 3.6 Hz), 7.10 (d, 1 H, *J* = 4.2 Hz), 4.75 (s, 2 H), 4.74 (s, 2H) [-OH peaks not identified]; ^{13}C NMR (characteristic peaks) ($(CD_3)_2SO$, 150 MHz) δ 181.5, 158.9, 157.8, 148.9, 143.0, 136.5, 134.0, 127.7, 125.0, 124.5, 109.7, 58.7 (2 C); HRMS (ESI+) *m/z* calcd for $C_{14}H_{13}O_5S_2$ $(M+H)^+$ 325.0199, found 325.0196.

Plasma Stability Assay

Balb C mouse plasma with K3 EDTA was purchased from Innovative Research™. Phosphate-buffered saline (PBS) pH 7.4 (1x) was purchased from GIBCO. Procaine hydrochloride (positive control) and procainamide hydrochloride (negative control) were purchased from Acros and used as is.

Plasma Preparation:

The plasma was thawed to room temperature and placed in a centrifuge at 3000 rpm for 10 min to pellet any insoluble material. The supernatant was diluted in PBS pH 7.4 (1X) to prepare a 1:1 solution (50% plasma v/v). The solution was warmed to 37 °C for 30 min while the stock compound solutions were prepared.

Compound Stock Solution Preparation:

Stock solutions of **1-1**, **1-15b**, **1-15f**, procaine HCl, and procainamide HCl in DMSO were prepared at 400 µM.

Testing Sample Preparation:

A solution of plasma/PBS (195 µL) was dispensed into 1.5 mL Eppendorf tubes (N = 3 per compound). Then, 5 µL of compound stock solution was added for a final DMSO concentration of 2.5%. The solution was mixed 4x by aspirating and dispensing with a pipette. Immediately after mixing, 50 µL of the test mixture was quenched by aspirating and dispensing into a 1.5 mL Eppendorf tube containing 400 µL of ice cold solution of acetonitrile and caffeine (internal standard). This aliquot marks the “no incubation” time point. The remaining 150 µL of the test solution was sealed and incubated at 37 °C on a gentle shaker (300 rpm). The quenching step was repeated as described above after 1.5 h and 3 h of incubation.

The quenched material was vortexed for 10 s, centrifuged at 3000 rpm for 10 minutes,

and filtered through 0.45 µM syringe filters into LC/MS vials. The samples were analyzed by high resolution LC/MS using mass guided peak search. The test compound peak was integrated and compared to the internal standard to determine the relative quantity of compound remaining.

3.3 CHAPTER 2 EXPERIMENTAL PART

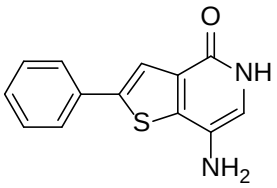

2-2

7-Amino-2-phenylthieno[3,2-*c*]pyridin-4(5*H*)-one (2-2).[111d]

Route 1:

A solution of **2-9** (0.280 g, 0.915 mmol) and conc. H_2SO_4 (7 mL) was heated to 80 °C, treated with conc. HNO_3 (0.5 mL), and heated at 80 °C for 1 h. The reaction mixture was allowed to cool to rt, stirred for 5 h, neutralized with 5 N NaOH, washed with water, and extracted with EtOAc. The combined organic layers were dried ($MgSO_4$), filtered, and concentrated to give a yellow solid that was purified by chromatography on SiO_2 (0 – 100% EtOAc/hexanes) to obtain crude 7- nitro-2-phenylthieno[3,2-*c*]pyridin-4(5*H*)-one (0.142 g, ca. 44%) as a yellow solid. The crude solid (0.0272 g) was dissolved in EtOH (50 mL) and was reduced and debrominated using a 10% Pd/C cartridge in an H-cube instrument (pressure: 1 atm, temp. 50 °C, flow rate 1 mL/min) for 1 h. The reaction mixture was evaporated under reduced pressure to obtain the crude product as a white powder which turned red upon standing at room temperature. The crude product was purified by SFC (MeOH, isocratic at 35% and 10 mL/min; retention time: 4.66 min) to obtain **3-2** (0.00370 g, 0.0153 mmol, 9% over 2 steps) as a pink solid.

Route 2:

A solution of HNO_3 (0.100 g, 1.10 mmol, 69% grade) in glacial AcOH (1 mL) was added to a solution of **2-13** (0.075 g, 0.33 mmol) in AcOH (2 mL). The yellow reaction mixture was stirred

at rt for 15.5 h and turned dark orange. It was diluted with water (15 mL) and the yellow precipitate was filtered and washed with water (3 x 5 mL) to yield a yellow solid. A solution of the solid in EtOAc was washed with water (15 mL), sat. aq. $NaHCO_3$ (2 x 15 mL), and brine (15 mL), dried (Na_2SO_4), and concentrated to yield a yellow residue (ca. 0.070 g) that was treated with 10% Pd/C (0.047 g, 0.044 mmol, 17 mol%) in EtOH (10 mL). The reaction flask was flushed with N_2 (3x) and then H_2 was bubbled through the solution. The reaction mixture was stirred at rt under H_2 (1 atm, balloon) for 5 h, filtered through basic Celite (EtOH), and concentrated to a dark residue that was purified by semi-prep SFC (MeOH, isocratic at 27% and 7.5 mL/min; collection/retention time: 7.25-10.25 min) to yield **2-2** (15.3 mg, 19% over 2 steps) as a yellow-brown solid: ^{1}H NMR ($(CD_3)_2SO$, 300 MHz) δ 10.85 (bs, 1 H), 7.83 (s, 1 H), 7.75 (d, 2 H, *J* = 7.2 Hz), 7.46 (t, 2 H, *J* = 7.2 Hz), 7.38-7.33 (m, 1 H), 6.66 (s, 1 H), 4.46 (s, 2 H); ^{13}C NMR ($(CD_3)_2SO$, 100 MHz) δ 156.5, 142.9, 141.0, 133.2, 131.1, 129.3, 128.2, 125.6, 124.3, 120.7, 112.21; HRMS (ESI+) *m/z* calcd for $C_{13}H_{11}ON_2S$ $(M+H)^+$ 243.0587, found 243.0586.

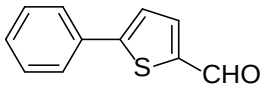

2-5

5-Phenylthiophene-2-carbaldehyde (2-5).[111d,129] A mixture of phenyl boronic acid (0.770 g, 6.32 mmol), Na_2CO_3 (1.21 g, 11.4 mmol), and $Pd(PPh_3)_4$ (0.300 g, 0.286 mmol) in a microwave vial was evacuated and refilled with Ar (3x), dissolved in deoxygenated 1,4-dioxane/H_2O (2:1, 17 mL), and treated with 5-bromothiophene-2-carboxaldehyde (**2-4**) (1.12 g, 5.69 mmol). The vial was sealed and heated in a microwave reactor at 90 °C for 2 h. The biphasic mixture was diluted with water (15 mL), and the precipitate was filtered and washed with water (100 mL). The residue was purified by chromatography on SiO_2 (0 – 25% EtOAc/hexanes) to yield **2-5**

(1.01 g, 95%) as a light pink solid: Mp 94.6-95.1 °C (CH_2Cl_2) (lit. 92-94 °C); IR (ATR) 3092, 1637, 1439, 1228, 1062 cm^{-1}; ^1H NMR ($CDCl_3$, 400 MHz) δ 9.89 (s, 1 H), 7.74 (d, 1 H, *J* = 3.6 Hz), 7.68-7.65 (m, 2 H), 7.45-7.37 (m, 4 H); ^{13}C NMR ($CDCl_3$, 100 MHz) δ 182.9, 154.4, 142.6, 137.5, 133.2, 129.6, 129.3, 126.5, 124.2; HRMS (ESI+) *m/z* calcd for $C_{11}H_9OS$ $(M+H)^+$ 189.0369, found 189.0368.

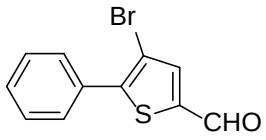

2-6

4-Bromo-5-phenylthiophene-2-carbaldehyde (2-6).[111d,130] Bromine (0.09 mL, 2 mmol) was added to a solution of **2-5** (0.300 g, 1.59 mmol) in $CHCl_3$/AcOH (1:1, 4 mL). The reaction mixture was shielded from light, stirred for 20 h, and diluted with EtOAc (15 mL). The organic layer was washed with sat. aq. $NaHCO_3$ (2 x 15 mL), aq. $Na_2S_2O_3$ (2 x 15 mL), and brine (15 mL), dried (Na_2SO_4), and concentrated to yield **2-6** (0.418 g, 98%) as yellow oil, which solidified upon standing to a light pink solid: Mp 81.7-82.5 °C (CH_2Cl_2) (lit. 83 °C); IR (ATR) 3051, 1677, 1663, 1430, 1217, 1124 cm^{-1}; ^1H NMR ($CDCl_3$, 400 MHz) δ 9.85 (s, 1 H), 7.72 (s, 1 H), 7.70- 7.67 (m, 2 H), 7.49-7.45 (m, 3 H); ^{13}C NMR ($CDCl_3$, 100 MHz) δ 181.9, 148.2, 141.5, 140.0, 131.9, 129.8, 129.1, 128.9, 108.9; HRMS (ESI+) *m/z* calcd for $C_{11}H_8BrOS$ $(M+H)^+$ 266.9474, found 266.9473.

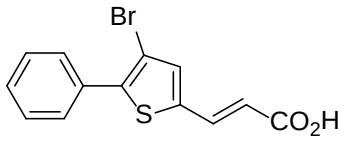

2-7

(*E*)-3-(4-Bromo-5-phenylthiophen-2-yl)acrylic acid (2-7).[111d] Malonic acid (0.094 g, 0.90 mmol) was added to a solution of **2-6** (0.200 g, 0.749 mmol) in pyridine (5 mL) and piperidine (0.25 mL). The reaction mixture was stirred at reflux for 5.5 h, allowed to cool to rt, poured over ice and dropwise treated with 12 N HCl (15 mL). The aqueous layer was extracted with EtOAc (100 mL) and the combined organic layers were washed with 1 N HCl (100 mL) and brine (100 mL), dried (Na_2SO_4), and concentrated to give **2-7** (0.203 g, 88%) as a yellow solid: Mp 169.1-171.9 °C (EtOAc); IR (ATR) 3300-2200 (br), 1676, 1614, 1413, 1273, 1195 cm^{-1}; ^1H NMR ($(CD_3)_2SO$, 400 MHz) δ 12.6 (bs, 1 H), 7.70 (d, 1 H, *J* = 16.0 Hz), 7.66-7.64 (m, 3 H), 7.55-7.45 (m, 3 H), 6.28 (d, 1 H, *J* = 16.0 Hz); ^{13}C NMR ($(CD_3)_2SO$, 100 MHz) δ 166.8, 139.6, 138.2, 135.1, 134.7, 131.6, 129.0, 128.9, 128.5, 119.1, 107.9; HRMS (ESI+) *m/z* calcd for $C_{13}H_{10}BrO_2S$ $(M+H)^+$ 308.9579, found 308.9578.

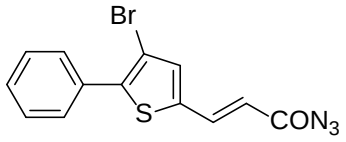

2-8

(*E*)-3-(4-Bromo-5-phenylthiophen-2-yl)acryloyl azide (2-8).[111d] A stirred suspension of **2-7** (0.650 g, 2.10 mmol) and DMF (0.1 mL) in toluene (10 mL) was treated dropwise with thionyl chloride (0.183 mL, 2.52 mmol) at room temperature, heated to reflux for 2.5 h, cooled to room temperature, and concentrated under reduced pressure to obtain crude acid chloride (0.660 g) as a brown oil that was used without further purification. A stirred suspension of NaN_3 (0.261 g, 4.03

mmol) in a mixture of toluene (2.5 mL) and water (2.5 mL) was treated dropwise with a solution of the crude oil (0.660 g) in toluene (2.5 mL) at 0 °C. The suspension was stirred for 1.5 h at room temperature. The toluene layer was then isolated and concentrated in vacuo, dissolved in EtOAc (5 mL), dried ($MgSO_4$), filtered, and concentrated under reduced pressure. The residue was purified by chromatography on SiO_2 (0 – 10% EtOAc/hexanes) to give **2-8** (0.310 g, 44% over 2 steps) as a yellow solid: IR (ATR) 2135, 1677, 1610, 1431, 1129 cm^{-1}; ^1H NMR (THF-*d*8, 500 MHz) δ 7.81 (d, 1 H, *J* = 15.5 Hz), 7.70-7.67 (m, 2 H), 7.54 (s, 1 H), 7.47-7.40 (m, 3 H), 6.34 (d, 1 H, *J* = 15.5 Hz); ^{13}C NMR (THF-*d*8, 75 MHz) δ 171.3, 142.7, 138.7, 137.9, 136.9, 132.9, 129.8, 129.4 (2 C), 119.3, 109.2; EIMS *m/z* 335 (50), 333 (35), 307 (95), 293 (55), 198 (95), 171 (100); HRMS (EI) *m/z* calcd for $C_{13}H_8BrN_3OS$ 332.9571, found 332.9571.

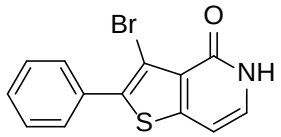

2-9

3-Bromo-2-phenylthieno[3,2-*c*]pyridin-4(5*H*)-one (2-9).[111d] A solution of azide **2-8** (0.101 g, 0.302 mmol) in diphenyl ether (2.5 mL) was heated in a microwave vial to 250 °C for 30 min. The dark brown reaction mixture was purified by chromatography on SiO_2 (20 – 70% EtOAc/hexanes) to give **2-9** (0.0481 g, 0.157 mmol, 52%) as a buff colored solid: Mp 239-240 °C; IR (ATR) 3313, 1684, 1638, 1602, 1591, 1494, 1440, 1192 cm^{-1}; ^1H NMR ($CDCl_3$, 300 MHz) δ 11.96 (bs, 1 H), 7.68-7.66 (m, 2 H), 7.50-7.46 (m, 3 H), 7.33 (d, 1 H, *J* = 6.6 Hz), 6.74 (d, 1 H, *J* = 6.6 Hz); ^{13}C NMR ($CDCl_3$, 125 MHz) δ 160.5, 148.9, 137.0, 132.5, 130.0, 129.6, 129.1, 128.8, 127.1, 105.7, 102.2; HRMS (TOF MS ES+) *m/z* calcd for $C_{13}H_9BrNOS$ $(M+H)^+$ 305.9588, found 305.9583.

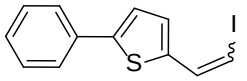

2-10

(*E*/*Z*)-2-(2-Iodovinyl)-5-phenylthiophene (2-10). NaHMDS (0.154 g, 0.787 mmol) in anhydrous THF (2 mL) was added dropwise to a suspension of **2-15** (0.446, 0.841 mmol) in anhydrous THF (5 mL) at 0 °C under N_2. The resulting mixture was stirred at rt for 10 min and then cooled to -78 °C. Aldehyde **2-5** (0.099 g, 0.53 mmol) in anhydrous THF (3 mL) was added dropwise and the mixture was stirred at -78 °C under N_2 for 40 min. The reaction was quenched with the addition of sat. aq. NH_4Cl (30 mL) and extracted with ether (30 mL). The organic layer was washed with water (30 mL) and brine (30 mL), dried (Na_2SO_4), and concentrated to an orange oil. The oil was purified by chromatography on SiO_2 (hexanes then 5% EtOAc/hexanes) to yield **2-10** (0.085 g, 52%) as a 1:1 *E*/*Z* mixture of a colorless solid: ^{1}H NMR ($CDCl_3$, 300 MHz) for the isomeric mixture δ 7.68-7.56 (m, 5 H), 7.46 (d, 1 H, *J* = 14.7 Hz), 7.40-7.29 (m, 8 H), 7.18 (d, 1 H, *J* = 3.6 Hz), 6.91 (d, 1 H, *J* = 3.9 Hz), 6.64 (d, 1 H, *J* = 15.0 Hz), 6.44 (d, 1 H, *J* = 8.4 Hz).

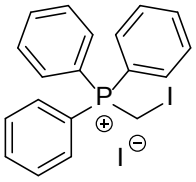

2-15

(Iodomethyl)triphenylphosphonium iodide (2-15).[115] Diiodomethane (1.25 mL, 15.5 mmol) was added to a solution of triphenylphosphine (**2-14**) (3.00 g, 11.4 mmol) in toluene (10 mL) in a vial under Ar. The vial was sealed and the resulting yellow solution was shielded from light with aluminum foil, stirred at reflux for 24 h, and allowed to cool to rt. The residue was filtered,

washed with cold toluene (100 mL), and dried to yield **2-15** (5.38 g, 89%) as a colorless solid: ^{1}H NMR ($(CD_3)_2SO$, 400 MHz) δ 7.94-7.74 (m, 15 H), 5.07 (d, 2 H, J_{HP} = 8.8 Hz).

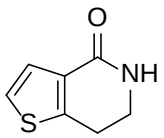

2-17

6,7-Dihydrothieno[3,2-*c*]pyridin-4(5*H*)-one (2-17).[111d,131] Thiophene-2-ethylamine (**2-16**) (1.0 mL, 8.4 mmol) was added dropwise to a three neck flask (one gas inlet, two rubber septa) containing a solution of triphosgene (1.25 g, 4.21 mmol) in anhydrous CH_2Cl_2 (12 mL) at 0 °C under Ar, followed by the addition of sat. aq. $NaHCO_3$ (12 mL) over 5 min. The resulting biphasic mixture was stirred at 0 °C under Ar for 5 h. The organic layer was dried (Na_2SO_4), passed through a short SiO_2 column (CH_2Cl_2), and concentrated to yield crude 2-(2-isocyanatoethyl)thiophene as an oil: IR (ATR) 2263 (NCO) cm^{-1}. A solution of this oil in anhydrous CH_2Cl_2 (25 mL) was added to a mixture of anhydrous $FeCl_3$ (1.36 g, 8.37 mmol) in anhydrous CH_2Cl_2 (100 mL) under N_2. The flask was equipped with a condenser and the reaction mixture was stirred at 50 °C for 40 min, poured into sat. aq. NH_4Cl (25 mL), extracted with CH_2Cl_2 (2 x 25 mL), and dried (Na_2SO_4). The solution was passed through a short basic Al_2O_3 column (10% MeOH/CH_2Cl_2) and concentrated to yield **2-17** (0.976 g, >90% pure based on NMR analysis, 71% over two steps) as a viscous dark oil with minor solvent impurities: ^{1}H NMR ($CDCl_3$, 400 MHz) δ 7.41 (d, 1 H, J = 5.2 Hz), 7.10 (d, 1 H, J = 5.2 Hz), 6.46 (bs, 1 H), 3.64 (dt, 2 H, J = 6.8, 2.8 Hz), 3.05 (t, 2 H, J = 6.8 Hz); ^{13}C NMR ($CDCl_3$, 100 MHz) δ 164.2, 146.3, 132.2, 126.0, 123.2, 41.3, 24.5.

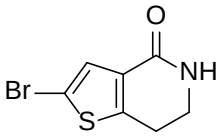

2-18

2-Bromo-6,7-dihydrothieno[3,2-*c*]pyridin-4(5*H*)-one (2-18).[111d,132] After addition of Br_2 (0.11 mL, 2.1 mmol) to a solution of **2-17** (0.300 g, 1.96 mmol) in AcOH (6 mL), the red reaction mixture was shielded from light and stirred at rt for 12 h, neutralized (Na_2CO_3), and diluted with EtOAc (30 mL). The organic layer was washed with sat. aq. $NaHCO_3$ (30 mL), aq. $Na_2S_2O_3$ (30 mL), and brine (30 mL), dried (Na_2SO_4), and concentrated to yield **2-18** (0.340 g, 75%) as a brown solid: Mp >100 °C (dec., CH_2Cl_2); IR (ATR) 3195, 3059, 2930, 1664, 1478, 1430, 1286 cm^{-1}; ^1H NMR ($CDCl_3$, 400 MHz) δ 7.36 (s, 1 H), 6.24 (bs, 1 H), 3.63 (dt, 2 H, *J* = 6.8, 2.8 Hz), 2.97 (t, 2 H, *J* = 6.8 Hz); ^{13}C NMR ($CDCl_3$, 100 MHz) δ 162.6, 147.4, 132.9, 128.5, 110.4, 41.2, 24.5; HRMS (ESI+) *m/z* calcd for C_7H_7BrNOS $(M+H)^+$ 231.9426, found 231.9425.

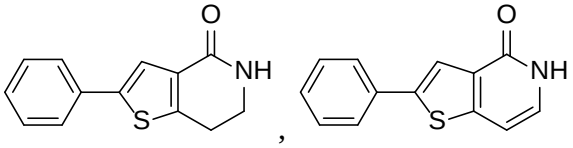

2-13a, **2-13**

2-Phenylthieno[3,2-*c*]pyridin-4(5*H*)-one (2-13).[111d,133] A mixture of bromide **2-18** (0.200 g, 0.862 mmol), phenyl boronic acid (0.127 g, 1.04 mmol), $Pd(PPh_3)_4$ (0.045 g, 0.043 mmol), and Na_2CO_3 (0.211 g, 2.00 mmol) in a microwave vial was flushed with Ar (3x), diluted with deoxygenated 1,4-dioxane/H_2O (2:1, 10 mL) and sealed. The reaction mixture was heated in an oil bath to 90 °C for 24 h, concentrated, and purified by chromatography on SiO_2 (50 – 100% EtOAc/hexanes) to yield 2-phenyl-6,7-dihydrothieno[3,2-*c*]pyridin-4(5*H*)-one (**2-13a**) as a crude solid (0.178 g) with minor aromatic impurities. The solid was typically used in the next step

without further purification. Analytically pure compound was acquired by washing with ether in a sonication bath: Mp 173.3-175.1 °C (CH_2Cl_2); IR (ATR) 3211 (br.), 3062, 2947, 2901, 1657, 1483, 1430, 754 cm^{-1}; ^1H NMR ($CDCl_3$, 400 MHz) δ 7.63 (s, 1 H), 7.59-7.56 (m, 2H), 7.39 7.36 (m, 2 H), 7.31-7.27 (m, 1 H), 6.75 (bs, 1 H), 3.67 (dt, 2 H, *J* = 6.8, 2.8 Hz), 3.06 (t, 2 H, *J* = 6.8 Hz); ^{13}C NMR ($CDCl_3$, 100 MHz) δ 164.1, 145.6, 142.3, 133.7, 133.1, 129.1, 128.0, 125.8, 121.3, 41.2, 24.5; HRMS (ESI+) *m/z* calcd for $C_{13}H_{12}NOS$ $(M+H)^+$ 230.0634, found 230.0632.

After addition of DDQ (0.218 g, 0.932 mmol) under an atmosphere of Ar to a solution of crude **2-13a** (0.178 g) in 1,4-dioxane (15 mL), the dark reaction mixture was stirred at 101 °C in a sealed vial under an Ar atmosphere for 1.5 d. Additional DDQ (0.218 g, 0.932 mmol) was added and heating was continued for another 24 h. The dark solution was concentrated to a crude brown solid that was purified by chromatography on SiO_2 (0-100% EtOAc/hexanes) to yield a crude light yellow solid with red and orange impurities. The crude solid was suspended in a small amount of EtOAc (<5 mL), filtered, and dried under vacuum to yield **2-13** (0.094 g, 48% over 2 steps) as light yellow solid: Mp >245 °C (dec., EtOAc); IR (ATR) 2828 (br), 1638, 1597, 1500, 1215, 749, 686 cm^{-1}; ^1H NMR ($(CD_3)_2SO$, 400 MHz) δ 11.47 (bs, 1 H), 7.86 (s, 1 H), 7.75 (d, 2 H, *J* = 7.2 Hz), 7.45 (t, 2 H, *J* = 7.2 Hz), 7.38-7.34 (m, 1 H), 7.27 (d, 1 H, *J* = 7.2 Hz), 6.85 (d, 1 H, *J* = 7.2 Hz); ^{13}C NMR ($(CD_3)_2SO$, 100 MHz) δ 158.6, 147.6, 141.2, 133.0, 131.6, 130.0, 129.3, 128.3, 125.7, 119.9, 100.9; HRMS (ESI+) *m/z* calcd for $C_{13}H_{10}NOS$ $(M+H)^+$ 228.0478, found 228.0474.

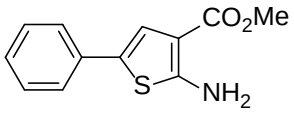

2-21

Methyl 2-amino-5-phenylthiophene-3-carboxylate (2-21).[111d,134] After addition of Et_3N (1.2 mL, 8.5 mmol) to a stirred mixture of phenylacetaldehyde (**2-20**) (1.0 mL, 8.4 mmol), methyl cyanoacetate (**2-24**) (0.80 mL, 8.8 mmol) and elemental sulfur (0.269 g, 8.40 mmol) in DMF (8.4 mL, 1 M), the reaction mixture was stirred at rt for 21 h and then diluted with water (10 mL). The yellow precipitate was filtered, washed with water (40 mL) and then hexanes (50 mL), and dried under vacuum to yield **2-21** (1.77 g, 90%) as a light yellow solid: Mp 183.8-185.1 °C (lit. 194.5 °C); IR (ATR) 3459, 3348, 2943, 1664, 1569, 1543, 1484, 1230 cm^{-1}; ^1H NMR ($(CD_3)_2SO$, 400 MHz) δ 7.50 (bs, 2 H), 7.46-7.43 (m, 2 H), 7.35-7.31 (m, 2 H), 7.24 (s, 1 H), 7.20-7.16 (m, 1 H), 3.73 (s, 3 H); ^{13}C NMR ($(CD_3)_2SO$, 100 MHz) δ 164.6, 163.5, 133.7, 128.9, 126.2, 124.0, 122.3, 121.0, 104.7, 50.7; HRMS (ESI+) *m/z* calcd for $C_{12}H_{12}NO_2S$ (M+H) 234.0583, found 234.0576.

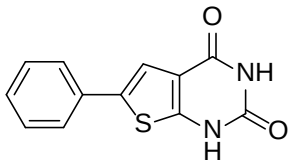

2-22

6-Phenylthieno[2,3-*d*]pyrimidine-2,4(1*H*,3*H*)-dione (2-22).[111d,135] Chlorosulfonyl isocyanate (0.15 mL, 1.7 mmol) was added slowly at -78 °C to a solution of **2-21** (0.200 g, 0.857 mmol) in CH_2Cl_2 (1.5 mL). The reaction mixture was allowed to warm to rt and stirred for 40 min. The slurry was concentrated and then diluted with wet 1,4-dioxane (4 mL), stirred at rt for 15 min and then at 85 °C for 30 min and treated with conc. NaOH (1 mL) so that the final concentration

of the base was 1 M. Heating at 85 °C was continued for 30 min and then the reaction mixture was allowed to cool to rt, diluted with water (5 mL), and acidified with conc. HCl with stirring until precipitation stopped. The precipitate was filtered, washed with water (20 mL), and dried under vacuum to yield **2-22** (0.120 g, 57%) as a colorless solid: Mp >300 °C (dec.); IR (ATR) 3159, 3044, 2806, 1707, 1653, 1555, 1256 cm^{-1}; ^{1}H NMR ($(CD_3)_2SO$, 400 MHz) δ 12.03 (s, 1 H), 11.21 (s, 1 H), 7.65-7.63 (m, 2 H), 7.55 (s, 1 H), 7.42-7.38 (m, 2 H), 7.32-7.29 (m, 1 H); ^{13}C NMR ($(CD_3)_2SO$, 100 MHz) δ 159.1, 151.4, 150.5, 133.3, 132.6, 129.2, 127.8, 125.1, 117.6, 116.2; HRMS (ESI+) *m/z* calcd for $C_{12}H_9N_2O_2S$ $(M+H)^+$ 245.0379, found 245.0378.

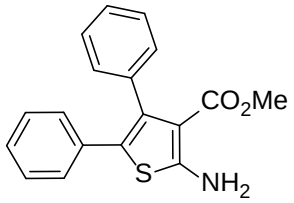

2-26

Methyl 2-amino-4,5-diphenylthiophene-3-carboxylate (2-26). Titanium tetrachloride (0.44 mL, 4.0 mmol) was added to a stirring solution of deoxybenzoin (**2-25**) (0.400 g, 1.98 mmol) and **2-24** (0.20 mL, 2.2 mmol) in CH_2Cl_2 (20 mL) at 0 °C under N_2. After stirring for 5 min, pyridine (0.34 mL, 4.1 mmol) was added dropwise at 0 °C under N_2. The mixture was stirred for 30 min at 0 °C and then for 22 h at rt. The solvent was removed under reduced pressure and the residue was diluted with EtOAc (15 mL). The organic layer was washed with 1N HCl (2 x 15 mL), water (15 mL), and brine (15 mL), dried (Na_2SO_4), and concentrated to a brown oil. The crude oil was dissolved in MeOH (10 mL) with sulfur (0.066 g, 2.1 mmol), morpholine (0.20 mL, 2.3 mmol), and acetic acid (0.04 mL, 0.7 mmol). The mixture was stirred at reflux for 2 d. The solution was diluted with water (10 mL) to induce precipitation. The precipitate was filtered, washed with

water (20 mL) and hexanes (20 mL), and dried to yield **2-26** (0.531 g, 87%) as a brown solid: Mp > 118 °C (dec.); IR (ATR) 3409, 3307, 1642, 1594, 1439, 1269, 1236, 692 cm^{-1}; ^{1}H NMR ($(CD_3)_2SO$, 400 MHz) δ 7.54 (bs, 2 H), 7.27-7.25 (m, 3 H), 7.14-7.06 (m, 5 H), 6.95-6.93 (m, 2 H), 3.37 (s, 3 H); ^{13}C NMR ($(CD_3)_2SO$, 100 MHz) δ 164.9, 163.4, 137.5, 135.9, 133.8, 129.8, 128.2, 127.5, 126.7, 126.3, 118.8, 105.2, 50.2; HRMS (ESI^+) *m/z* calcd for $C_{18}H_{16}NO_2S$ $(M+H)^+$ 310.0896, found 310.0898.

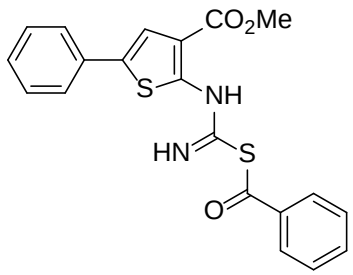

2-28 (tentative structural assignment)

Methyl 2-(3-benzoylthioureido)-5-phenylthiophene-3-carboxylate (2-28).[111d] A solution of benzoyl chloride (0.50 mL, 4.3 mmol) and anhydrous ammonium thiocyanate (0.489 g, 6.43 mmol) in anhydrous CH_3CN (10 mL) was stirred at reflux for 30 min under N_2 and then treated with a suspension of **2-21** (0.500 g, 2.14 mmol) in anhydrous CH_3CN (5 mL). The reaction mixture was stirred for 6 h at reflux, cooled, and the precipitate was filtered, washed with water (75 mL), and dried under vacuum to yield **2-28** (0.583 g, 69%) as a fine bright yellow powder: Mp 229.6-231.2 °C (CH_3CN); IR (ATR) 3275, 2943, 1694, 1670, 1508, 1221 cm^{-1}; ^{1}H NMR ($CDCl_3$, 400 MHz) δ 14.78 (bs, 1 H), 9.17 (bs, 1 H), 7.98-7.96 (m, 2 H), 7.67-7.61 (m, 3 H), 7.57-7.52 (m, 3 H), 7.41-7.37 (m, 2 H), 7.32-7.27 (m, 1 H), 4.02 (s, 3 H); ^{13}C NMR ($CDCl_3$, 100 MHz) δ 174.0, 165.5, 164.9, 147.7, 134.8, 133.9, 133.7, 131.5, 129.3, 129.1, 127.9 (2 C), 125.9,

120.4, 118.3, 52.4; HRMS (ESI+) *m/z* calcd for $C_{20}H_{17}N_2O_3S_2$ $(M+H)^+$ 397.0675, found 397.0673.

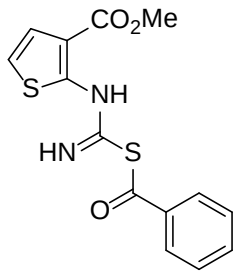

2-29 (tentative structural assignment)

Methyl 2-(3-benzoylthioureido)thiophene-3-carboxylate (2-29).[111d] A mixture of benzoyl chloride (0.59 mL, 5.1 mmol) and anhydrous ammonium thiocyanate (0.581 g, 7.63 mmol) in anhydrous CH_3CN (10 mL) was stirred at reflux for 30 min under N_2, treated with a suspension of **2-27** (0.400 g, 2.54 mmol) in anhydrous CH_3CN (5 mL), and stirred for 6 h at reflux and then cooled to 0 °C. The precipitate was filtered, washed with cold CH_3CN (50 mL) and then water (75 mL), and dried under vacuum to yield **2-29** (0.543 g, 67%) as a yellow solid: Mp 179.7-181.6 °C (EtOH); IR (ATR) 3422, 2934, 1683, 1543, 1148 cm^{-1}; ^1H NMR ($CDCl_3$, 400 MHz) δ 14.77 (bs, 1 H), 9.16 (bs, 1 H), 7.97-7.95 (m, 2 H), 7.66-7.62 (m, 1 H), 7.55-7.51 (m, 2 H), 7.37 (d, 1 H, *J* = 6.0 Hz), 6.85 (dd, 1 H, *J* = 5.6, 0.4 Hz), 3.99 (s, 3 H); ^{13}C NMR ($CDCl_3$, 100 MHz) δ 174.4, 165.5, 165.0, 148.7, 133.9, 131.6, 129.3, 127.9, 125.1, 117.5, 117.4, 52.3; HRMS (ESI+) *m/z* calcd for $C_{14}H_{13}N_2O_3S_2$ $(M+H)^+$ 321.0362, found 321.0360.

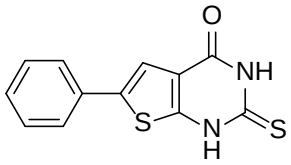

2-30

6-Phenyl-2-thioxo-2,3-dihydrothieno[2,3-*d*]pyrimidin-4(1*H*)-one (2-30).[111d,136] A suspension of **2-28** (0.100 g, 0.252 mmol) and KOH (0.100 g, 1.78 mmol) in EtOH (5 mL) was stirred at reflux for 14 h, cooled to rt, and acidified with aq. HCl. The colorless precipitate was filtered and washed with water (20 mL). The solid was then precipitated from EtOH, filtered and dried under vacuum to yield **2-30** (0.032 g, 49%) as an off-white solid: Mp >230 °C (dec., EtOH) (lit. >305 °C, dec.); IR (ATR) 3059, 2932, 1653, 1543, 1199, 1126, 744 cm^{-1}; ^{1}H NMR ($(CD_3)_2SO$, 400 MHz) δ 13.54 (bs, 1 H), 12.51 (bs, 1 H), 7.69 (d, 2 H, *J* = 7.6 Hz), 7.65 (s, 1 H), 7.43 (t, 2 H, *J* = 7.6 Hz), 7.36-7.33 (m, 1 H); ^{13}C NMR ($(CD_3)_2SO$, 100 MHz) δ 173.4, 156.5, 150.8, 135.9, 132.3, 129.3, 128.3, 125.4, 119.8, 117.5; HRMS (ESI+) *m/z* calcd for $C_{12}H_9N_2OS_2$ $(M+H)^+$ 261.0151, found 261.0148.

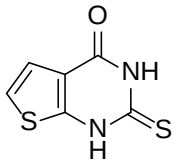

2-31

2-Thioxo-2,3-dihydrothieno[2,3-*d*]pyrimidin-4(1*H*)-one (2-31).[111d,137] A suspension of **2-29** (0.350 g, 1.09 mmol) and KOH (0.350 g, 6.24 mmol) in EtOH (15 mL) was stirred at reflux for 19 h, cooled to rt and concentrated under reduced pressure. The residue was diluted with 1 N HCl (25 mL). The precipitate was filtered and washed with water (50 mL) to yield a brown solid. The solid was stirred in hot EtOH, cooled, filtered and dried under vacuum to yield **2-31** (0.115

g, 57%) as a fine yellow powder: Mp >280 °C (dec., EtOH) (lit. 305-307 °C, EtOH); IR (ATR) 3059, 2898, 1629, 1553, 1523, 1450, 1187, 1128, 701 cm^{-1}; ^{1}H NMR ($(CD_3)_2SO$, 400 MHz) δ 13.44 (bs, 1 H), 12.44 (bs, 1 H), 7.27 (d, 1 H, *J* = 5.6 Hz), 7.20 (d, 1 H, *J* = 5.6 Hz); ^{13}C NMR ($(CD_3)_2SO$, 100 MHz) δ 173.5, 156.7, 151.7, 121.8, 119.8, 118.7; HRMS (ESI+) *m/z* calcd for $C_6H_5N_2OS_2$ $(M+H)^+$ 184.9838, found 184.9838.

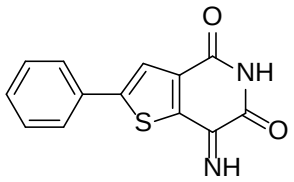

2-32

7-Imino-2-phenylthieno[3,2-*c*]pyridine-4,6(5*H*,7*H*)-dione (2-32).[111d] A solution of **2-2** (32.51 mg, 0.1342 mmol) in MeOH (30 mL) in a 50 mL Pyrex® round bottom flask was placed 15 cm away from a 23 W compact fluorescent lamp and stirred at 23-24 °C until the starting material was consumed (2.5 days), as determined by high resolution LC/MS. Brown product **2-32** started to precipitate after 1 day. The mixture was concentrated under reduced pressure to remove about half of the solvent and the brown precipitate was filtered, washed with MeOH (5 mL) and dried under vacuum to yield a brown solid (14.86 mg). The filtrate was concentrated under reduced pressure to remove all of the solvent. The brown residue was washed with MeOH (5 mL) and dried under vacuum to yield a brown solid (11.72 mg). The solids were combined to yield **2-32** (26.58 mg, 77%) as an amorphous brown solid. Both precipitates had the same purity based on 1H NMR analysis. Yellow-green crystals were obtained from the slow evaporation of a solution of **2-32** in MeCN: Mp >260 °C (dec., MeOH); IR (ATR) 3239, 3095, 2823, 1695, 1598, 1453 cm^{-1}; ^{1}H NMR ($(CD_3)_2SO$, 400 MHz) δ 11.87 (bs, 1H), 11.59 (s, 1 H), 7.98 (s, 1 H), 7.87 (d, 2 H,

J = 6.8 Hz), 7.52-7.43 (m, 3 H); ^{13}C NMR ($(CD_3)_2SO$, 100 MHz) δ 160.1, 157.9, 153.4, 149.3, 141.9, 136.8 132.0, 129.6, 129.5, 126.2, 122.1; HRMS (ESI+) *m/z* calcd for $C_{13}H_9O_2N_2S$ $(M+H)^+$ 257.0379, found 257.0378. The X-ray structure of **2-32** was deposited with the Cambridge Crystallographic Data Centre (CCDC 1476250).

Reactions Conducted in the Lilly Automated Synthesis Lab

General Procedure for Suzuki-Miyaura Cross-Coupling and Aromatization

A mixture of halide **2-18** (1 mmol), aryl boronic acid (1.5 equiv.), and Na_2CO_3 (2.3 equiv.) in dioxane (7.8 mL) and water (2.6 mL) was deoxygenated by a passing through it a stream of N_2 for 15 min. Then, $Pd(PPh_3)_4$ (5 mol%) was added and the resulting mixture was stirred at 90 °C for 24 h, allowed to cool, passed through diatomaceous earth rinsing with EtOAc, and concentrated to a yield crude product **2-38**.

A mixture of crude **2-38** and DDQ (3.5 equiv.) in dioxane (12 mL) was stirred at 90 °C for 24 h, passed through a Celite cartridge rinsing with EtOAc, and concentrated to yield crude reaction product **2-40**. The product was purified by mass-guided HPLC in the Automated Purification Lab (APL).

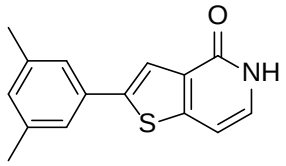

2-40b

2-(3,5-Dimethylphenyl)thieno[3,2-*c*]pyridin-4(5*H*)-one (2-40b). Isolated as a brown solid (116 mg, 45%): ^{1}H NMR ($(CD_3)_2SO$, 400 MHz) δ 11.45 (bs, 1H), 7.81 (s, 1 H), 7.37 (s, 2 H), 7.26 (t, 1 H, *J* = 6.8 Hz), 7.01 (s, 1 H), 6.84 (d, 1 H, *J* = 6.8 Hz), 2.33 (s, 6 H).

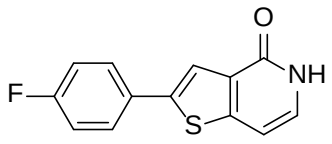

2-40c

2-(4-Fluorophenyl)thieno[3,2-*c*]pyridin-4(5*H*)-one (2-40c). Isolated as a brown solid (64.8 mg, 26%): ^{1}H NMR ($(CD_3)_2SO$, 400 MHz) δ 11.47 (bs, 1H), 7.84 (s, 1 H), 7.83-7.79 (m, 2 H), 7.32-7.26 (m, 3 H), 6.86 (d, 1 H, *J* = 6.8 Hz).

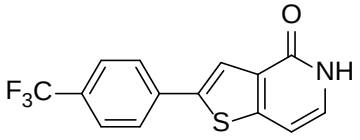

2-40d

2-(4-(Trifluoromethyl)phenyl)thieno[3,2-*c*]pyridin-4(5*H*)-one (2-40d). Isolated as a brown solid (108 mg, 36%): ^{1}H NMR ($(CD_3)_2SO$, 400 MHz) δ 11.54 (bs, 1H), 8.05 (s, 1 H), 7.99 (d, 2 H, *J* = 8.0 Hz), 7.80 (d, 2 H, *J* = 8.0 Hz), 7.32 (t, 1 H, *J* = 6.4 Hz), 6.90 (d, 1 H, *J* = 7.2 Hz).

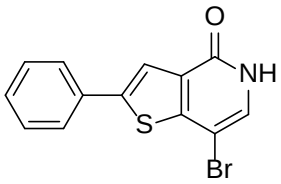

2-41a

7-Bromo-2-phenylthieno[3,2-*c*]pyridin-4(5*H*)-one (2-41a).[133] A solution of NBS in DMF (1.3 equiv., 0.15 M) was added slowly over 10 min to a mixture of **2-13** (0.442 mmol) in DMF (1 mL). The resulting mixture was stirred at 25 C for 12 h, passed through Celite rinsing with EtOAc, concentrated, and purified by mass-guided HPLC in APL to yield **2-41a** (99.9 mg, 74%,

78% BRSM) as an off-white solid: ^{1}H NMR ($(CD_3)_2SO$, 400 MHz) δ 11.81 (bs, 1H), 8.01 (s, 1 H), 7.83-7.80 (m, 2 H), 7.60 (s, 1 H), 7.50-7.46 (m, 2 H), 7.42-7.36 (m, 1 H).

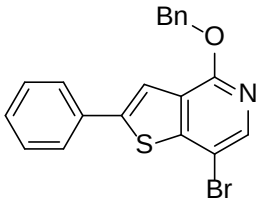

2-42a

4-(Benzyloxy)-7-bromo-2-phenylthieno[3,2-*c*]pyridine (2-42a). A mixture of **2-41a** (0.25 mmol), BnBr (1.2 equiv.), and K_2CO_3 (1 equiv.) in dioxane (4 mL) was stirred at 70 °C for 16 h, passed through Celite rinsing with EtOAc, concentrated, and purified by mass-guided HPLC in APL to yield **2-42a** (49.0 mg, 49%) as a light tan solid: ^{1}H NMR ($(CD_3)_2SO$, 400 MHz) δ 8.13 (s, 1 H), 8.03 (s, 1 H), 7.82-7.80 (m, 2 H), 7.49-7.46 (m, 2 H), 7.42-7.28 (m, 6 H), 5.22 (s, 2 H).

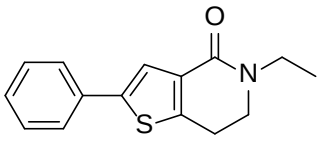

39e

5-Ethyl-2-phenyl-6,7-dihydrothieno[3,2-*c*]pyridin-4(5*H*)-one (2-39e). Iodoethane (4.1 mmol) was added to a mixture of **2-13a** (1.92 mmol) and a solution of KO*t*-Bu in THF (3.1 mmol, 1 M) at 25 °C. The resulting mixture was stirred at 55 °C for 20 h, passed through Celite rinsing with EtOAc, concentrated, and purified by mass-guided HPLC in APL to yield **2-39e** (182 mg, 37%, 53% BRSM) as an off-white solid: ^{1}H NMR ($(CD_3)_2SO$, 400 MHz) δ 7.67-7.65 (m, 2 H), 7.60 (s, 1 H), 7.45-7.41 (m, 2 H), 7.35-7.31 (m, 1 H), 3.65 (t, 2 H, J = 6.8 Hz), 3.47 (q, 2 H, J = 7.2 Hz), 3.09 (t, 2 H, J = 6.8 Hz), 1.10 (t, 3 H, J = 7.2 Hz).

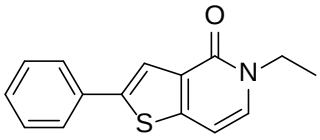

2-40e

5-Ethyl-2-phenylthieno[3,2-*c*]pyridin-4(5*H*)-one (2-40e). A mixture of **2-39e** (0.706 mmol) and DDQ (3.5 equiv.) in dioxane (11 mL) was stirred at 90 °C for 20 h, passed through Celite rinsing with EtOAc, concentrated, and purified by mass-guided HPLC in APL to yield **2-40e** (160 mg, 89%) as a tan solid: ^{1}H NMR ($(CD_3)_2SO$, 400 MHz) δ 7.88 (s, 1 H), 7.77-7.75 (m, 2 H), 7.61 (d, 1 H, *J* = 7.2 Hz), 7.48-7.44 (m, 2 H), 7.39-7.35 (m, 1 H), 6.93 (d, 1 H, *J* = 7.2 Hz), 4.02 (q, 2 H, *J* = 7.2 Hz), 1.26 (t, 3 H, *J* = 7.2 Hz); ^{13}C NMR ($(CD_3)_2SO$, 100 MHz) δ 158.0, 146.8, 142.2, 134.1, 133.4, 131.6, 129.7, 128.8, 126.2, 120.7, 101.8, 43.7, 15.2.

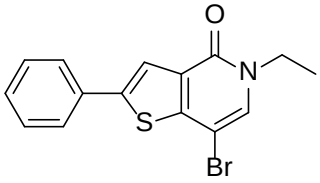

2-41e

7-Bromo-5-ethyl-2-phenylthieno[3,2-*c*]pyridin-4(5*H*)-one (2-41e). A solution of NBS in DMF (1.4 equiv., 0.2 M) was added over 10 min to a mixture of **2-40e** (0.588 mmol) in DMF (0.5 mL) at 25 °C. The resulting mixture was stirred at 35 °C for 12 h, passed through Celite rinsing with EtOAc, concentrated, and purified by mass-guided HPLC in APL to yield **2-41e** (97.9 mg, 50%, 56% BRSM) as a brown solid: ^{1}H NMR ($(CD_3)_2SO$, 400 MHz) δ 8.03 (s, 1 H), 8.02 (s, 1 H), 7.83-7.81 (m, 2 H), 7.50-7.46 (m, 2 H), 7.42-7.83 (m, 1 H), 4.03 (q, 2 H, *J* = 7.2 Hz), 1.27 (t, 3 H, *J* = 7.2 Hz).

APPENDIX

SUPPLEMENTARY FIGURES AND SCHEMES

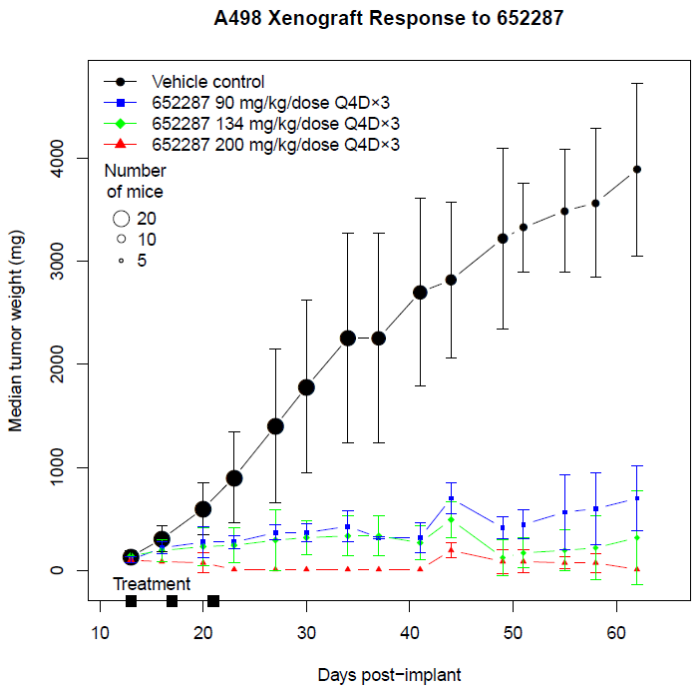

Figure 18. A498 cell line xenograft studies in mice with compound **1-1**. Drug treatment was administered by intravenous injections every 4 days for a total of three injections.[45]

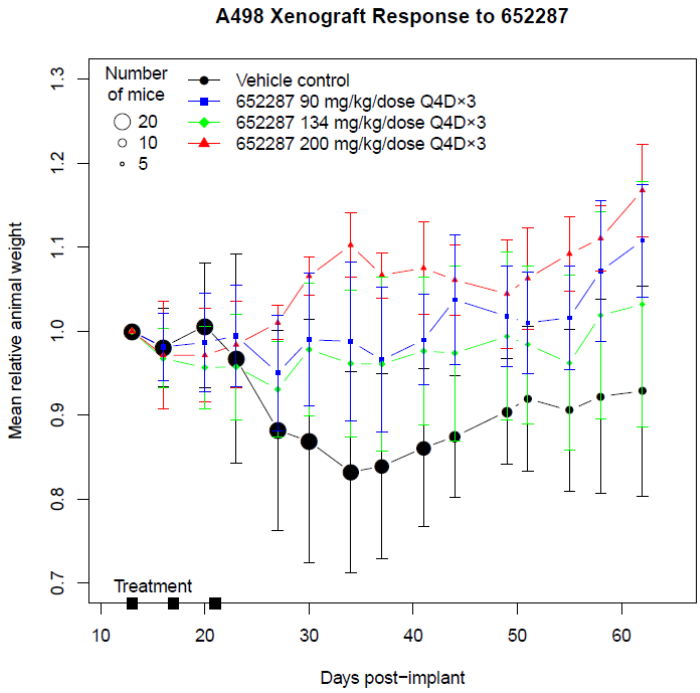

Figure 19. Mean mouse weight response to NSC 652287 (**1-1**) in A498 xenograft study.[45]

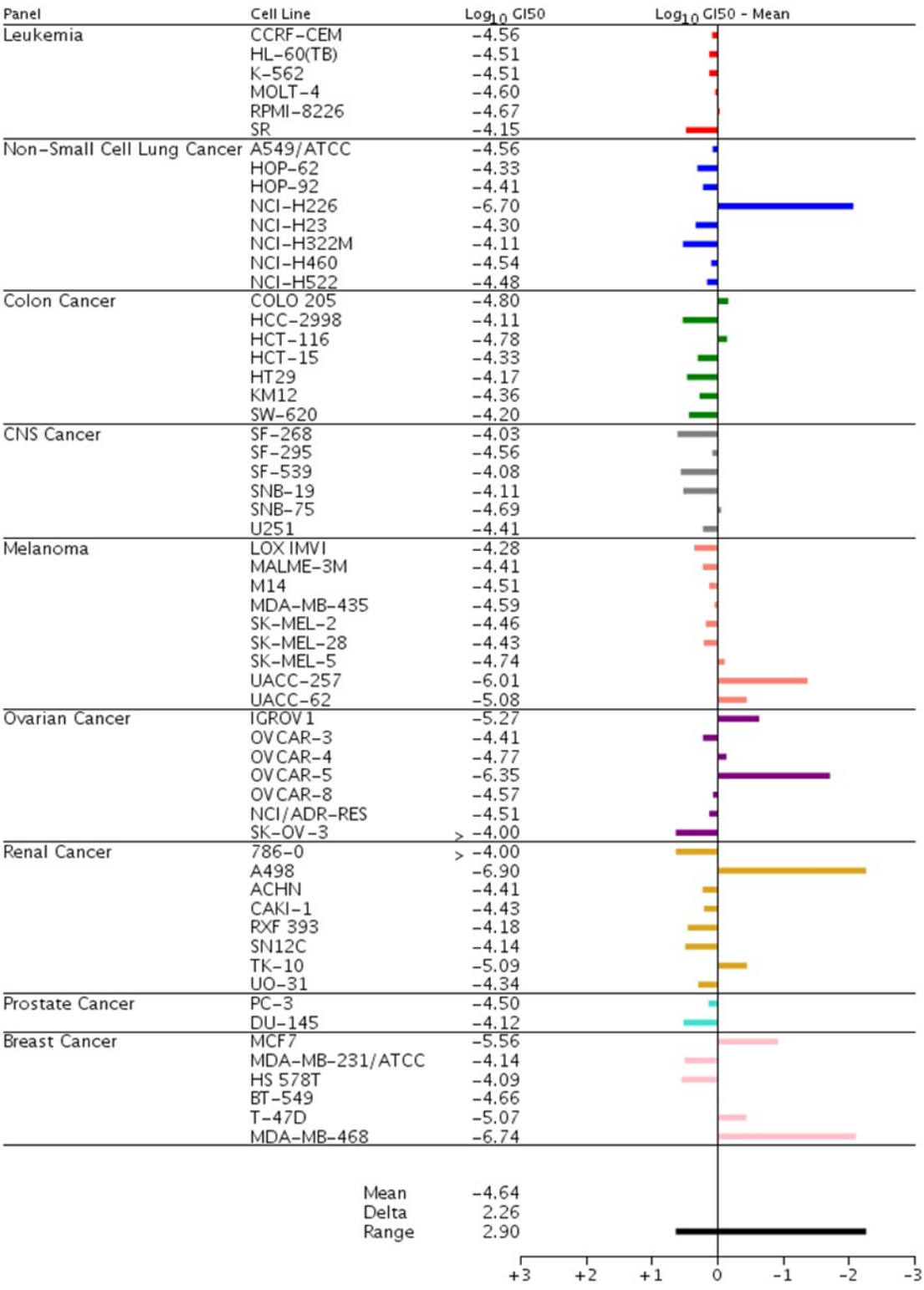

Figure 20. NCI-60 cell panel displaying mean $\log_{10}$ GI_{50} for compound **1-15b**.[45]

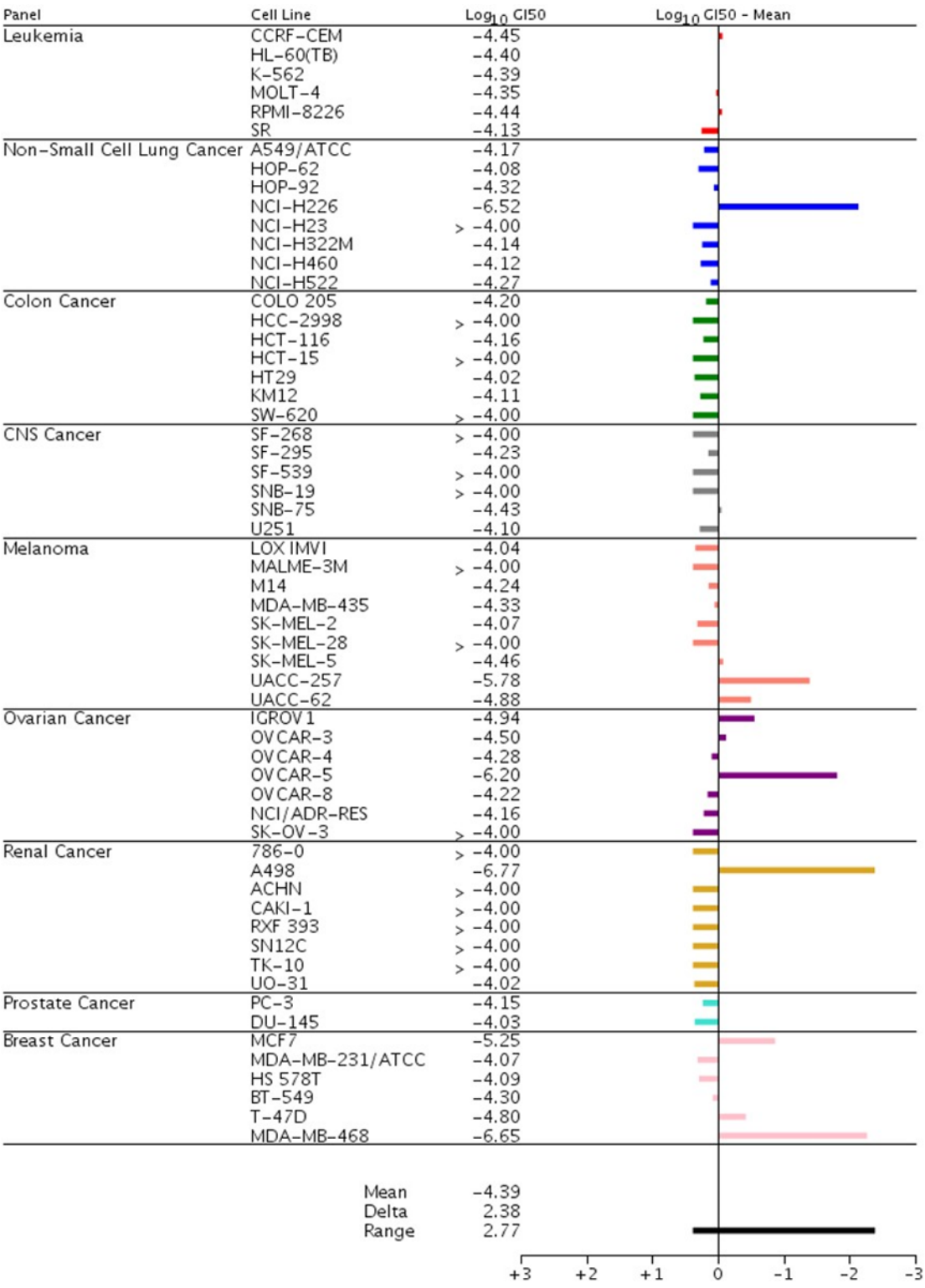

Figure 21. NCI-60 cell panel displaying mean $\log_{10}$ GI_{50} for compound **1-15c**.[45]

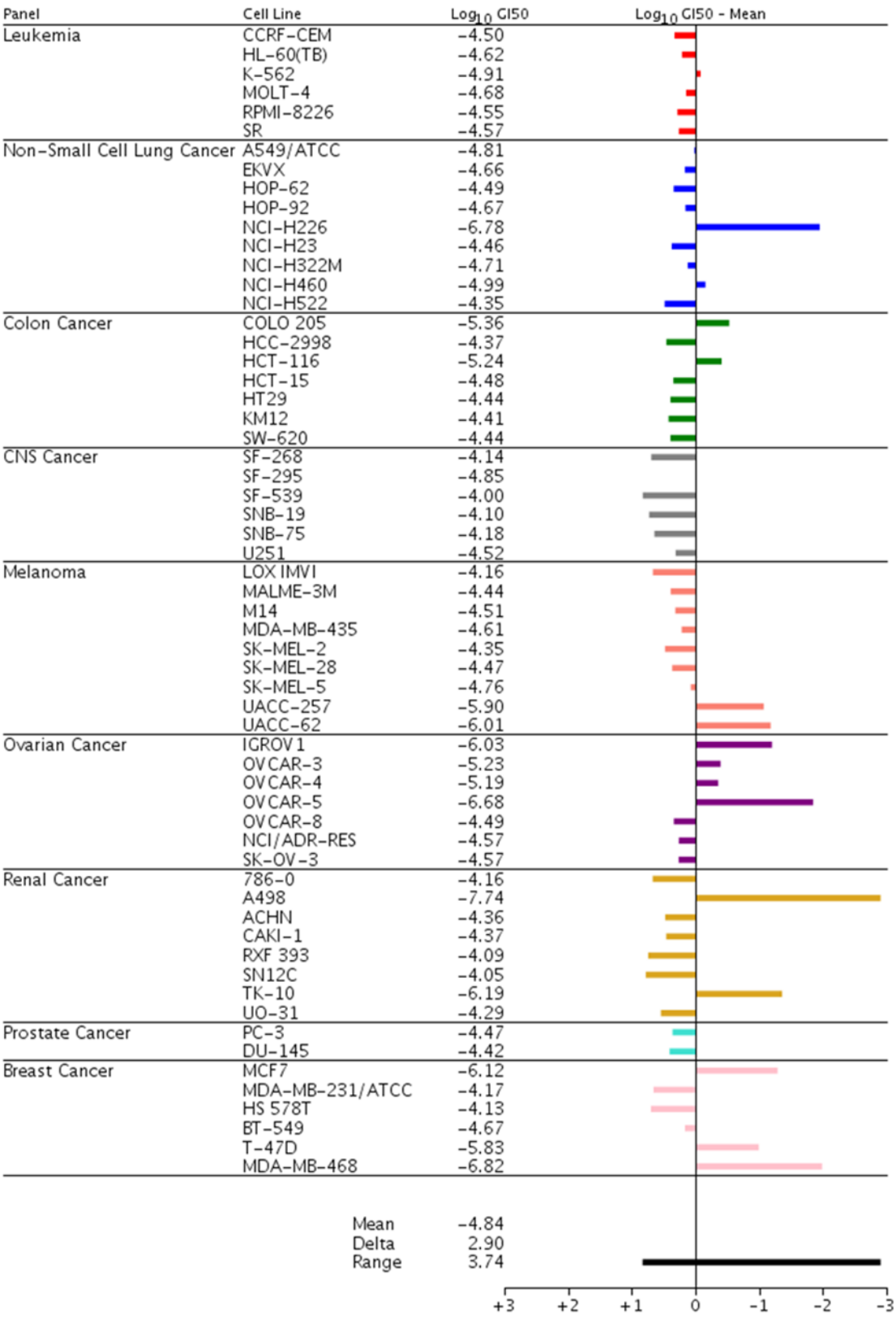

Figure 22. NCI-60 cell panel displaying mean $\log_{10}$ GI_{50} for compound **1-15f**.[45]

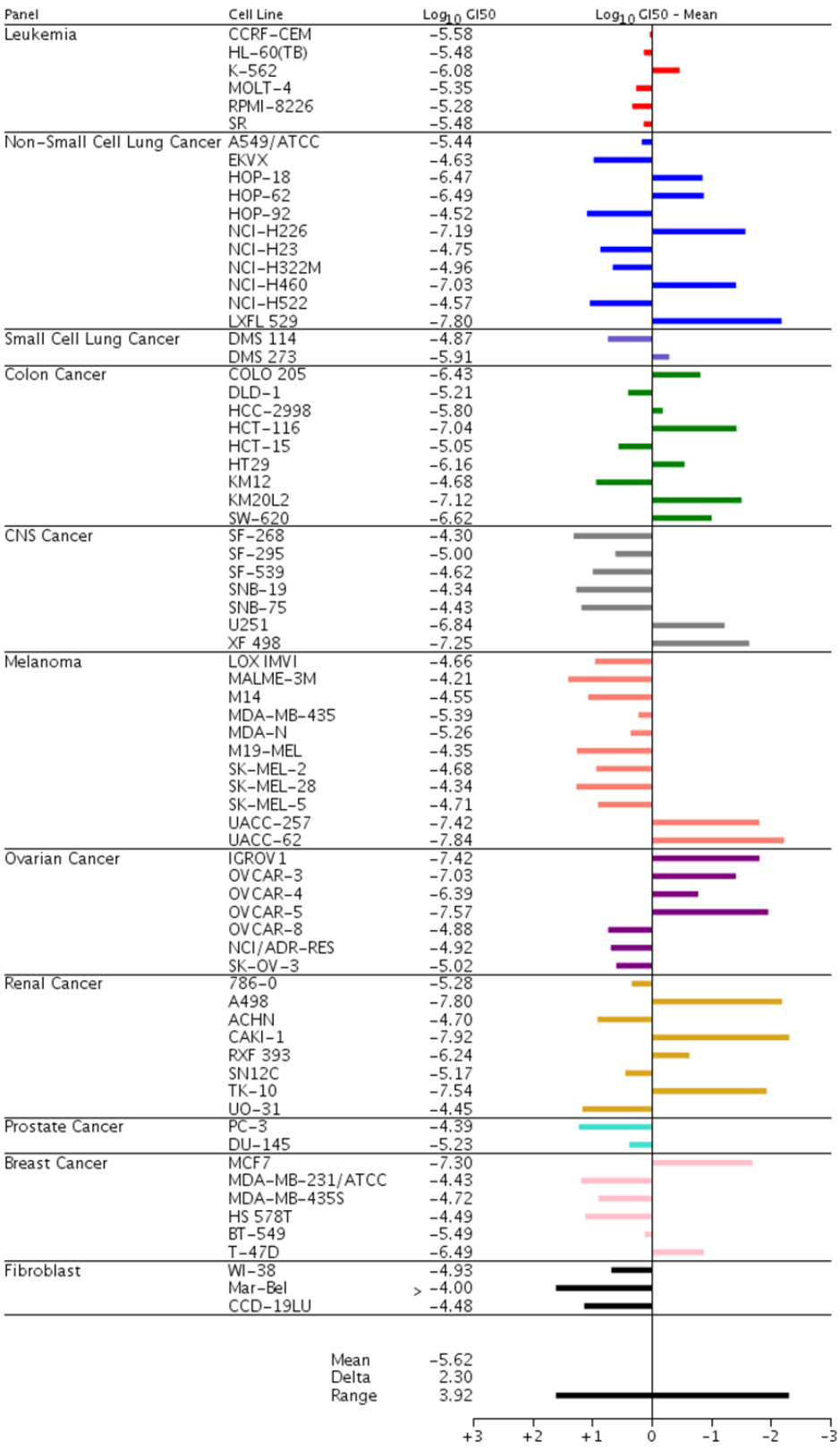

Figure 23. NCI-60 cell panel displaying mean $\log_{10}$ GI_{50} for the broadly cytotoxic triad **1-1**.[45]

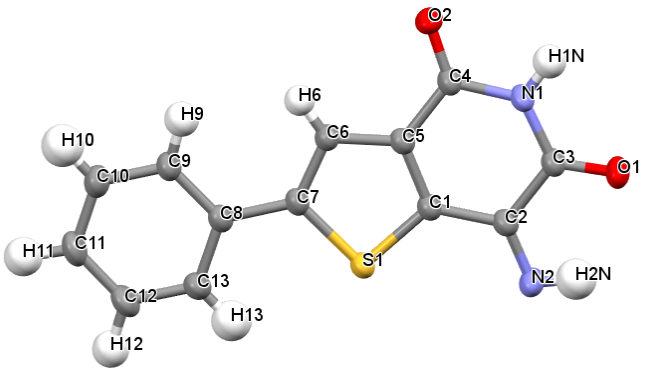

Figure 24. Crystal Structure of **2-32**.[138]

Table 10. Sample and crystal data for **2-32**.

Identification code	salamoun	
Chemical formula	$C_{13}H_8N_2O_2S$	
Formula weight	256.27 g/mol	
Temperature	230(2) K	
Wavelength	1.54178 Å	
Crystal size	0.005 x 0.080 x 0.160 mm	
Crystal habit	clear yellow plate	
Crystal system	triclinic	
Space group	P -1	
Unit cell dimensions	a = 6.4286(3) Å	α = 89.263(2)°
	b = 7.4520(3) Å	β = 78.416(2)°
	c = 11.7070(5) Å	γ = 84.742(2)°
Volume	547.09(4) $Å^3$	
Z	2	
Density (calculated)	1.556 g/cm^3	
Absorption coefficient	2.595 mm^{-1}	
F(000)	264	

Table 11. Data collection and structure refinement for **2-32**.

Diffractometer	Bruker Apex II CCD	
Radiation source	IMuS micro-focus, Cu	
Theta range for data collection	3.85 to 68.30°	
Index ranges	-7<=h<=7, -7<=k<=8, -14<=l<=14	
Reflections collected	8782	
Independent reflections	1955 [R(int) = 0.0429]	
Coverage of independent reflections	97.7%	
Absorption correction	multi-scan	
Max. and min. transmission	0.9870 and 0.6820	
Refinement method	Full-matrix least-squares on F^2	
Refinement program	SHELXL-2014/6 (Sheldrick, 2014)	
Function minimized	$\Sigma\ w(F_o^2 - F_c^2)^2$	
Data / restraints / parameters	1955 / 0 / 195	
Goodness-of-fit on F^2	1.479	
Δ/σ_{max}	0.001	
Final R indices	1761 data; $I>2\sigma(I)$	R1 = 0.0424, wR2 = 0.1274
	all data	R1 = 0.0468, wR2 = 0.1306
Weighting scheme	$w=1/[\sigma^2(F_o^2)+(0.0680P)^2]$ where $P=(F_o^2+2F_c^2)/3$	
Largest diff. peak and hole	0.283 and -0.451 eÅ^{-3}	
R.M.S. deviation from mean	0.075 eÅ^{-3}	

Table 12. Atomic coordinates and equivalent isotropic atomic displacement parameters (Å^2) for **2-32**.

U(eq) is defined as one third of the trace of the orthogonalized U_{ij} tensor.

	x/a	**y/b**	**z/c**	**U(eq)**
S1	0.68246(8)	0.20728(7)	0.57834(4)	0.0287(2)
C1	0.4811(3)	0.3040(3)	0.68347(18)	0.0257(5)
N1	0.1143(3)	0.4623(2)	0.82919(15)	0.0299(4)
O1	0.2640(3)	0.4168(2)	0.98717(14)	0.0385(4)
C2	0.4866(3)	0.3262(3)	0.80546(19)	0.0272(5)
N2	0.6501(3)	0.2810(3)	0.84828(17)	0.0348(5)
O2	0.9599(2)	0.5162(2)	0.67332(14)	0.0368(4)

	x/a	y/b	z/c	U(eq)
C3	0.2793(3)	0.4055(3)	0.88206(18)	0.0276(5)
C4	0.1132(3)	0.4522(3)	0.71031(19)	0.0272(5)
C5	0.3047(3)	0.3598(3)	0.63786(18)	0.0249(5)
C6	0.3305(3)	0.3230(3)	0.51801(18)	0.0254(5)
C7	0.5295(3)	0.2380(3)	0.47253(18)	0.0251(4)
C8	0.6133(3)	0.1783(3)	0.35150(17)	0.0262(5)
C9	0.4862(4)	0.2040(3)	0.26786(19)	0.0320(5)
C10	0.5611(4)	0.1460(3)	0.1547(2)	0.0372(5)
C11	0.7650(4)	0.0618(3)	0.1213(2)	0.0403(6)
C12	0.8937(4)	0.0362(3)	0.2031(2)	0.0404(6)
C13	0.8189(4)	0.0937(3)	0.3166(2)	0.0328(5)

Table 13. Bond lengths (Å) for **2-32**.

S1-C1	1.709(2)	S1-C7	1.730(2)
C1-C5	1.377(3)	C1-C2	1.448(3)
N1-C3	1.365(3)	N1-C4	1.396(3)
N1-H1N	0.93(3)	O1-C3	1.218(3)
C2-N2	1.270(3)	C2-C3	1.522(3)
N2-H2N	0.83(4)	O2-C4	1.211(3)
C4-C5	1.466(3)	C5-C6	1.407(3)
C6-C7	1.381(3)	C6-H6	0.88(3)
C7-C8	1.470(3)	C8-C13	1.396(3)
C8-C9	1.397(3)	C9-C10	1.376(3)
C9-H9	0.98(3)	C10-C11	1.384(3)
C10-H10	0.95(3)	C11-C12	1.386(4)
C11-H11	0.98(3)	C12-C13	1.379(3)
C12-H12	1.01(3)	C13-H13	0.93(3)

Table 14. Bond angles (°) for **2-32**.

C1-S1-C7	92.09(10)	C5-C1-C2	122.5(2)
C5-C1-S1	111.09(16)	C2-C1-S1	126.37(17)
C3-N1-C4	126.54(19)	C3-N1-H1N	119.9(16)
C4-N1-H1N	113.4(17)	N2-C2-C1	123.4(2)
N2-C2-C3	121.0(2)	C1-C2-C3	115.54(18)
C2-N2-H2N	108.(2)	O1-C3-N1	121.9(2)
O1-C3-C2	120.18(19)	N1-C3-C2	117.96(18)

O2-C4-N1	120.11(19)	O2-C4-C5	124.23(19)
N1-C4-C5	115.65(18)	C1-C5-C6	113.66(19)
C1-C5-C4	121.34(19)	C6-C5-C4	124.98(18)
C7-C6-C5	111.96(19)	C7-C6-H6	120.6(18)
C5-C6-H6	127.5(18)	C6-C7-C8	127.46(19)
C6-C7-S1	111.19(16)	C8-C7-S1	121.35(16)
C13-C8-C9	118.0(2)	C13-C8-C7	121.7(2)
C9-C8-C7	120.20(19)	C10-C9-C8	120.9(2)
C10-C9-H9	117.3(17)	C8-C9-H9	121.6(17)
C9-C10-C11	120.5(2)	C9-C10-H10	120.(2)
C11-C10-H10	119.(2)	C10-C11-C12	119.3(2)
C10-C11-H11	117.5(18)	C12-C11-H11	123.1(18)
C13-C12-C11	120.3(2)	C13-C12-H12	118.7(18)
C11-C12-H12	120.9(18)	C12-C13-C8	120.9(2)
C12-C13-H13	121.(2)	C8-C13-H13	118.(2)

Table 15. Anisotropic atomic displacement parameters (Å^2) for **2-32**.
The anisotropic atomic displacement factor exponent takes the form: $-2\pi^2[h^2 a^{*2} U_{11} + ... + 2 h k a^* b^* U_{12}]$

	U_{11}	U_{22}	U_{33}	U_{23}	U_{13}	U_{12}
S1	0.0250(3)	0.0355(4)	0.0244(3)	-0.0055(2)	-0.0041(2)	0.0035(2)
C1	0.0247(10)	0.0273(11)	0.0248(11)	-0.0032(7)	-0.0039(8)	-0.0019(8)
N1	0.0229(9)	0.0411(11)	0.0243(9)	-0.0078(7)	-0.0031(8)	0.0023(7)
O1	0.0336(9)	0.0575(11)	0.0230(8)	-0.0079(7)	-0.0052(7)	0.0025(7)
C2	0.0248(10)	0.0289(11)	0.0270(11)	-0.0031(8)	-0.0032(9)	-0.0021(8)
N2	0.0293(10)	0.0501(12)	0.0252(10)	-0.0043(8)	-0.0080(8)	0.0023(8)
O2	0.0261(8)	0.0541(11)	0.0296(9)	-0.0042(7)	-0.0089(7)	0.0075(7)
C3	0.0260(11)	0.0319(11)	0.0245(11)	-0.0039(8)	-0.0036(9)	-0.0028(8)
C4	0.0255(10)	0.0312(12)	0.0248(10)	-0.0051(8)	-0.0044(9)	-0.0029(8)
C5	0.0245(10)	0.0243(11)	0.0254(10)	-0.0023(8)	-0.0033(8)	-0.0024(8)
C6	0.0267(10)	0.0261(11)	0.0238(10)	-0.0015(8)	-0.0060(9)	-0.0024(8)
C7	0.0280(10)	0.0234(10)	0.0231(10)	-0.0025(7)	-0.0031(8)	-0.0025(7)
C8	0.0282(11)	0.0254(11)	0.0237(11)	-0.0008(8)	-0.0019(9)	-0.0022(8)
C9	0.0309(11)	0.0393(13)	0.0241(11)	-0.0039(9)	-0.0034(9)	0.0012(9)
C10	0.0420(13)	0.0442(14)	0.0249(12)	-0.0019(9)	-0.0067(10)	-0.0008(10)
C11	0.0443(13)	0.0469(14)	0.0249(11)	-0.0072(9)	0.0028(10)	0.0007(10)
C12	0.0358(13)	0.0472(15)	0.0323(12)	-0.0074(10)	0.0039(10)	0.0054(10)
C13	0.0306(11)	0.0356(12)	0.0303(12)	-0.0036(9)	-0.0047(10)	0.0040(9)

Table 16. Hydrogen atomic coordinates and isotropic atomic displacement parameters ($Å^2$) for **2-32**.

	x/a	y/b	z/c	U(eq)
H1N	-0.017(5)	0.503(3)	0.874(3)	0.042(7)
H2N	0.622(5)	0.311(4)	0.918(3)	0.062(10)
H6	0.237(4)	0.348(3)	0.473(2)	0.035(7)
H9	0.338(5)	0.255(4)	0.288(2)	0.045(8)
H10	0.473(5)	0.164(4)	0.099(3)	0.067(10)
H11	0.812(5)	0.025(4)	0.040(3)	0.056(8)
H12	1.046(5)	-0.016(4)	0.180(3)	0.051(8)
H13	0.903(5)	0.076(4)	0.372(3)	0.061(9)

BIBLIOGRAPHY

1. *National Cancer Institute;* Cancer Stat Facts: Kidney and Renal Pelvis Cancer. https://seer.cancer.gov/statfacts/html/kidrp.html. (*accessed* July, 2017).

2. Mattei, J.; da Silva, R. D.; Sehrt, D.; Molina, W. R.; Kim, F. J. *Cancer Lett.* **2014**, *343*, 156.

3. (a) Atkins, M. B.; Ernstoff, M. S.; Figlin, R. A.; Flaherty, K. T.; George, D. J.; Kaelin, W. G.; Kwon, E. D.; Libermann, T. A.; Linehan, W. M.; McDermott, D. F.; Ochoa, A. C.; Pantuck, A. J.; Rini, B. I.; Rosen, M. A.; Sosman, J. A.; Sukhatme, V. P.; Vieweg, J. W.; Wood, C. G.; King, L. *Clin. Cancer Res.* **2007**, *13*, 667; (b) Rini, B. I. *J. Clin. Oncol.* **2009**, *27*, 3225; (c) Su, D.; Stamatakis, L.; Singer, E. A.; Srinivasan, R. *Curr. Opin. Oncol.* **2014**, *26*, 321.

4. Buczek, M.; Escudier, B.; Bartnik, E.; Szczylik, C.; Czarnecka, A. *Biochim. Biophys. Acta* **2014**, *1845*, 31.

5. Bauer, A.; Bronstrup, M. *Nat. Prod. Rep.* **2014**, *31*, 35.

6. *American Cancer Society;* Targeted Therapies for Kidney Cancer. https://www.cancer.org/cancer/kidney-cancer/treating/targeted-therapy.html. (*accessed* July, 2017).

7. Brown, C. *Nature* **2016**, *537*, S106.

8. Sonpavde, G.; Hutson, T. E.; Rini, B. I. *Expert Opin. Invest. Drugs* **2008**, *17*, 741.

9. Moffat, J. G.; Rudolph, J.; Bailey, D. *Nat. Rev. Drug Discov.* **2014**, *13*, 588.

10. Shoemaker, R. H. *Nat. Rev. Cancer* **2006**, *6*, 813.

11. Vichai, V.; Kirtikara, K. *Nat. Protoc.* **2006**, *1*, 1112.

12. Zaharevitz, D. W.; Holbeck, S. L.; Bowerman, C.; Svetlik, P. A. *J. Mol. Graph. Model.* **2002**, *20*, 297.

13. Monks, A.; Scudiero, D. A.; Johnson, G. S.; Paull, K. D.; Sausville, E. A. *Anticancer Drug Des.* **1997**, *12*, 533.

14. Mertins, S. D.; Myers, T. G.; Hollingshead, M.; Dykes, D.; Bodde, E.; Tsai, P.; Jefferis, C. A.; Gupta, R.; Linehan, W. M.; Alley, M.; Bates, S. E. *Clin. Cancer Res.* **2001**, *7*, 620.

15. Rivera, M. I.; Stinson, S. F.; Vistica, D. T.; Jorden, J. L.; Kenney, S.; Sausville, E. A. *Biochem. Pharmacol.* **1999**, *57*, 1283.

16. (a) Dalvie, D. K.; Kalgutkar, A. S.; Khojasteh-Bakht, S. C.; Obach, R. S.; O'Donnell, J. P. *Chem. Res. Toxicol.* **2002**, *15*, 269; (b) Gramec, D.; Peterlin Mašič, L.; Sollner Dolenc, M. *Chem. Res. Toxicol.* **2014**, *27*, 1344.

17. Sperry, J. B.; Wright, D. L. *Curr. Opin. Drug Discov. Devel.* **2005**, *8*, 723.

18. Dansette, P. M.; Rosi, J.; Bertho, G.; Mansuy, D. *Chem. Res. Toxicol.* **2012**, *25*, 348.

19. Montuschi, P.; Ciabattoni, G. *J. Med. Chem.* **2015**, *58*, 4131.

20. Wu, G.; Vashishtha, S. C.; Erve, J. C. L. *Chem. Res. Toxicol.* **2010**, *23*, 1393.

21. Perzborn, E.; Roehrig, S.; Straub, A.; Kubitza, D.; Misselwitz, F. *Nat. Rev. Drug Discov.* **2011**, *10*, 61.

22. (a) Arnason, J. T.; Philogène, B. J. R.; Morand, P.; Imrie, K.; Iyengar, S.; Duval, F.; Soucy-Breau, C.; Scaiano, J. C.; Werstiuk, N. H.; Hasspieler, B.; Downe, A. E. R. In *Insecticides of Plant Origin*; American Chemical Society: 1989; Vol. 387, p 164; (b) Marles, R. J.; Hudson, J. B.; Graham, E. A.; Soucy-Breau, C.; Morand, P.; Compadre, R. L.; Compadre, C. M.; Towers, G. H. N.; Arnason, J. T. *Photochem. Photobiol.* **1992**, *56*, 479; (c) Juang, S. H.; Lung, C. C.; Hsu, P. C.; Hsu, K. S.; Li, Y. C.; Hong, P. C.; Shiah, H. S.; Kuo, C. C.; Huang, C. W.; Wang, Y. C.; Huang, L.; Chen, T. S.; Chen, S. F.; Fu, K. C.; Hsu, C. L.; Lin, M. J.; Chang, C. j.; Ashendel, C. L.; Chan, T. C. K.; Chou, K. M.; Chang, J. Y. *Mol. Cancer Ther.* **2007**, *6*, 193; (d) Lin, J.; Jin, X.; Bu, Y.; Cao, D.; Zhang,

N.; Li, S.; Sun, Q.; Tan, C.; Gao, C.; Jiang, Y. *Org. Biomol. Chem.* **2012**, *10*, 9734; (e) Xi, F.-M.; Li, C.-T.; Han, J.; Yu, S.-S.; Wu, Z.-J.; Chen, W.-S. *Bioorg. Med. Chem.* **2014**, *22*, 6515.

23. Kim, D. S. H. L.; Ashendel, C. L.; Zhou, Q.; Chang, C.-t.; Lee, E.-S.; Chang, C.-j. *Bioorg. Med. Chem. Lett.* **1998**, *8*, 2695.

24. Capobianco, M. L.; Barbarella, G.; Manetto, A. *Molecules* **2012**, *17*, 910.

25. (a) Brown, C. J.; Lain, S.; Verma, C. S.; Fersht, A. R.; Lane, D. P. *Nat. Rev. Cancer* **2009**, *9*, 862; (b) Chène, P. *Nat. Rev. Cancer* **2003**, *3*, 102; (c) Hoe, K. K.; Verma, C. S.; Lane, D. P. *Nat. Rev. Drug Discov.* **2014**, *13*, 217; (d) Vu, B.; Vassilev, L. In *Small-Molecule Inhibitors of Protein-Protein Interactions*; Vassilev, L., Fry, D., Eds.; Springer Berlin Heidelberg: 2011; Vol. 348, p 151.

26. Issaeva, N.; Bozko, P.; Enge, M.; Protopopova, M.; Verhoef, L. G. G. C.; Masucci, M.; Pramanik, A.; Selivanova, G. *Nat. Med.* **2004**, *10*, 1321.

27. Vassilev, L. T.; Vu, B. T.; Graves, B.; Carvajal, D.; Podlaski, F.; Filipovic, Z.; Kong, N.; Kammlott, U.; Lukacs, C.; Klein, C.; Fotouhi, N.; Liu, E. A. *Science* **2004**, *303*, 844.

28. Poyurovsky, M. V.; Katz, C.; Laptenko, O.; Beckerman, R.; Lokshin, M.; Ahn, J.; Byeon, I.-J. L.; Gabizon, R.; Mattia, M.; Zupnick, A.; Brown, L. M.; Friedler, A.; Prives, C. *Nat. Struct. Mol. Biol.* **2010**, *17*, 982.

29. Zhao, Y.; Aguilar, A.; Bernard, D.; Wang, S. *J. Med. Chem.* **2015**, *58*, 1038.

30. Krajewski, M.; Ozdowy, P.; D'Silva, L.; Rothweiler, U.; Holak, T. A. *Nat. Med.* **2005**, *11*, 1135.

31. (a) Zhao, C. Y.; Grinkevich, V.; Nikulenkov, F.; Bao, W.; Selivanova, G. *Cell Cycle* **2010**, *9*, 1847; (b) Jones, R. J.; Bjorklund, C. C.; Baladandayuthapani, V.; Kuhn, D. J.; Orlowski, R. Z. *Mol. Cancer Ther.* **2012**, *11*, 2243; (c) Burmakin, M.; Shi, Y.; Hedström, E.; Kogner, P.; Selivanova, G. *Clin. Cancer Res.* **2013**, *19*, 5092.

32. Wanzel, M.; Vischedyk, J. B.; Gittler, M. P.; Gremke, N.; Seiz, J. R.; Hefter, M.; Noack, M.; Savai, R.; Mernberger, M.; Charles, J. P.; Schneikert, J.; Bretz, A. C.; Nist, A.; Stiewe, T. *Nat. Chem. Biol.* **2016**, *12*, 22.

33. Fuchs, J. E.; Spitzer, G. M.; Javed, A.; Biela, A.; Kreutz, C.; Wellenzohn, B.; Liedl, K. R. *J. Chem. Inf. Model.* **2011**, *51*, 2223.

34. Nieves-Neira, W.; Rivera, M. I.; Kohlhagen, G.; Hursey, M. L.; Pourquier, P.; Sausville, E. A.; Pommier, Y. *Mol. Pharmacol.* **1999**, *56*, 478.

35. Phillips, L. R.; Jorden, J. L.; Rivera, M. I.; Upadhyay, K.; Wolfe, T. L.; Stinson, S. F. *J. Chromatogr. B* **2002**, *767*, 27.

36. Dijkman, W. P.; Groothuis, D. E.; Fraaije, M. W. *Angew. Chem. Int. Ed.* **2014**, *53*, 6515.

37. de Lange, J.; Verlaan-de Vries, M.; Teunisse, A. F. A. S.; Jochemsen, A. G. *Cell Death Differ.* **2012**, *19*, 980.

38. Lou, J. J. W.; Chua, Y. L.; Chew, E. H.; Gao, J.; Bushell, M.; Hagen, T. *PLoS ONE* **2010**, *5*, e10522.

39. Weilbacher, A.; Gutekunst, M.; Oren, M.; Aulitzky, W. E.; van der Kuip, H. *Cell Death Dis.* **2014**, *5*, e1318.

40. Rees, M. G.; Seashore-Ludlow, B.; Cheah, J. H.; Adams, D. J.; Price, E. V.; Gill, S.; Javaid, S.; Coletti, M. E.; Jones, V. L.; Bodycombe, N. E.; Soule, C. K.; Alexander, B.; Li, A.; Montgomery, P.; Kotz, J. D.; Hon, C. S.-Y.; Munoz, B.; Liefeld, T.; Dancik, V.; Haber, D. A.; Clish, C. B.; Bittker, J. A.; Palmer, M.; Wagner, B. K.; Clemons, P. A.; Shamji, A. F.; Schreiber, S. L. *Nat. Chem. Biol.* **2016**, *12*, 109.

41. Xu, J.; Eriksson, S. E.; Cebula, M.; Sandalova, T.; Hedstrom, E.; Pader, I.; Cheng, Q.; Myers, C. R.; Antholine, W. E.; Nagy, P.; Hellman, U.; Selivanova, G.; Lindqvist, Y.; Arner, E. S. J. *Cell Death Dis.* **2015**, *6*, e1616.

42. Kaelin Jr, W. G. *Nat. Rev. Cancer* **2017**, *17*, 425.

43. Division of Cancer Treatment and Diagnosis, *National Cancer Institute*. *Unpublished results*.

44. Moffat, J. G.; Vincent, F.; Lee, J. A.; Eder, J.; Prunotto, M. *Nat. Rev. Drug Discov.* **2017**, *16*, 531.

45. Developmental Therapeutics Program, *National Cancer Institute*. *Unpublished results*.

46. (a) Ishida, H.; Yui, K.; Aso, Y.; Otsubo, T.; Ogura, F. *Bull. Chem. Soc. Jpn.* **1990**, *63*, 2828; (b) Chang, C. T.; Yang, Y.-L. Eur. Pat. Appl. EP866066 A1 19980923, 1998.

47. (a) McFarland, J. W.; Howe, B. M.; Lehmkuhler, J. D.; Myers, D. C. *J. Heterocycl. Chem.* **1995**, *32*, 1747; (b) Chang, C. T.; Ashendel, C. L.; Kim, D. PCT Int. Appl. WO9746225A1 19971211, 1997.

48. Salamoun, J.; Anderson, S.; Burnett, J. C.; Gussio, R.; Wipf, P. *Org. Lett.* **2014**, *16*, 2034.

49. (a) Contributions by Shelby Anderson and Dr. Christopher Rosenker, *University of Pittsburgh, Department of Chemistry*. ; (b) Littke, A. F.; Dai, C.; Fu, G. C. *J. Am. Chem. Soc.* **2000**, *122*, 4020.

50. Martin, R.; Buchwald, S. L. *Acc. Chem. Res.* **2008**, *41*, 1461.

51. Bruno, N. C.; Tudge, M. T.; Buchwald, S. L. *Chem. Sci.* **2013**, *4*, 916.

52. Lipton, M. F.; Mauragis, M. A.; Maloney, M. T.; Veley, M. F.; VanderBor, D. W.; Newby, J. J.; Appell, R. B.; Daugs, E. D. *Org. Process Res. Dev.* **2003**, *7*, 385.

53. (a) Handy, S. T.; Zhang, Y. *Chem. Commun.* **2006**, 299; (b) Garcia, Y.; Schoenebeck, F.; Legault, C. Y.; Merlic, C. A.; Houk, K. N. *J. Am. Chem. Soc.* **2009**, *131*, 6632; (c) Legault, C. Y.; Garcia, Y.; Merlic, C. A.; Houk, K. N. *J. Am. Chem. Soc.* **2007**, *129*, 12664.

54. Konkol, K. L.; Rasmussen, S. C. *Organometallics* **2016**, *35*, 3234.

55. Miyata, Y.; Terayama, M.; Minari, T.; Nishinaga, T.; Nemoto, T.; Isoda, S.; Komatsu, K. *Chem. Asian J.* **2007**, *2*, 1492.

56. (a) Vedejs, E.; Luchetta, L. M. *J. Org. Chem.* **1998**, *64*, 1011; (b) Flegeau, E. F.; Popkin, M. E.; Greaney, M. F. *J. Org. Chem.* **2008**, *73*, 3303; (c) Schnürch, M.; Flasik, R.; Khan, A. F.; Spina, M.; Mihovilovic, M. D.; Stanetty, P. *Eur. J. Org. Chem.* **2006**, 3283.

57. (a) Verrier, C.; Lassalas, P.; Théveau, L.; Quéguiner, G.; Trécourt, F.; Marsais, F.; Hoarau, C. *Beilstein J. Org. Chem.* **2011**, *7*, 1584; (b) Verrier, C.; Martin, T.; Hoarau, C.; Marsais, F. *J. Org. Chem.* **2008**, *73*, 7383.

58. Théveau, L.; Verrier, C.; Lassalas, P.; Martin, T.; Dupas, G.; Querolle, O.; Hijfte, L. V.; Marsais, F.; Hoarau, C. *Chem. Eur. J.* **2011**, *17*, 14450.

59. Bach, T.; Krüger, L. *Eur. J. Org. Chem.* **1999**, 2045.

60. Potratz, S.; Mishra, A.; Bäuerle, P. *Beilstein J. Org. Chem.* **2012**, *8*, 683.

61. (a) Harmon, R. E.; Stanley, F.; Gupta, S. K.; Johnson, J. *J. Org. Chem.* **1970**, *35*, 3444; (b) Hermes, M. E.; Marsh, F. D. *J. Am. Chem. Soc.* **1967**, *89*, 4760.

62. Perdew, J. P.; Wang, Y. *Phys. Rev. B* **1992**, *45*, 13244.

63. Gidron, O.; Bendikov, M. *Angew. Chem. Int. Ed.* **2014**, *53*, 2546.

64. (a) Troy, A. B. *Curr. Drug Discov. Technol.* **2015**, *12*, 3; (b) *National Cancer Institute;* Targeted Cancer Therapies. https://www.cancer.gov/about-cancer/treatment/types/targeted-therapies/targeted-therapies-fact-sheet. (*accessed* July, 2017).

65. (a) Alex, A. A.; Millan, D. S. In *Drug Design Strategies: Quantitative Approaches*; The Royal Society of Chemistry: 2012, p 108; (b) Curry, S. *Interdiscip. Sci. Rev.* **2015**, *40*, 308; (c) Merino, F.; Raunser, S. *Angew. Chem. Int. Ed.* **2017**, *56*, 2846; (d) Venien-Bryan, C.; Li, Z.; Vuillard, L.; Boutin, J. A. *Acta Cryst.* **2017**, *F73*, 174.

66. (a) Chang, J.; Kim, Y.; Kwon, H. J. *Nat. Prod. Rep.* **2016**, *33*, 719; (b) Wright, M. H.; Sieber, S. A. *Nat. Prod. Rep.* **2016**, *33*, 681; (c) Kapoor, S.; Waldmann, H.; Ziegler, S. *Bioorg. Med. Chem.* **2016**, *24*, 3232; (d) Abet, V.; Mariani, A.; Truscott, F. R.; Britton, S.; Rodriguez, R. *Bioorg. Med. Chem.* **2014**, *22*, 4474.

67. (a) Molina, D. M.; Jafari, R.; Ignatushchenko, M.; Seki, T.; Larsson, E. A.; Dan, C.; Sreekumar, L.; Cao, Y.; Nordlund, P. *Science* **2013**, *341*, 84; (b) Savitski, M. M.; Reinhard, F. B. M.; Franken, H.; Werner, T.; Savitski, M. F.; Eberhard, D.; Molina, D. M.; Jafari, R.; Dovega, R. B.; Klaeger, S.; Kuster, B.; Nordlund, P.; Bantscheff, M.; Drewes, G. *Science* **2014**, *346*, 1255784; (c) Molina, D. M.; Nordlund, P. *Annu. Rev. Pharmacol. Toxicol.* **2016**, *56*, 141.

68. Main contributions by Dr. Steven Mullet and Prof. Nathan Yates, *University of Pittsburgh, Biomedical Mass Spectrometry Center*. *Unpublished results*.

69. Tyanova, S.; Temu, T.; Cox, J. *Nat. Protoc.* **2016**, *11*, 2301.

70. Kimura, Y.; Furuhata, T.; Urano, T.; Hirata, K.; Nakamura, Y.; Tokino, T. *Genomics* **1997**, *41*, 477.

71. Smart, D. K.; Ortiz, K. L.; Mattson, D.; Bradbury, C. M.; Bisht, K. S.; Sieck, L. K.; Brechbiel, M. W.; Gius, D. *Cancer Res.* **2004**, *64*, 6716.

72. Hayes, J. D.; Strange, R. C. *Pharmacology* **2000**, *61*, 154.

73. Bulock, K. G.; Beardsley, G. P.; Anderson, K. S. *J. Biol. Chem.* **2002**, *277*, 22168.

74. Penning, T. M.; Byrns, M. C. *Ann. N. Y. Acad. Sci.* **2009**, *1155*, 33.

75. Lyons, J.; Landis, C. A.; Harsh, G.; Vallar, L.; Grunewald, K.; Feichtinger, H.; Duh, Q. Y.; Clark, O. H.; Kawasaki, E.; Bourne, H. R.; et, a. *Science* **1990**, *249*, 655.

76. Gamage, N.; Barnett, A.; Hempel, N.; Duggleby, R. G.; Windmill, K. F.; Martin, J. L.; McManus, M. E. *Toxicol. Sci.* **2006**, *90*, 5.

77. Bateman, R. L.; Rauh, D.; Tavshanjian, B.; Shokat, K. M. *J. Biol. Chem.* **2008**, *283*, 35756.

78. Kukalev, A.; Nord, Y.; Palmberg, C.; Bergman, T.; Percipalle, P. *Nat. Struct. Mol. Biol.* **2005**, *12*, 238.

79. Gibbs, P. E. M.; Miralem, T.; Maines, M. D. *Front. Pharmacol.* **2015**, *6*, 119.

80. Honda, K.; Yamada, T.; Endo, R.; Ino, Y.; Gotoh, M.; Tsuda, H.; Yamada, Y.; Chiba, H.; Hirohashi, S. *J. Cell Biol.* **1998**, *140*, 1383.

81. Menendez, J. A.; Lupu, R. *Nat. Rev. Cancer* **2007**, *7*, 763.

82. Rescher, U.; Gerke, V. *J. Cell Sci.* **2004**, *117*, 2631.

83. Dostanic, I.; Schultz, J. E. J.; Lorenz, J. N.; Lingrel, J. B. *J. Biol. Chem.* **2004**, *279*, 54053.

84. (a) Sacco, F.; Perfetto, L.; Castagnoli, L.; Cesareni, G. *FEBS Lett.* **2012**, *586*, 2732; (b) Jin, J.; Pawson, T. *Phil. Trans. R. Soc. B* **2012**, *367*, 2540.

85. (a) Alonso, A.; Pulido, R. *FEBS J.* **2016**, *283*, 1404; (b) Chen, M. J.; Dixon, J. E.; Manning, G. *Sci. Signal.* **2017**, *10*.

86. (a) Lazo, J. S.; Wipf, P. *Curr. Opin. Invest. Drugs* **2009**, *10*, 1297; (b) Santos, R.; Ursu, O.; Gaulton, A.; Bento, A. P.; Donadi, R. S.; Bologa, C. G.; Karlsson, A.; Al-Lazikani, B.; Hersey, A.; Oprea, T. I.; Overington, J. P. *Nat. Rev. Drug Discov.* **2017**, *16*, 19.

87. Yu, Z.-H.; Zhang, Z.-Y. *Chem. Rev.* **2017**, ASAP.

88. (a) Barr, A. J. *Future Med. Chem.* **2010**, *2*, 1563; (b) Bialy, L.; Waldmann, H. *Angew. Chem. Int. Ed.* **2005**, *44*, 3814; (c) McConnell, J. L.; Wadzinski, B. E. *Mol. Pharmacol.* **2009**, *75*, 1249; (d) Vintonyak, V. V.; Waldmann, H.; Rauh, D. *Bioorg. Med. Chem.* **2011**, *19*, 2145; (e) Salamoun, J. M.; Wipf, P. *J. Med. Chem.* **2016**, *59*, 7771.

89. (a) Stephens, B. J.; Han, H.; Gokhale, V.; Von Hoff, D. D. *Mol. Cancer Ther.* **2005**, *4*, 1653; (b) Bessette, D.; Qiu, D.; Pallen, C. *Cancer Metastasis Rev.* **2008**, *27*, 231; (c) Sharlow, E. R.; Wipf, P.; McQueeney, K. E.; Bakan, A.; Lazo, J. S. *Expert Opin. Invest. Drugs* **2014**, *23*, 661.

90. Saha, S.; Bardelli, A.; Buckhaults, P.; Velculescu, V. E.; Rago, C.; Croix, B. S.; Romans, K. E.; Choti, M. A.; Lengauer, C.; Kinzler, K. W.; Vogelstein, B. *Science* **2001**, *294*, 1343.

91. (a) Zimmerman, M. W.; Homanics, G. E.; Lazo, J. S. *PLoS ONE* **2013**, *8*, e58300; (b) Zimmerman, M. W.; McQueeney, K. E.; Isenberg, J. S.; Pitt, B. R.; Wasserloos, K. A.; Homanics, G. E.; Lazo, J. S. *J. Biol. Chem.* **2014**, *289*, 5904.

92. Wang, H.; Quah, S. Y.; Dong, J. M.; Manser, E.; Tang, J. P.; Zeng, Q. *Cancer Res.* **2007**, *67*, 2922.

93. Fiordalisi, J. J.; Keller, P. J.; Cox, A. D. *Cancer Res.* **2006**, *66*, 3153.

94. Ming, J.; Liu, N.; Gu, Y.; Qui, X.; Wang, E. H. *Pathology* **2009**, *41*, 118.

95. (a) Liang, F.; Liang, J.; Wang, W.-Q.; Sun, J.-P.; Udho, E.; Zhang, Z.-Y. *J. Biol. Chem.* **2007**, *282*, 5413; (b) Abdollahi, P.; Vandsemb, E. N.; Hjort, M. A.; Misund, K.; Holien, T.; Sponaas, A.-M.; Rø, T. B.; Slørdahl, T. S.; Børset, M. *Mol. Cancer Res.* **2017**, *15*, 69.

96. Lazo, J. S.; Wipf, P. *Oncol. Res.* **2003**, *13*, 347.

97. (a) Kozlov, G.; Cheng, J.; Ziomek, E.; Banville, D.; Gehring, K.; Ekiel, I. *J. Biol. Chem.* **2004**, *279*, 11882; (b) Jeong, D. G.; Kim, S. J.; Kim, J. H.; Son, J. H.; Park, M. R.; Lim, S. M.; Yoon, T.-S.; Ryu, S. E. *J. Mol. Biol.* **2005**, *345*, 401.

98. Pathak, M. K.; Dhawan, D.; Lindner, D. J.; Borden, E. C.; Farver, C.; Yi, T. *Mol. Cancer Ther*. **2002**, *1*, 1255.

99. (a) Munde, M.; Lee, M.; Neidle, S.; Arafa, R.; Boykin, D. W.; Liu, Y.; Bailly, C.; Wilson, W. D. *J. Am. Chem. Soc.* **2007**, *129*, 5688; (b) Antony, S.; Marchand, C.; Stephen, A. G.; Thibaut, L.; Agama, K. K.; Fisher, R. J.; Pommier, Y. *Nucleic Acids Res.* **2007**, *35*, 4474.

100. Choi, S.-K.; Oh, H.-M.; Lee, S.-K.; Jeong, D. G.; Ryu, S. E.; Son, K.-H.; Han, D. C.; Sung, N.-D.; Baek, N.-I.; Kwon, B.-M. *Nat. Prod. Res.* **2006**, *20*, 341.

101. Shadnia, H.; Wright, J. S. *Chem. Res. Toxicol.* **2008**, *21*, 1197.

102. Schultz, T. W.; Yarbrough, J. W.; Hunter, R. S.; Aptula, A. O. *Chem. Res. Toxicol.* **2007**, *20*, 1359.

103. Han, Y.-M.; Lee, S.-K.; Jeong, D. G.; Ryu, S. E.; Han, D. C.; Kim, D. K.; Kwon, B.-M. *Bioorg. Med. Chem. Lett.* **2012**, *22*, 323.

104. Chou, L.-C.; Chen, C.-T.; Lee, J.-C.; Way, T.-D.; Huang, C.-H.; Huang, S.-M.; Teng, C.-M.; Yamori, T.; Wu, T.-S.; Sun, C.-M.; Chien, D.-S.; Qian, K.; Morris-Natschke, S. L.; Lee, K.-H.; Huang, L.-J.; Kuo, S.-C. *J. Med. Chem.* **2010**, *53*, 1616.

105. Mendgen, T.; Steuer, C.; Klein, C. D. *J. Med. Chem.* **2011**, *55*, 743.

106. (a) Stockwell, B. R. *Nat. Rev. Genet.* **2000**, *1*, 116; (b) Schreiber, S. L.; Kotz, J. D.; Li, M.; Aubé, J.; Austin, C. P.; Reed, J. C.; Rosen, H.; White, E. L.; Sklar, L. A.; Lindsley, C. W.; Alexander, B. R.; Bittker, J. A.; Clemons, P. A.; de Souza, A.; Foley, M. A.; Palmer, M.; Shamji, A. F.; Wawer, M. J.; McManus, O.; Wu, M.; Zou, B.; Yu, H.; Golden, J. E.; Schoenen, F. J.; Simeonov, A.; Jadhav, A.; Jackson, M. R.; Pinkerton, A. B.; Chung, T. D. Y.; Griffin, P. R.; Cravatt, B. F.; Hodder, P. S.; Roush, W. R.; Roberts, E.; Chung, D.-H.; Jonsson, C. B.; Noah, J. W.; Severson, W. E.; Ananthan, S.; Edwards, B.; Oprea, T. I.; Conn, P. J.; Hopkins, C. R.; Wood, M. R.; Stauffer, S. R.; Emmitte, K. A.; Brady, L. S.; Driscoll, J.; Li, I. Y.; Loomis, C. R.; Margolis, R. N.; Michelotti, E.; Perry, M. E.; Pillai, A.; Yao, Y. *Cell* **2015**, *161*, 1252.

107. Ahn, J. H.; Kim, S. J.; Park, W. S.; Cho, S. Y.; Ha, J. D.; Kim, S. S.; Kang, S. K.; Jeong, D. G.; Jung, S.-K.; Lee, S.-H.; Kim, H. M.; Park, S. K.; Lee, K. H.; Lee, C. W.; Ryu, S. E.; Choi, J.-K. *Bioorg. Med. Chem. Lett.* **2006**, *16*, 2996.

108. Min, G.; Lee, S.-K.; Kim, H.-N.; Han, Y.-M.; Lee, R.-H.; Jeong, D. G.; Han, D. C.; Kwon, B.-M. *Bioorg. Med. Chem. Lett.* **2013**, *23*, 3769.

109. Daouti, S.; Li, W.-h.; Qian, H.; Huang, K.-S.; Holmgren, J.; Levin, W.; Reik, L.; McGady, D. L.; Gillespie, P.; Perrotta, A.; Bian, H.; Reidhaar-Olson, J. F.; Bliss, S. A.; Olivier, A. R.; Sergi, J. A.; Fry, D.; Danho, W.; Ritland, S.; Fotouhi, N.; Heimbrook, D.; Niu, H. *Cancer Res.* **2008**, *68*, 1162.

110. Stepan, A. F.; Walker, D. P.; Bauman, J.; Price, D. A.; Baillie, T. A.; Kalgutkar, A. S.; Aleo, M. D. *Chem. Res. Toxicol.* **2011**, *24*, 1345.

111. (a) New, J. S.; Christopher, W. L.; Yevich, J. P.; Butler, R.; Schlemmer, R. F.; VanderMaelen, C. P.; Cipollina, J. A. *J. Med. Chem.* **1989**, *32*, 1147; (b) Gentile, G.; Bernasconi, G.; Pozzan, A.; Merlo, G.; Marzorati, P.; Bamborough, P.; Bax, B.; Bridges, A.; Brough, C.; Carter, P.; Cutler, G.; Neu, M.; Takada, M. *Bioorg. Med. Chem. Lett.* **2011**, *21*, 4823; (c) Li, L.; Degardin, M.; Lavergne, T.; Malyshev, D. A.; Dhami, K.; Ordoukhanian, P.; Romesberg, F. E. *J. Am. Chem. Soc.* **2014**, *136*, 826; (d) Salamoun, J. M.; McQueeney, K. E.; Patil, K.; Geib, S. J.; Sharlow, E. R.; Lazo, J. S.; Wipf, P. *Org. Biomol. Chem.* **2016**, *14*, 6398.

112. Patil, K. *University of Pittsburgh, Department of Chemistry*.

113. (a) Chien-Chang, C.; Li-Yueh, C.; Rung-Yuan, L.; Che-Yi, C.; Shenghong, A. D. *Heterocyles* **2009**, *78*, 2979; (b) Uriz, P.; Serra, M.; Salagre, P.; Castillon, S.; Claver, C.; Fernandez, E. *Tetrahedron Lett.* **2002**, *43*, 1673.

114. Jessen, H. J.; Schumacher, A.; Schmid, F.; Pfaltz, A.; Gademann, K. *Org. Lett.* **2011**, *13*, 4368.

115. Dias, L. C.; Ferreira, M. A. B. *J. Org. Chem.* **2012**, *77*, 4046.

116. Biehl, E. In *Metalation of Azoles and Related Five-Membered Ring Heterocycles*; Gribble, G. W., Ed.; Springer Berlin Heidelberg: 2012; Vol. 29, p 347.

117. Tormyshev, V. M.; Trukhin, D. V.; Rogozhnikova, O. Y.; Mikhalina, T. V.; Troitskaya, T. I.; Flinn, A. *Synlett* **2006**, 2559.

118. (a) George, M. V.; Bhat, V. *Chem. Rev.* **1979**, *79*, 447; (b) Cossy, J.; Belotti, D. *Tetrahedron Lett.* **2001**, *42*, 4329; (c) Simpson, D. S.; Katavic, P. L.; Lozama, A.; Harding, W. W.; Parrish, D.; Deschamps, J. R.; Dersch, C. M.; Partilla, J. S.; Rothman, R. B.; Navarro, H.; Prisinzano, T. E. *J. Med. Chem.* **2007**, *50*, 3596.

119. (a) Kim, I.; Min, M.; Kang, D.; Kim, K.; Hong, S. *Org. Lett.* **2017**, *19*, 1394; (b) Lima, C. G. S.; de M. Lima, T.; Duarte, M.; Jurberg, I. D.; Paixão, M. W. *ACS Catal.* **2016**, *6*, 1389; (c) Gocke, E.; Chételat, A. A.; Csato, M.; McGarvey, D. J.; Jakob-Roetne, R.; Kirchner, S.; Muster, W.; Potthast, M.; Widmer, U. *Mutat. Res.* **2003**, *535*, 43.

120. (a) Benz, S.; Nötzli, S.; Siegel, J. S.; Eberli, D.; Jessen, H. J. *J. Med. Chem.* **2013**, *56*, 10171; (b) Turan, I. S.; Yildiz, D.; Turksoy, A.; Gunaydin, G.; Akkaya, E. U. *Angew. Chem. Int. Ed.* **2016**, *55*, 2875.

121. Ling, K.-Q.; Ye, J.-H.; Chen, X.-Y.; Ma, D.-J.; Xu, J.-H. *Tetrahedron* **1999**, *55*, 9185.

122. (a) Henry, R. A.; Heller, C. A.; Moore, D. W. *J. Org. Chem.* **1975**, *40*, 1760; (b) Tahara, S.; Shigetsuna, M.; Otomasu, H. *Chem. Pharm. Bull.* **1982**, *30*, 3133.

123. McQueeney, K. E.; Sharlow, E. R.; Lazo, J. S., *University of Virginia, Department of Pharmacology. Unpublished results*.

124. (a) Li, J.; Ballmer, S. G.; Gillis, E. P.; Fujii, S.; Schmidt, M. J.; Palazzolo, A. M. E.; Lehmann, J. W.; Morehouse, G. F.; Burke, M. D. *Science* **2015**, *347*, 1221; (b) Ley, S. V.; Fitzpatrick, D. E.; Myers, R. M.; Battilocchio, C.; Ingham, R. J. *Angew. Chem. Int. Ed.* **2015**, *54*, 10122.

125. Baranczak, A.; Tu, N. P.; Marjanovic, J.; Searle, P. A.; Vasudevan, A.; Djuric, S. W. *ACS Med. Chem. Lett.* **2017**, *8*, 461.

126. (a) *Eli Lilly & Company;* Open Innovation Drug Discovery Program. https://openinnovation.lilly.com/dd/. (*accessed* July, 2017); (b) Godfrey, A. G.; Masquelin, T.; Hemmerle, H. *Drug Discov. Today* **2013**, *18*, 795.

127. In collaboration with Christopher Beadle, *Eli Lilly & Company*. *Unplublished results*.

128. Chao, J.; Taveras, A. G.; Chao, J.; Aki, C.; Dwyer, M.; Yu, Y.; Purakkattle, B.; Rindgen, D.; Jakway, J.; Hipkin, W.; Fosetta, J.; Fan, X.; Lundell, D.; Fine, J.; Minnicozzi, M.; Phillips, J.; Merritt, J. R. *Bioorg. Med. Chem. Lett.* **2007**, *17*, 3778.

129. Molander, G. A.; Iannazzo, L. *J. Org. Chem.* **2011**, *76*, 9182.

130. Milner, P. J.; Yang, Y.; Buchwald, S. L. *Organometallics* **2015**, *34*, 4775.

131. Milen, M.; Ábrányi-Balogh, P.; Dancsó, A.; Drahos, L.; Keglevich, G. *Heteroatom Chem.* **2013**, *24*, 124.

132. Bock, M. G.; Gaul, C.; Gummadi, V. R.; Moebitz, H.; Sengupta, S. PCT Int. Appl. WO2012035078 A1 20120322, 2012.

133. Burkitt, S.; Cardozo, M.; Cushing, T.; DeGraffenreid, M.; Farthing, C.; Hao, X.; Jaen, J.; Jiao, X.; Kopecky, D.; Labelle, M. PCT Int. Appl. WO2004041285 A1 20040521, 2004.

134. Gopinath, P.; Chandrasekaran, S. *J. Org. Chem.* **2011**, *76*, 700.

135. González Cabrera, D.; Le Manach, C.; Douelle, F.; Younis, Y.; Feng, T.-S.; Paquet, T.; Nchinda, A. T.; Street, L. J.; Taylor, D.; de Kock, C.; Wiesner, L.; Duffy, S.; White, K. L.; Zabiulla, K. M.; Sambandan, Y.; Bashyam, S.; Waterson, D.; Witty, M. J.; Charman, S. A.; Avery, V. M.; Wittlin, S.; Chibale, K. *J. Med. Chem.* **2014**, *57*, 1014.

136. Modica, M.; Santagati, M.; Russo, F.; Parotti, L.; De Gioia, L.; Selvaggini, C.; Salmona, M.; Mennini, T. *J. Med. Chem.* **1997**, *40*, 574.

137. Song, Y.-H.; Son, H. Y. *J. Heterocycl. Chem.* **2011**, *48*, 597.

138. Geib, S. J. , *University of Pittsburgh, Department of Chemistry*.